2019-06-01

Characterizing the Function of PAS kinase in Cellular Metabolism and Neurodegenerative Disease

Jenny Adele Pape
Brigham Young University

Characterizing the Function of PAS kinase in Cellular Metabolism and Neurodegenerative Disease

Jenny Adele Pape

A dissertation submitted to the faculty of
Brigham Young University
in partial fulfillment of the requirements for the degree of

Doctor of Philosophy

Julianne H. Grose, Chair
Laura C. Bridgewater
David M. Thomson
K. Scott Weber

Department of Microbiology and Molecular Biology

Brigham Young University

ABSTRACT

Characterizing the Function of PAS kinase in Cellular Metabolism and

Neurodegenerative Disease

Jenny Adele Pape
Department of Microbiology and Molecular Biology, BYU
Doctor of Philosophy

PAS kinase 1 (Psk1) is a sensory protein kinase responsible for activating and deactivating many pathways in the cell. Dysregulation of PAS kinase can lead to a variety of diseases, ranging from obesity to cancer to neurodegenerative disease. Herein, we provide an in-depth analysis of two known interacting partners of PAS kinase, Centromere binding factor 1 (Cbf1) and poly(A)- binding protein binding protein 1 (Pbp1). PAS kinase phosphorylates Cbf1 inhibiting its function and decreasing respiration in yeast. In agreement, *CBF1*-deficient exhibit decreased respiration. Although the number of mitochondria is not altered by *CBF1*-deficiency, a mitochondrial proteomics analysis revealed an altered mitochondrial composition. Through beta-galactosidase assays and western blot, we showed direct transcriptional control of Atp3 (a subunit of the mitochondrial F_1-ATP synthase complex), and the yeast lipid genes Lac1 and Lag1 by Cbf1. Furthermore, we confirmed the human homolog of Cbf1, USF1, as a substrate of PAS kinase *in vitro* and provided the first evidence for the role of USF1 in respiration. Our model suggests that PAS kinase decreases respiration through the inhibition of Cbf1, partitioning glucose away from respiration and towards lipid synthesis. We expanded on the role of PAS kinase in glucose regulation through a mouse study including wild-type and PAS kinase deficient mice on either a normal chow or high-fat-high-sugar diet. Our results showed increased respiration in PAS kinase deficient males only on a normal chow diet. PAS kinase-deficiency was not shown to protect against weight gain when on a high-fat high-sugar diet, but it did significantly protect from liver triglyceride accumulation. Interestingly, females were protected from triglyceride accumulation regardless of genotype. This suggests that sex may be masking the effects of PAS kinase.

The second identified substrate of PAS kinase discussed is Pbp1. The human homolog of Pbp1 is ataxin-2, mutations in which are a known risk factor for amyotrophic lateral sclerosis (ALS). As diet and sex have been shown to be important factors regarding PAS kinase function, they also are strong contributing factors to ALS and are extensively reviewed herein. Pbp1 is known to be sequestered by PAS kinase under glucose depravation, and it can sequester additional proteins along with it to regulate different cellular pathways. To shed light on the pathways affected by Pbp1, we performed a yeast two-hybrid assay and mass spectrometry, identifying 32 novel interacting partners of Pbp1 (ataxin-2). We provide further analysis of the direct binding partner Ptc6, measuring mitophagy, mitochondrial content, colocalization, and respiration. This work elucidates novel molecular mechanisms behind the function of PAS kinase and yields valuable insights into the role of PAS kinase in disease.

Keywords: PAS kinase, Cbf1, USF1, respiration, glucose allocation, ALS, neurodegenerative, ataxin-2, Pbp1, stress granules, Ptc6, mitophagy

ACKNOWLEDGEMENTS

I would like to thank my mentor and friend, Julianne Grose. I am grateful for her time talking through experiments, reviewing my writing, and teaching me techniques in the lab. Her high standard for excellence has pushed me and challenged me throughout my education, making me a better scientist.

I would like to thank my graduate committee as well as other faculty I have had the opportunity to learn from. Thank you for always being willing to share your advice, encouragement, and criticism. I could not have succeeded without your help.

I would also like to thank my fellow lab members, both past and present. They have been there to troubleshoot with me when experiments fail and celebrate with me when I succeed. Thank you for keeping a positive atmosphere in our lab and making it feel like a home away from home.

I would like to thank my family and friends for their unwavering support. Thank you for your patience as I have tried to balance school and life. Thank you for always listening to me talk about my research and nodding along even if you don't get it. Finally, I would like to give a big thank you to my husband, Braden, for his love, support, and patience.

TABLE OF CONTENTS

LIST OF TABLES

LIST OF FIGURES

CHAPTER 1: PAS kinase Works through its Substrates to Regulate Metabolism and Neurodegenerative Disease

1.1 Introduction

A cells ability to appropriately sense and allocate nutrients in their environment is essential to the health of the cell. Without proper maintenance, metabolic disease such as diabetes, heart disease, and cancer may develop. Sensory protein kinases are key regulators of metabolic processes, with the ability to sense nutrients in the environment and respond by activating and deactivating many different pathways within the cell. By developing drugs that target specific protein kinases, it may be possible to restore healthy cellular pathways that have developed due to disease.

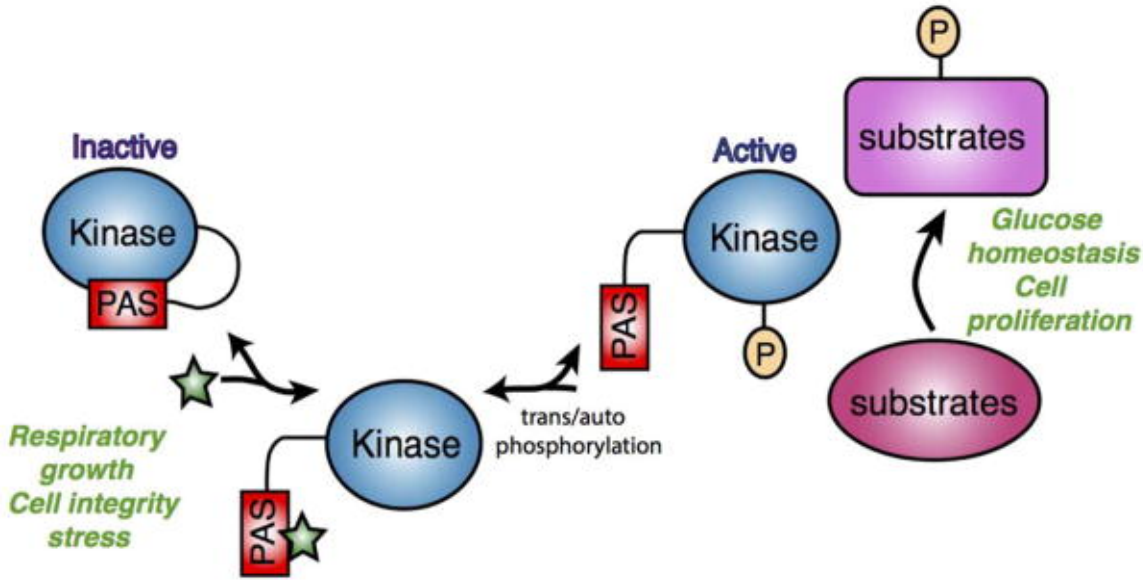

Figure 1.1 A model of PAS kinase activation and function [1].

The protein PAS (Per-Arnt-Sim) kinase is a nutrient sensory protein kinase that responds to glucose and regulates its allocation throughout the cell. PAS kinase contains both a serine/threonine catalytic kinase domain and a regulatory PAS (Per-ARNT-Sim) domain [2]. In the model for PAS kinase regulation and function, the N-terminal of the PAS domain binds and

inhibits the serine/threonine c-terminal kinase domain in cis. To activate the kinase, it is hypothesized that small metabolites bind to the PAS domain, releasing and thereby activating the catalytic kinase domain (Figure 1.1) [3]. This suggests that PAS kinase may work to modulate cellular growth based on nutrient availability.

PAS kinase is highly conserved between yeast, mice, and man. Initial studies in mice revealed no significant differences in development, growth or reproduction between wild-type (WT) and PAS kinase knockout (KO) mice. However, when placed on a high fat diet, PAS kinase knockout mice exhibited weight gain (Figure 1.2), increased triglyceride accumulation, glucose tolerance and insulin sensitivity comparable to their wild-type littermates. Each of these levels were significantly elevated in the wild-type mice on a high fat diet. [4].

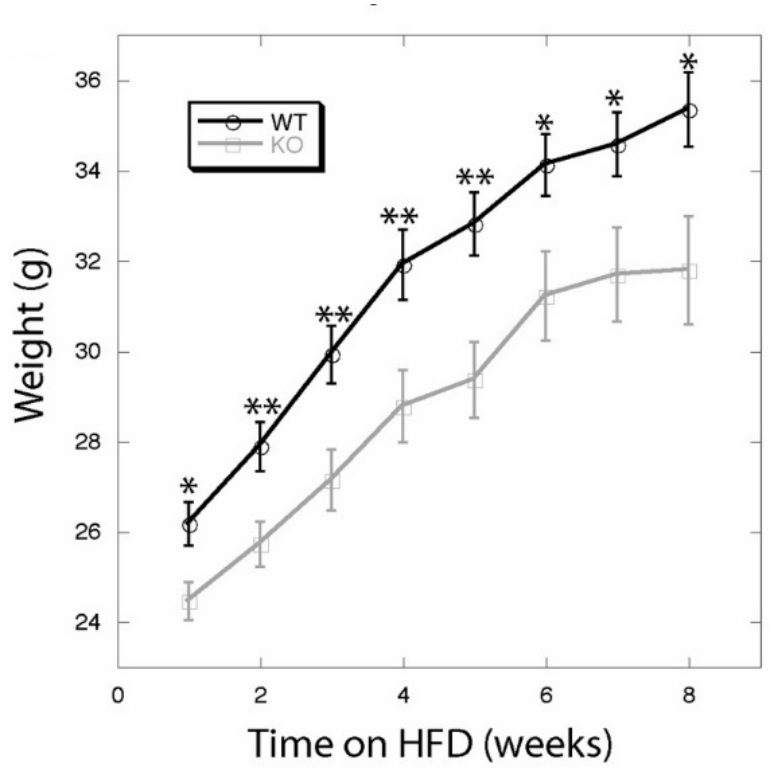

Figure 1.2 WT mice on a HFD gain significantly more weight than KO mice on a HFD [4].

Despite its importance, little is known about the molecular mechanisms of PAS kinase function including the substrates it acts on. Yeast two hybrid assays and co-purification were performed to better understand the specific molecular pathways being utilized by PAS kinase. These experiments revealed 93 putative binding partners of PAS kinase. Of these 93 partners, a remarkable 73% appeared to have a human homolog, whereas only 20-30% of the yeast proteome is reportedly conserved in humans [5]. This supports the evolutionary conservation of PAS kinase and its critical role in regulating central metabolic pathways. One protein of the two proteins that were collected from both the yeast two hybrid assay and co-purification was Pbp1. Pbp1 is a largely uncharacterized a poly(A)-binding protein (Pab1)-binding protein associated with stress granule formation. In-vitro kinase assays revealed PAS kinase dependent phosphorylation of Pbp1 as well as PAS kinase dependent phosphorylation of Pbp1's human homolog, Ataxin-2. Pbp1 is the yeast homolog of human ataxin-2 (Figure 1.3) [6].

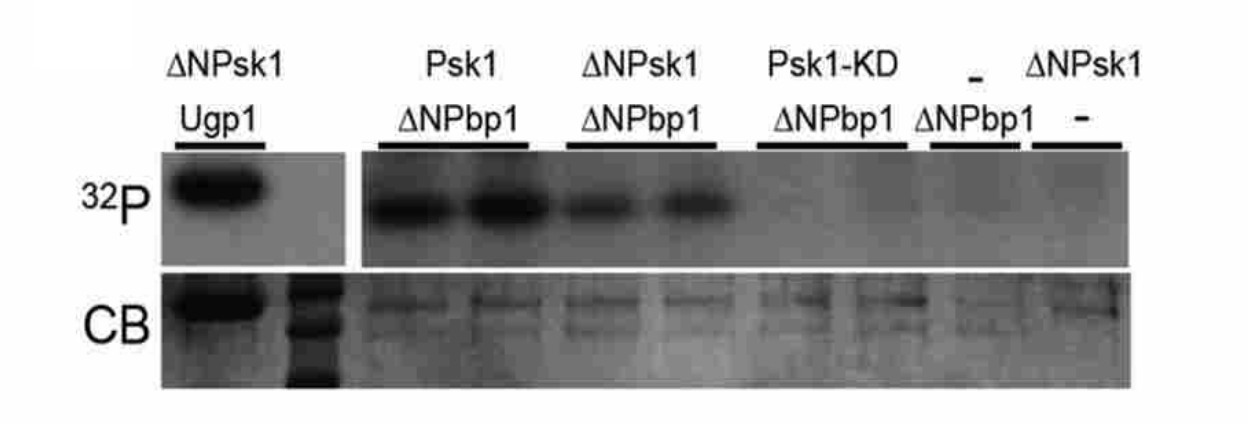

Figure 1.3 Evidence for direct phosphorylation of Pbp1 by PAS kinase [6].

In 2010, it was found that mutations in ataxin-2 significantly increased the risk for amyotrophic lateral sclerosis (ALS) [10]. ALS is a neurodegenerative disorder that causes muscle weakness, disability, and eventually fatal paralysis normally within 3-5 years of diagnosis. The etiology of the disease is still unknown, with only about 10% of ALS cases being

familial, the rest being sporadic [7]. Riluzole is the only drug has been developed and shown to have an impact on survival in ALS, yet it is still unclear how it works with ALS [8, 9]. Currently the mainstay treatment for ALS is symptomatic management through multidisciplinary care, such as respiratory management, counseling, pain management, and communication therapy [10]. It therefore is imperative to identify and understand disease related genes to develop effective treatment for ALS.

Ataxin-2 is thought to increase one's risk for ALS through its association with TAR DNA binding protein (TDP-43). [11]. TDP-43 has recently been identified as the major disease causing protein in ALS [12]. TDP-43 positive ubiquinated neuronal cytoplasmic inclusions have been found in the spinal motor neurons in 97% of all ALS cases [13]. It has been shown that lowering ataxin-2 levels in both yeast and flies will protect against TDP-43 aggregation and toxicity [11]. In TDP-43 transgenic mice, complete loss of ataxin-2 extended the survival of mice by over 80% (Figure 1.4) [13].

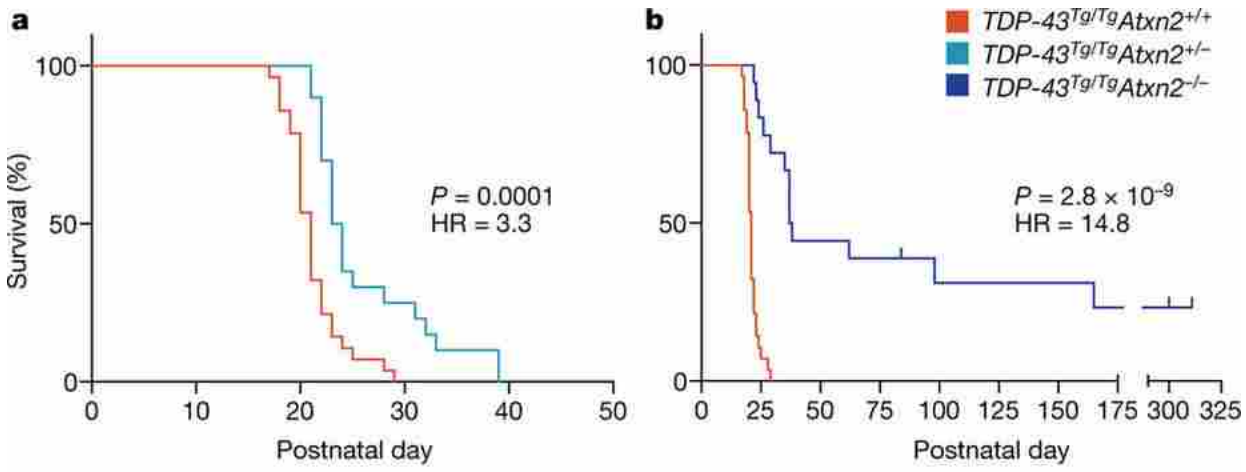

Figure 1.4 Reducing the level of ataxin-2 extends lifespan in TDP-43 transgenic mice [13].

As mentioned above, PAS kinase directly phosphorylates and activates the yeast ataxin-2 homolog, Pbp1 [6, 14] . Under normal conditions, PAS kinase causes overexpression of Pbp1 or ataxin-2 in yeast. However, PAS kinase deficiency decreases toxicity due to the inability to overexpress Pbp1. In addition, PAS kinase decreases the amount of Pbp1 and ataxin-2 localization to stress granules. Pbp1 and PAS kinase were recently shown to be required for the sequestration of the nutrient sensing TORC1 at stress granules in yeast and there is some evidence for this conservation of function in mammalian cells (Figure 1.5) [15]. TORC1 is a central regulator of cell growth and proliferation and is essential for cell survival. Together, these results suggest that PAS kinase inhibition may reduce the activity and/or levels of ataxin-2, and rescue TORC1 inhibition. PAS kinase could be an ideal target to lower levels of ataxin-2.

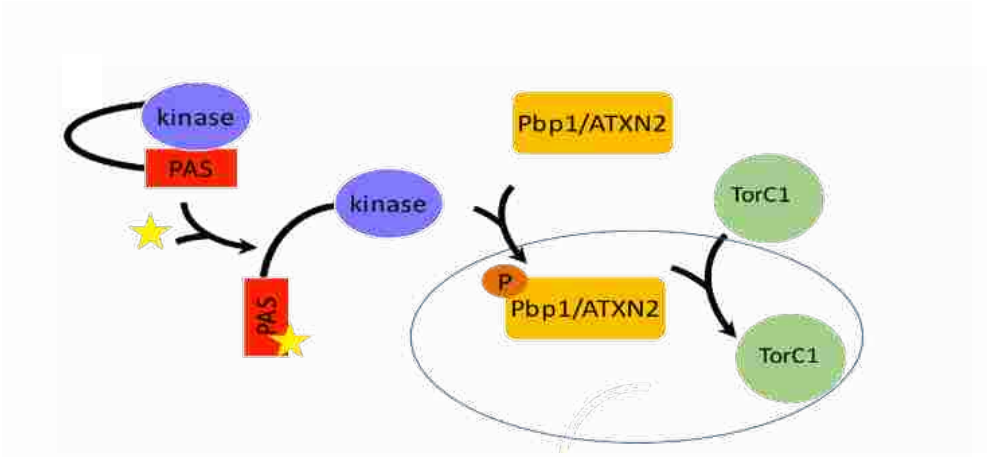

Figure 1.5 A model for PAS kinase dependent phosphorylation and activation of Pbp1/ataxin-2 which leads to inhibition of TORC1 through its sequestration at stress granules [6].

1.2 Summary of research chapters

Chapter 2 outlines our efforts to characterize a novel substrate of PAS kinase, Centromere binding factor 1 (Cbf1). We show that while PAS-kinase deficient yeast exhibit increased respiration, Cbf1-deficient yeast exhibit decreased respiration. We identify ATP3, a subunit of the mitochondrial F1-ATP synthase complex, as a contributing factor to the decrease

in respiration. We also discover a Cbf1 dependent regulation of Lac1 and Lag1, two genes involved in the synthesis of ceramides in yeast. Finally, we also show that the human homolog of Cbf1, Upstream transcription factor 1 (USF1), behaves similarly to Cbf1.

In Chapter 3 we provide further characterization of PAS kinase deficient mice. Typically, male mice are used to study PAS kinase as they present with more intense phenotypes. However, in our study we included both male and female mice, and while some phenotypes were similar, we saw many unexpected differences. In addition, our mice were put on either a normal chow (NC) diet or a high-fat high-sugar (HFHS) diet that more accurately reflects the Western Diet found in today's society. We show PAS kinase dependent changes in respiration via respiration, western blot, ATP assays, and weight analysis. In addition, we provide an in-depth hepatic triglyceride profiling that verifies PAS kinase deficiency can protect against triglyceride accumulation.

Chapter 4 is a review paper discussing how diet and metabolic health influence ALS risk, onset, progression, and survival time. In addition, we highlight various sex differences seen in ALS. PAS kinase has been shown to regulation Ataxin-2, a risk factor for ALS. Due to the sex-dependent changes reported in chapter 3, this review provides insight into how diet, metabolic health, and sex may influence molecular pathways in ALS and helps to understand how to better design experiments in ALS models in order to uncover novel phenotypes.

Chapter 5 is an unpublished study focused on identifying the interacting partners of Pbp1 as well as the characterization of an interacting partner, Ptc6, that regulates mitochondrial health in the cell.

REFERENCES

1. DeMille, D., et al. PAS kinase: A nutrient sensing regulator of glucose homeostasis. *IUBMB Life.* 2013. 65(11). p. 921-9.

2. Rutter, J., et al., PAS kinase: an evolutionarily conserved PAS domain-regulated serine/threonine kinase. Proc Natl Acad Sci U S A, 2001. 98(16): p. 8991-6.

3. Amezcua, C.A., et al., Structure and interactions of PAS kinase N-terminal PAS domain: model for intramolecular kinase regulation. Structure, 2002. 10(10): p. 1349-61.

4. Hao, H.X. and J. Rutter, The role of PAS kinase in regulating energy metabolism. IUBMB Life, 2008. 60(4): p. 204-9.

5. DeMille, D., et al., A comprehensive protein-protein interactome for yeast PAS kinase 1 reveals direct inhibition of respiration through the phosphorylation of Cbf1. Mol Biol Cell, 2014. 25(14): p. 2199-215.

6. DeMille, D., et al., PAS kinase is activated by direct SNF1-dependent phosphorylation and mediates inhibition of TORC1 through the phosphorylation and activation of Pbp1. Mol Biol Cell, 2015. 26(3): p. 569-82.12. Byrne, S., et al., Rate of familial amyotrophic lateral sclerosis: a systematic review and meta-analysis. J Neurol Neurosurg Psychiatry, 2011. 82(6): p. 623-7.

7. Miller, R.G., J.D. Mitchell, and D.H. Moore, Riluzole for amyotrophic lateral sclerosis (ALS)/motor neuron disease (MND). Cochrane Database Syst Rev, 2012(3): p. CD001447.

8. Kennel, P., et al., Riluzole prolongs survival and delays muscle strength deterioration in mice with progressive motor neuronopathy (pmn). J Neurol Sci, 2000. 180(1-2): p. 55-61.

9. Van den Berg, J.P., et al., Multidisciplinary ALS care improves quality of life in patients with ALS. Neurology, 2005. 65(8): p. 1264-1267.

10. Elden, A.C., et al., Ataxin-2 intermediate-length polyglutamine expansions are associated with increased risk for ALS. Nature, 2010. 466(7310): p. 1069-75.

11. Mackenzie, I.R.A. and R. Rademakers, The role of TDP-43 in amyotrophic lateral sclerosis and frontotemporal dementia. Current opinion in neurology, 2008. 21(6): p. 693-700.

12. Scotter, E.L., H.-J. Chen, and C.E. Shaw, TDP-43 Proteinopathy and ALS: Insights into Disease Mechanisms and Therapeutic Targets. Neurotherapeutics, 2015. 12(2): p. 352-363.

13. Becker, L.A., et al., Therapeutic reduction of ataxin-2 extends lifespan and reduces pathology in TDP-43 mice. Nature, 2017. 544(7650): p. 367-371.

14. Logroscino, G., Motor neuron disease: Are diabetes and amyotrophic lateral sclerosis related? Nat Rev Neurol, 2015. 11(9): p. 488-90.

15. Takahara, T. and T. Maeda, Transient sequestration of TORC1 into stress granules during heat stress. Mol Cell, 2012. 47(2): p. 242-52.

CHAPTER 2: The Regulation of Cbf1 by PAS kinase is a Pivotal Control Point for Lipogenesis vs. Respiration in Saccharomyces cerevisiae

The following chapter is taken from an article published in Genes, Genomics, and Genetics Journal. All content and figures have been formatted for this dissertation but it is otherwise unchanged.

2.1 Abstract

PAS kinase 1 (Psk1) is a key regulator of respiration in *Saccharomyces cerevisiae*. Herein the molecular mechanisms of this regulation are explored through the characterization of its substrate, Centromere binding factor 1 (Cbf1). *CBF1*-deficient yeast displayed a significant decrease in cellular respiration, while PAS kinase-deficient yeast, or yeast harboring a Cbf1 phosphosite mutant (T211A) displayed a significant increase. Transmission electron micrographs showed an increased number of mitochondria in PAS kinase-deficient yeast consistent with the increase in respiration. Although the *CBF1*-deficient yeast did not appear to have an altered number of mitochondria, a mitochondrial proteomics study revealed significant differences in the mitochondrial composition of *CBF1*-deficient yeast including altered Atp3 levels, a subunit of the mitochondrial F_1-ATP synthase complex. Both beta-galactosidase reporter assays and western blot analysis confirmed direct transcriptional control of *ATP3* by Cbf1. In addition, we confirmed the regulation of yeast lipid genes *LAC1* and *LAG1* by Cbf1. The human homolog of Cbf1, Upstream transcription factor 1 (USF1), is also known to be involved in lipid biogenesis. Herein, we provide the first evidence for a role of USF1 in respiration since it appeared to complement Cbf1 in vivo as determined by respiration phenotypes. In addition, we confirmed

USF1 as a substrate of human PAS kinase (hPASK) in vitro. Combined, our data supports a model in which Cbf1/USF1 functions to partition glucose towards respiration and away from lipid biogenesis, while PAS kinase inhibits respiration in part through the inhibition of Cbf1/USF1.

2.2 Introduction

Proper resource allocation is fundamental to the success of any system. In cellular organisms, it is crucial to sense available nutrients and astutely allocate them among several pathways including growth, storage and energy metabolism. If nutrients are not properly allocated, e.g. when too many nutrients are diverted to one pathway, it comes at the expense of another important pathway and often leads to diseases such as obesity, diabetes and cancer. One of the mechanisms that cells have evolved to help coordinate resource allocation are nutrient sensing protein kinases.

PAS kinase is a highly conserved sensory kinase with both a sensory PAS (Per-ARNT-Sim) domain and a serine/threonine kinase domain [1]. It is a key player in sensing and allocating glucose in eukaryotic cells (reviewed in [2-8]). Additionally, PAS kinase is activated both in yeast and mammalian cells under conditions that activate respiratory metabolism [9, 10]. This occurs in yeast when cells are grown on carbon sources other than glucose and in mammalian cells under conditions of high glucose.

PAS kinase is not only activated by respiratory conditions, but is also implicated in regulating respiratory metabolism itself. PAS kinase-deficient mice ($PASK^{-/-}$) have a hypermetabolic phenotype in that they consume more oxygen and give off more CO_2 and heat when placed on a high-fat diet [11]. In contrast, $PASK^{-/-}$ mice also accumulate significantly less hepatic lipids when placed on the high-fat diet and PAS kinase knockdown or inhibition also

decreases triglyceride in hepatic cell lines. These data suggest that PAS kinase is allocating glucose away from respiration towards lipid storage in wild type mice. However, the mechanisms behind these phenotypes are largely unknown. We recently identified a novel substrate of yeast PAS kinase 1 (Psk1), Centromere binding factor 1 (Cbf1), that could be an important player in the mechanisms behind these phenotypes [12].

Cbf1 is a general transcription factor conserved from yeast to man [13-15]. Its human homolog, Upstream transcription factor 1 (USF1), is a key regulator of genes involved in lipid homeostasis and USF1 mutations are strongly correlated with hyperlipidemia [16-20]. In yeast, transcriptome data suggests that Cbf1 regulates a wide variety of genes including those involved in respiration and lipid biogenesis, as well as amino acid biosynthesis [15, 21, 22]. We recently provided evidence for decreased respiration in *CBF1*-deficient yeast and for the PAS kinase-dependent phosphorylation and inhibition of Cbf1 [12]. The altered respiration observed in yeast lacking *CBF1* or PAS kinase may be due to many effects within the cell such as 1) effects on total mitochondrial mass or 2) electron transport chain expression or activity. Here we further characterized the mechanisms behind PAS kinase and Cbf1 respiratory function in yeast. Specifically, we report the differences observed in mitochondrial area between wild type, *CBF1*-deficient and PAS kinase-deficient yeast and present the mitochondrial proteomes of these yeast. In addition, we confirm the role of *CBF1* in regulating the yeast lipid genes *LAC1* and *LAG1* and provided evidence that they are downregulated by *CBF1* under the same conditions that *ATG3* is upregulated. Evidence is also provided for USF1 being a conserved PAS kinase substrate through in vitro kinase assays as well as yeast complementation assays. Combined, our data supports a model in which Cbf1/USF1 partitions glucose towards respiration at the expense of lipid biogenesis, while PAS kinase inhibits Cbf1/USF1 favoring lipid biogenesis.

2.3 Materials and methods

2.3.1 Growth assays and vector construction

A list of strains, plasmids and primers used in this study are provided in Table 2.1. All plasmids constructed for this study were made using standard polymerase chain reactions (PCR) followed by restriction digests using enzymes from New England Biolabs [23]. Human USF1 was PCR amplified using primers 3456/3457 from plasmid pCMV6-USF1 (OriGene, SC 1227700). *CBF1*-deficient yeast acquire suppressors at a rapid rate. Therefore, all cultures were streaked fresh from frozen and used as quickly as small colonies appeared.

Table 2.1 Strains, plasmids and primers used in this study

Strain	Background	Genotype	Abbreviation	a/α	Reference or source
JGY1	W303	*his3, leu2, lys2, met15, trp1, ura3*	WT	a	David Stillman, University of Utah
JGY4	W303	*psk1*::his3, *psk2*::kan-MX4, *leu2*, *lys2*, *met15*, *trp1*, *ura3*	*psk1psk2*	a	[9]
JGY43	BY4741	*his3-1, leu2-0, met15-0, ura3-0*	WT	a	[51]
JGY1227	BY4741	*cbf1*::kan-MX4*, his3-1, leu2-0, met15-0, ura3-0*	*cbf1*	a	[51]
JGY1244	BY4741	*psk1*::hph-MX4*, psk2*::nat-MX4*, his3-1, leu2-0, met15-0, ura3-0*	*psk1psk2*	a	This study
JGY1261	BY4741	*psk1*::hph-MX4*, psk2*::nat-MX4*, cbf1*::kan-MX4, *his3-1, leu2-0, met15-0, ura3-0*	*psk1psk2cbf1*	a	This study
JGY1348	BY4741	*psk1*::kan-MX4*, his3-1, leu2-0, met15-0, ura3-0*	*psk1*	a	[51]
JGY1349	BY4741	*psk2*::kan-MX4*, his3-1, leu2-0, met15-0, ura3-0*	*psk2*	a	[51]
JHG504	BL21DE3	F^- ompT hsdSB(rB^-mB^-) gal dcm (DE3)	BL21		Novagen

Plasmid	Gene	Description	Backbone	Yeast Origin	Selection	Reference or source
pJG121	EV	Empty pRS415 plasmid	pRS415	CEN	LEU	(Simons et al, 1987)
pJG173	*PSK2*	pGAL1-10-PSK2-HIS/HA	pRS426	2u	URA	(Grose et al., 2007)
pJG210	*UGP1*	Ugp1-HIS	pHIS-parallel		AMP	(Smith et al, 2007)
pJG725	EV	pAdh-myc	pRS416	CEN	URA	[12]
pJG858	PSK1	pGAL1-10-PSK1-HIS/HA	pRS426	2u	URA	(DeMille et al., 2014)
pJG1009	EV	pET15b with James Y2H MCS	pET15b		AMP	[12]
pJG1025	*IPP1*	*IPP1* into pET15b (pJG1009)	pET15b		AMP	[12]
pJG1031	*CBF1*	*CBF1* into pET15b	pET15b		AMP	[12]
pJG1232	*USF1*	USF1 in pCMV	pCMV6-XL5		AMP	OriGene
pJG1233	*USF1*	USF1 into pET15b	pET15b		AMP	This study
pJG1246	*USF1*	USF1 into pJG725	pRS415	CEN	URA	This study
pJG1314	*LACZ*	*LACZ* into pJG121	pRS415	CEN	LEU	This study
pJG1315	*ATP3*	*ATP3-LACZ*	pRS415	CEN	LEU	This study
pJG1316	*COX4*	*COX4-LACZ*	pRS415	CEN	LEU	This study
pJG1317	*HAP4*	*HAP4-LACZ*	pRS415	CEN	LEU	This study

pJG1318	*NDI1*	*NDI1-LACZ*	pRS415	CEN	LEU	This study
pJG1320	*QCR6*	*QCR6-LACZ*	pRS415	CEN	LEU	This study
pJG1321	*LAC1*	*LAC1-LACZ*	pRS415	CEN	LEU	This study
pJG1322	*LAG1*	*LAG1-LACZ*	pRS415	CEN	LEU	This study
pJG1335	*CBF1*	T211A-Cbf1 into pJG725	pRS416	CEN	URA	This study
pJG1336	*CBF1*	T212A-Cbf1 into pJG725	pRS416	CEN	URA	This study

Primer	Sequence
JG3440	GGCCTCGAGCATTTTCTGTCGCTCTTATGATCC
JG3441	GGCAAGCTTTGTCCACATAGCTCTTGTTTATTGA
JG3442	GGCCTCGAGCCTCTTGTCCATTATCTTCGGGA
JG3443	GGCAAGCTTTGATGTCATGTTGTCGTTATTTCTTC
JG3457	GGCCTCGAGGTTGCTGTCATTCTTGATGACG
JG3458	CGAATTCATGAAGGGGCAGCAGAAAACAGCTG
JG3652	GGCCTCGAGGTATAATGTACCTTTGTTCCCTACAC
JG3683	GGCAAGCTTATGACCATGATTACGGATTCACTGG
JG3684	GGCGGATCCTTTTTGACACCAGACCAACTGGTAATG
JG3669	GGCAAGCTTTAGAAAAGTCTTTGCGGTCATGATTC
JG3670	GGCCTCGAGTTTCATCAAGGACTAAAGTTTTCTTATG
JG3671	GGCAAGCTTTGATACAATTCTTGACAACATGACTAC
JG3672	GGCCTCGAGGGCAAGCTTGACCTTTACTTTCCTCTCTAAAAGCC
JG3673	GGCAAGCTTTTCCAACATGCCCATTTTCTATTTC
JG3674	GGCCTCGAGCGAACAGCACAAGACGCGTATCAC
JG3675	GGCAAGCTTTAGTGAAAGCATTGTGCTTGTTATC
JG3676	GGCCTCGAGGCGGATTCCAAAGGCGTCCTTC
JG3679	GGCAAGCTTCTTCGATAGCATAGTGGTTTTTAG
JG3680	GGCCTCGAGGACCGGCGCTACCCGGTTAAG
JG3741	GGCAAGCTT GATGTAGGGCATTACTTCTTTGATG
JG3799	GGAAGAAATGTTTATCACCAGATGGAGAACCAATGAGCGG
JG3800	CCGCTCATTGGTTCTCCATCTGGTGATAAACATTTCTTCC
JG3801	GTCGTATTATTGAGTCACCAGCTTTATTCCATGGCGGG
JG3802	CCCGCCATGGAATAAAGCTGGTGACTCAATAATACGAC

2.3.2 In vitro kinase assays

Full-length HIS-tagged yeast Psk1 (pJG858), Psk2 (pJG173) and Ugp1 (pJG210) proteins were purified from yeast (JGY4), while Cbf1 (pJG1031) and USF1 (pJG1233) proteins were from BL21DE3 *E. coli* (JHG504) as previously described [24] using Ni-NTA (Qiagen, Chatsworth, CA) chromotography. hPASK was expressed in Sf9 insect cells using the BAC-to-BAC baculovirus expression system (GIBCO/BRL) as previously described (Rutter et al. 2001) and purified using Ni-NTA (Qiagen, Chatsworth, CA) chromatography.

For yeast in vitro kinase assays, purified proteins were incubated with and without Psk1 in a 30 uL reaction containing 1x kinase buffer as previously described (DeMille et al., 2014). For in vitro kinase assays using purified USF1 and hPASK proteins, reactions were run similar to

the yeast proteins except for the following: 1 mM ATP was used and reactions were incubated for 30 minutes. Ipp1 (expressed from plasmid pJG1025) was purified similarly as Cbf1 and USF1, and was used as a negative control to show specificity of hPASK with USF1.

2.3.3 Mitochondrial respiration

Yeast strains not transformed with a plasmid (wild type (JGY43), *psk1psk2* (JGY1244), *psk1* (JGY1348) and *psk2* (JGY1349)) were grown in YPAD overnight, diluted 1:100 in YPAGly/EtOH and grown for 13 hours. Wild type yeast (JGY43) transformed with an empty vector (pJG725), or *CBF1*-deficient yeast (JGY1227) transformed with either empty vector (pJG725), wild type Cbf1 (pJG1125), T211A-Cbf1 (pJG1335), T212A-Cbf1 (pJG1336), or USF1 (pJG1246) were grown in selective SD-Ura media until saturated, diluted 1:100 in SGly/EtOH-Ura and grown an additional 24-26 hours. The OD600 was taken to ensure equal growth among strains. In experiments requiring the *CBF1*-deficient yeast, yeast were freshly streaked from the freezer 48 hours prior to use to avoid selection of suppressors which were commonly seen. High-resolution O_2 consumption was determined at 37˚C using the Oroboros O_2K Oxygraph (Innsbruck, Austria). Samples were centrifuged at 5000 x g for 5 min and resuspended in warm mitochondrial respiration buffer 05 (MiR05; 0.5 mM EGTA, 10 mM KH2PO4, 3 mM MgCl2-6 H2O, 60 mM K-lactobionate, 20 mM HEPES, 110 mM sucrose, 1 mg/ml fatty acid free BSA, pH 7.1). After addition of sample, the chambers were hyperoxygenated to ~350 nmol/ml. Following this, routine respiration was determined by measuring O_2 consumption in the absence of any substrate (routine). Next, EtOH was added and then the uncoupler carbonyl cyanide p-(trifluoromethoxy)phenylhydrazone (FCCP; 70 μM) as a measure of maximal electron transport system capacity (E). Finally, respiration was inhibited by the addition of the cytochrome c oxidase inhibitor, azide (20 mM) eliciting a state of residual

oxygen consumption (ROX), which provided a control for all values. Samples were run in triplicate and averaged.

2.3.4 TEM imaging

Wild type (JGY43), *cbf1* (JGY1227) and *psk1psk2* (JGY1244) yeast were grown overnight in YPAD then diluted into YPAraffinose and grown until OD600 ~0.5. Cell size was measured using a Moxi Flow micro cytometer (ORFLO Technologies, Hailey, ID). Permanganate fixation protocol described by Perkins and McCaffery (Perkins and McCaffery, 2007) was followed. Samples were sectioned at 80 nm using a RMC MTX ultramicrotome with a diamond knife then post stained with Reynold's Lead Citrate for 10 min. Cells were observed in a Tecnai T-12 transmission electron microscope and images recorded digitally. Mitochondrial quantification was determined using AxioVision Rel 4.8 Software (Zeiss) as described by Braun et al. (Braun et al., 2006). Each strain was examined in duplicate with wild type n=74, *cbf1* n=73, *psk1psk2* n=69 images total per yeast strain obtained with the following criteria: 1. the image of the cell must be at least 3 um across to ensure the slice included a majority of the cell 2. the cell image must bear a visible nucleus 3. the cell image must appear to have an intact cell wall and 4. the cell image must be fairly uniform in shape to exclude cells that are budding.

2.3.5 Mitochondrial isolation

Wild type (JGY 43), *cbf1* (JGY1227) and *psk1psk2* (JGY1244) yeast were grown in triplicate overnight in YPAD, diluted 1:100 into YPAGly/EtOH, and grown until OD600 ~1.0-2.0. Preparation of Isolated Mitochondria by Differenting Centrifugation (Diekert et al., 2001) was followed with the exception of Lyticase (Sigma) being used in place of Zymolase. Mitochondria were quantified using the Bradford assay. For mass spectrometry analysis, 10 uL of sample were diluted with 6X SDS sample buffer to a final concentration of 1X, and samples

were separated on 12% SDS-PAGE until the loading dye had migrated approximately 1 cm. Bands were then obtained using a razor blade, and submitted to the UCSD Biomolecular and Proteomics Mass Spectrometry Facility for in-gel digestion and mass spectrometry analysis. One sample from JGY1227 failed to give data and was resubmitted for mass spectrometry analysis in solution (without being run on SDS-PAGE).

2.3.6 In gel digest of MS samples

Gel slices were cut to 1 mm by 1 mm cubes and destained 3 times by first washing with 100 ul of 100 mM ammonium bicarbonate for 15 minutes, followed by addition of the same volume of acetonitrile (ACN) for 15 minutes [25]. The supernatant was removed and samples were dried in a speedvac. Samples were then reduced by mixing with 200 µl of 100 mM ammonium bicarbonate-10 mM DTT and incubated at 56°C for 30 minutes. The liquid was removed and 200 ul of 100 mM ammonium bicarbonate-55 mM *iodoacetamide* was added to gel pieces and incubated at room temperature in the dark for 20 minutes. After the removal of the supernatant and one wash with 100 mM ammonium bicarbonate for 15 minutes, the same volume of ACN was added to dehydrate the gel pieces. The solution was then removed and samples were dried in a speedvac. For digestion, enough solution of ice-cold trypsin (0.01 ug/ul) in 50 mM ammonium bicarbonate was added to cover the gel pieces and set on ice for 30 min. After complete rehydration, the excess trypsin solution was removed, replaced with fresh 50 mM ammonium bicarbonate, and left overnight at 37°C. The peptides were extracted twice by the addition of 50 µl of 0.2% formic acid and 5% ACN and vortex mixing at room temperature for 30 min. The supernatant was removed and saved. A total of 50 µl of 50% ACN-0.2% formic acid was added to the sample, which was vortexed again at room temperature for 30 min. The supernatant was removed and combined with the supernatant from the first extraction. The

combined extractions were analyzed directly by liquid chromatography (LC) in combination with tandem mass spectroscopy (MS/MS) using electrospray ionization.

2.3.7 Preparation of MS samples in solution

Protein samples were diluted in TNE (50 mM Tris pH 8.0, 100 mM NaCl, 1 mM EDTA) buffer. RapiGest SF reagent (Waters Corp.) was added to the mix to a final concentration of 0.1% and samples were boiled for 5 min. TCEP (Tris (2-carboxyethyl) phosphine) was added to 1 mM (final concentration) and the samples were incubated at 37°C for 30 min. Subsequently, the samples were carboxymethylated with 0.5 mg/ml of iodoacetamide for 30 min at 37°C followed by neutralization with 2 mM TCEP (final concentration). Proteins samples prepared as above were digested with trypsin (trypsin:protein ratio - 1:50) overnight at 37°C. RapiGest was degraded and removed by treating the samples with 250 mM HCl at 37°C for 1 h followed by centrifugation at 14000 rpm for 30 min at 4°C. The soluble fraction was then added to a new tube and the peptides were extracted and desalted using C18 desalting columns (Thermo Scientific, PI-87782) [25-27].

2.3.8 LC-MS/MS analysis

Trypsin-digested peptides were analyzed by ultra high pressure liquid chromatography (UPLC) coupled with tandem mass spectroscopy (LC-MS/MS) using nano-spray ionization. The nano-spray ionization experiments were performed using a TripleTof 5600 hybrid mass spectrometer (ABSCIEX) interfaced with nano-scale reversed-phase UPLC (Waters corporation nano ACQUITY) using a 20 cm-75 micron ID glass capillary packed with 2.5-µm C18 [130] CSH^{TM} beads (Waters corporation). Peptides were eluted from the C18 column into the mass spectrometer using a linear gradient (5–80%) of ACN (Acetonitrile) at a flow rate of 250 µl/min for 1 h. The buffers used to create the ACN gradient were: Buffer A (98% H_2O, 2% ACN, 0.1%

formic acid, and 0.005% TFA) and Buffer B (100% ACN, 0.1% formic acid, and 0.005% TFA). MS/MS data were acquired in a data-dependent manner in which the MS1 data was acquired for 250 ms at m/z of 400 to 1250 Da and the MS/MS data was acquired from m/z of 50 to 2,000 Da. The Independent data acquisition (IDA) parameters were as follows; MS1-TOF acquisition time of 250 milliseconds, followed by 50 MS2 events of 48 milliseconds acquisition time for each event. The threshold to trigger MS2 event was set to 150 counts when the ion had the charge state +2, +3 and +4. The ion exclusion time was set to 4 seconds. Finally, the collected data were analyzed using Protein Pilot 4.5 (ABSCIEX) for peptide identifications for in gel samples, or Protein Pilot 5.0 (ABSCIEX) for the single sample submitted in solution.

2.3.9 Mitochondrial protein western blot

Mitochondria was isolated from wild type (JGY 43), *cbf1* (JGY1227) and *psk1psk2* (JGY1244) yeast using the same method listed previously. Protein concentration was determined using the Bradford protein assay. An equal amount of protein was loaded to each well of a 10% SDS-PAGE gel, separated, then transferred onto a nitrocellulose membrane. After incubation with 5% nonfat milk in TBST, the membrane was washed two times with TBS and probed with the selected antibody: Atp3 (the gamma subunit of the F_1 sector of the F_0F_1ATP synthase, 1:5000, Invitrogen), Qcr7 (Subunit 7 of ubiquinol cytochrome-c reductase, complex III, 1:5000, a generous gift from Dr. Martin Ott, (Gruschke S., et al., 2012)), Cox13 (Subunit VIa of cytochrome c oxidase, complex IV, 1:1000, a generous gift from Dr. Martin Ott, unpublished), and porin (1:5000, Abcam). Membranes were washed two times with TBST and once with TBS then incubated with a 1:1000 dilution of horseradish peroxidase-conjugated anti-mouse or anti-rabbit antibodies for 2 hours. Blots were rinsed and then developed using the WesternBright ECL kit (Advansta Inc) according to the manufacturer's protocol. Each blot was stripped by

washing the blot in Amresco gentle-review stripping buffer for 30 minutes and probed a second time with a different antibody following the steps listed above. We ensured data was collected for each antibody on both a fresh blot and a stripped blot, except for Atp3 which was only done on a fresh blot due to sensitivity to the stripping buffer. Each biological replicate (n=≥4) was run in duplicate as a technical control. Bands were quantified using the ImageJ software.

2.3.10 ß-galactosidase reporter assays

A LacZ reporter plasmid (pJG1314) was constructed by amplifying LacZ from BL21DE3 *E. coli* with primers JG3683 and JG3684, digesting with HindIII/BamHI and ligating into a similarly digested pRS415 vector (pJG121). Promoter regions (*LAC1* (JG3440/JG3441), *LAG1* (JG3442/JG3443), *ATP3* (JG3671/JG3672), *COX4* (JG3675/JG3676), *HAP4* (JG3669/JG3670), *NDI1* (JG3679/JG3680), and *QCR6* (JG3673/JG3674)) were amplified from wild type yeast template (JGY43) and cloned into the XhoI/HindIII sites of pJG1314. Yeast strains (wild type (JGY43), *cbf1* (JGY1227) *psk1psk2* (JGY1244) and *psk1psk2cbf1* (JGY1261)) were transformed with LacZ fusion plasmids containing each promoter region (pJG1321, (p*LAC1*-LacZ), pJG1322 (p*LAG1*-LacZ), pJG1315 (p*ATP3*-LacZ), pJG1316 (*pCOX4*-LacZ), pJG1317 (p*HAP4*-LacZ), pJG1318 (p*NDI1*-LacZ), pJG1320 (p*QCR6*-LacZ), grown in selective SD-Leu media for 2 days, diluted 1:50 in fresh media and grown until OD600 ~0.5-1.0. ß-galactosidase assays were performed as previously described by Stebbins and Triezenberg (Stebbins et al, 2004). Cell extracts were normalized by the Bradford assay to ensure equal amounts of total protein were used. Each strain was analyzed six times and averages were determined.

2.3.11 Gel shift assays

Promoter regions for *LAC1 (*JG3440/JG3441), *LAG1* (JG3442/JG3443), *ATP3* (JG3671/JG3672), and *PSK1* (JG3741/JG3652) were PCR amplified from wild type yeast

template (JGY43). *ATP3** and *PSK1** promoter binding mutants were made by site-directed mutagenesis at the Cbf1 binding site using oligos JG3799/JG3800 (*ATP3**) and JG3801/JG3802 (*PSK1*)* and were PCR amplified. Reaction mixes (20 ul) contained the PCR amplified promoter region, either 0 ul, 3 ng, or 6 ng of purified Cbf1 protein, and gel shift binding buffer (10 mM tris (pH 7.4), 1 mM EDTA, 50 mM KCl). Reaction mixes were incubated at room temperature for 20 minutes and analyzed by electrophoresis using 2% agarose gels.

2.3.12 ATP assays

Wild type (JGY43), *cbf1* (JGY1227) and *psk1psk2* (JGY1244) yeast were grown overnight in YPAD at 30°C, then shifted to room temperature for 24 hours (to avoid suppressor accumulation in the *cbf1* strain through prolonged growth at 30°C) before dilution 1:50 into fresh YPAD and grown for 2 hours. Cultures were then centrifuged and resuspended in 5 mL YPA-Glycerol/EtOH and grown until OD600 ~0.3-0.5, about 4 hours. ATP was then measured using the Promega Bac-titer Glo bioluminescent assay. A standard was generated using a known concentration of ATP provided in the kit. ATP levels were normalized to viable cell counts by plating diluted cells on YPAD.

2.3.13 ROS assays

Flow cytometry was utilized to quantify the total intracellular reactive oxygen species (cell-ROS) and mitochondrial total reactive oxygen species (mit-ROS) adapted from (Perez et al., 2014). The oxidant sensitive, cell permeant fluorescent probes H_2DCFDA(Invitrogen) and dihydrohodamine 123 (DHR123, Invitrogen) were used to measure cell-ROS and mit-ROS respectively. Strains were grown in 2% YPAD overnight and then diluted 1:50 in YPAraffinose and grown for 4 hours. Samples were aliquoted and immediately, loaded with either H_2DCFDA or DHR123 and incubated at 30˚C for 2 hours in the dark. Cells were then diluted with PBS

buffer and immediately quantified by flow cytometry. The fluorescence was monitored in the emission fluorescence channel FL1. The populations of cells were gated in the forward scatter and side scatter dot plots to eliminate dead cells and cellular debris. Flowjo analytical software was used in order to quantify ROS levels between the strains.

2.3.14 Respiration plate assays

Wild type yeast transformed with an empty vector (pJG725) or *cbf1* yeast (JGY1227) transformed with plasmids containing wild type Cbf1 (pJG1125), the empty vector, or USF1 (pJG1246) were grown 2 days in SD-Ura liquid media. Cultures were serially diluted (1/10) in water and spotted to both selective synthetic glycerol/EtOH, raffinose, or glucose plates (control) and incubated for 2-3 days at 30˚C.

2.4 Results

2.4.1 Psk1 inhibits respiration through phosphorylation of Cbf1 at T211

In our recent publication, the combination of threonines 211 and 212 of Cbf1 were important for Psk1 phosphorylation and inhibition of respiration [12]. We further investigated each of these two sites individually (T211A and T212A) through in vitro kinase assays. Mutation of the T211 site dramatically reduced the ability of Psk1 to phosphorylate Cbf1, suggesting that it is the critical site for Psk1 phosphorylation (Figure 2.1A). Additionally, *CBF1*-deficient yeast transformed with the T211A mutant displayed a higher respiratory rate in vivo compared to both wild type *CBF1* and the T212A phosphomutant (Figure 2.1B). Both phosphomimetic forms of T211 (T211D and T211E) were not significantly different from the controls (data not shown), suggesting that the phosphomimetic mutations do not mimic Psk1 phosphorylation. The phosphomimetic form of UDP-glucose pyrophosphorylase (Ugp1), a well-characterized substrate of yeast PAS kinase, also did not mimic phospho-Ugp1 [7].

2.4.2 Evidence for respiratory control as a specialized function of PAS kinase 1 (Psk1)

In budding yeast there are two orthologs of PAS kinase, Psk1 and Psk2 [1], which have high sequence similarity and are partially redundant in function [28]. Many duplicated genes arose from a whole genome duplication event that occurred in an early ancestor of yeast [29-33]. From this, duplicated proteins either gained accessory functions allowing for their selection and maintenance, or were selected against and lost. The conservation of both Psk1 and Psk2 suggests differential functions for these proteins, however, both proteins phosphorylate the well-characterized substrate Ugp1 (Smith et al., 2017). To test whether Cbf1 is a substrate of both Psk1 and Psk2, in vitro kinase assays were performed (Figure 2.1C). Only weak phosphorylation of wild type Cbf1 by Psk2 was observed (lower band) suggesting that Psk1 is the major intracellular regulator of Cbf1. Note that Psk1and Psk2 autophosphorylation was observed (upper ^{32}P bands) and Psk2-dependent phosphorylation of Ugp1 (its known substrate) was observed, indicating that the Psk2 protein was active. No phosphorylation of Cbf1 was seen previously when using the kinase dead mutant of PAS kinase as control (Demille *et al.,* 2014).

In vitro kinase assays, however, can be artifactual due to misfolded protein, the presence of protein contaminants, differential activities due to purification artifacts etc, making in vivo assays for Psk2 respiratory function a necessary verification (Figure 2.1D). We recently showed that *PSK1PSK2*-deficient yeast have an increased respiration rate, while *CBF1*-deficient yeast display a significant decrease when compared to wild type yeast [12]. To determine whether this respiratory control is a specialized function of Psk1, we assayed respiration rates in the individual mutant yeast (*psk1* and *psk2*) compared to wild type and the double mutant (*psk1psk2*) (Figure 2.1D). Both *psk1psk2* and *psk1* yeast had significantly higher maximal respiration rates (respiration in the presence of the uncoupler FCCP) compared to wild type. There was no

significant difference between *psk2* and wild type yeast. These in vivo results are consistent with the apparent decrease of Psk2 protein under respiratory conditions [9] as well as the decreased in vitro phosphorylation of Cbf1 by Psk2 (Figure 2.1C), and support Psk1 as the primary ortholog responsible for regulating respiration in yeast.

2.4.3 PAS kinase-deficient yeast have increased mitochondrial area

The observed effects on respiration could be due to several different alterations in the cell including changes in mitochondrial mass. To test the hypothesis that PAS kinase decreases respiration by down-regulating mitochondrial biogenesis pathways, mitochondria were viewed by transmission electron microscopy and both the number and total area of mitochondria were quantified in wild type, *cbf1* and *psk1psk2* yeast (Figure 2.1E & 2.1F). *PSK1PSK2*-deficient yeast showed a significant increase in both the number of mitochondria per cell as well as average mitochondrial area per total cell. These PAS kinase effects are consistent with the respiration phenotype; however, Cbf1 only trended towards a decreased number of mitochondria per cell without reaching significance. Thus, PAS kinase appeared to affect respiration by additional Cbf1-independent pathways in both the assays for mitochondrial area and the respiration assays (Figure 2.1D & 2.1F, and DeMille et al., 2014).

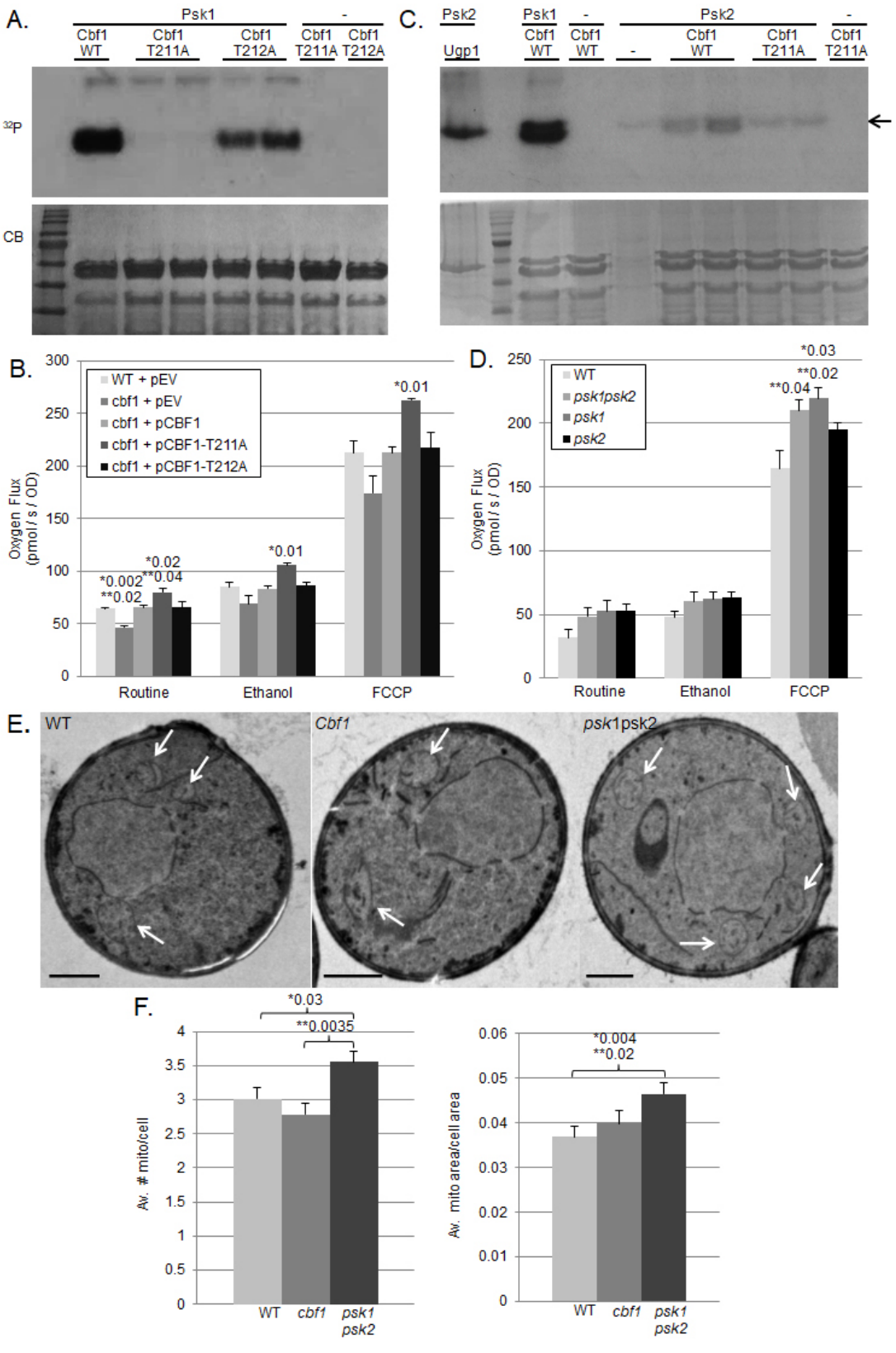
A.
Psk1
Cbf1 WT
Cbf1 T211A
Cbf1 T212A
-
Cbf1 T211A
Cbf1 T212A
32P
CB
C.
Psk2
Ugp1
Psk1
Cbf1 WT
-
Cbf1 WT
Psk2
-
Cbf1 WT
Cbf1 T211A
-
Cbf1 T211A
B.
WT + pEV
cbf1 + pEV
cbf1 + pCBF1
cbf1 + pCBF1-T211A
cbf1 + pCBF1-T212A
Oxygen Flux (pmol / s / OD)
*0.002
**0.02
*0.02
**0.04
*0.01
*0.01
Routine
Ethanol
FCCP
D.
WT
psk1psk2
psk1
psk2
Oxygen Flux (pmol / s / OD)
*0.03
**0.02
**0.04
Routine
Ethanol
FCCP
E.
WT
Cbf1
psk1psk2
F.
*0.03
**0.0035
Av. # mito/cell
WT
cbf1
psk1 psk2
*0.004
**0.02
Av. mito area/cell area
WT
cbf1
psk1 psk2

Figure 2.1 Psk1-dependent phosphorylation of Cbf1 at T211 controlled respiration. (A & C) In vitro kinase assays using purified Psk1 or Psk2, and Cbf1 wild type (WT) or mutant proteins incubated with radiolabeled-ATP. Ugp1 was a positive Psk2 control and Cbf1 purification yielded two bands visible in the Coomassie Brilliant Blue (CB) panel. Kinase reactions were separated by SDS PAGE, stained CB and imaged using autoradiography (32P). Black arrow in C indicates Cbf1. (B) WT or CBF1-deficient (cbf1) yeast transformed with indicated plasmids were grown in S-glycerol/EtOH media and respiration rates measured using an Oroboros O2K Oxygraph. Routine respiration was measured, then ethanol added, and finally, an uncoupler (FCCP) was added to represent maximal respiration. (D) WT, psk1psk2, psk1 or psk2 yeast were grown in YPAglycerol/EtOH and respiration measured as in B. (E) Representative pictures from transmission electron microscopy of WT, cbf1 and PAS kinase-deficient (psk1psk2) yeast. Each yeast strain was grown in duplicate, fixed with permanganate (Perkins and McCaffery, 2007), stained with Reynold's Lead Citrate, then observed in a Technai T-12 transmission electron microscope. White arrows indicate mitochondria. Scale bars= 1uM. (F) quantification of electron micrographs was determined using AxioVision Software (74 images were used for WT, 73 for cbf1, and 69 for psk1psk2). Error bars represent SEM. Significant p-values of data analyzed using pair wise Student's T-Test(*) and one-way analysis of variance (ANOVA) with Tukey's HSD post hoc test (**) are shown.

2.4.4 Mass spectrometry reveals a dramatically altered mitochondrial proteome in *CBF1*-deficient yeast

The fact that there was no obvious, statistical difference between mitochondrial number or area in the wild type and *CBF1*-deficient yeast suggests other mechanisms of respiratory regulation**.** In order to assess the major differences in the mitochondrial proteome of *CBF1*-deficient yeast, mitochondria were purified from wild type, *CBF1*-deficient, and *PSK1PSK2*-deficient yeast in triplicate, and subjected to analysis by mass spectrometry (see supplementary data 1 files for all total proteins retrieved). Surprisingly, although no difference in mitochondrial area was seen on a per cell basis when assessed by electron microscopy, the total amount of mitochondrial protein harvested per 0.5 liter yeast cultures was greatly reduced, consistent with the previously observed growth defects on respiratory carbon sources [12]. In fact, normalizing to total cells using a flow cytometer appeared not to control for this difference because the *CBF1*-deficient yeast culture contains a large proportion of alive but very sick yeast. That is, when *CBF1*-deficient and wild type yeast are grown in glycerol/ETOH for six hours, normalized by OD600 and then plated on YPAD, at 48 hours there is huge decrease in *CBF1*-deficient colonies that arise. Thus, the 'sick' *CBF1*-deficient yeast may have more fragile mitochondria.

This led to decreased detection of mitochondrial proteins in the *CBF1*-deficient samples when assessed by mass spectrometry, with the total number of proteins detected for wild type yeast (598+/-30.6 proteins) and *PSK1PSK2*-deficient yeast (580 +/- 62.4 proteins) being over seven times that from the *CBF1*-deficient yeast (79.7 +/- 11.5 proteins). Thus, a direct comparison of the total proteins retrieved from the three strains is hampered by the lower yield (the *CBF1*-deficient yeast lacked a majority of the mitochondrial proteins detected in the wild type and *PSK1PSK2*-deficient samples). To try to compensate for this discrepancy, we matched the number of proteins retrieved from the wild type and *PSK1PSK2*-deficient yeast directly to the *CBF1*-deficient yeast by comparing the same number of total proteins from the wild type and *PSK1PSK2*-deficient yeast (proteins were chosen starting with the highest confidence proteins until the same number of proteins were retrieved). This approach revealed several key differences between the strains. Although there are 51 proteins common to all three strains (42 of which are directly involved in respiration, Table 2S.1), there are 50 additional proteins (26 directly involved in respiration) common to both the wild type and *PSK1PSK2*-deficient yeast that are not found in the *CBF1*-deficient yeast (this analysis is provided in Table 2S.1).

Volcano plots were also used to analyze the mass spectrometry data by plotting the ANOVA p-value and log2(ratio) of the fold difference of all proteins retrieved (Figure 2.2A). Forty-three proteins were identified as significantly different between the samples and their changes are presented as a heat map in Fig. 2.2B. Of these 43 proteins, five were TCA cycle enzymes (Cit1, Idh1, Kdg1, Fum1 and Mdh1), two were ATP synthase Subunits (Atp3 and Atp15), several are mitochondrial transporters of small molecules (such as Ald4, Mcy1, Pda1, Lpd1), and two are involved in mitochondrial protein import (Tim44 and Ssc1). There were also several involved in the maintenance of mitochondrial DNA and reactive oxygen species (ROS)

production and defense. The porin (Por1) protein, often used as an indication of total mitochondria, was also selectively reduced. In addition to these classic mitochondrial proteins, several glycolytic enzymes as well as enzymes known to associate with the outer mitochondrial membrane were found. A few enzymes associated with the peroxisome, cytosolic ER and nucleus were also reported. A figure representing the location, and in some cases the function, of each of these 43 hits is provided in Fig. 2.2C. Of the 43 proteins, 40 appeared to have increased expression in the wild type versus *CBF1*-deficient yeast (they are decreased in the knockout strain), while three appeared to have decreased expression.

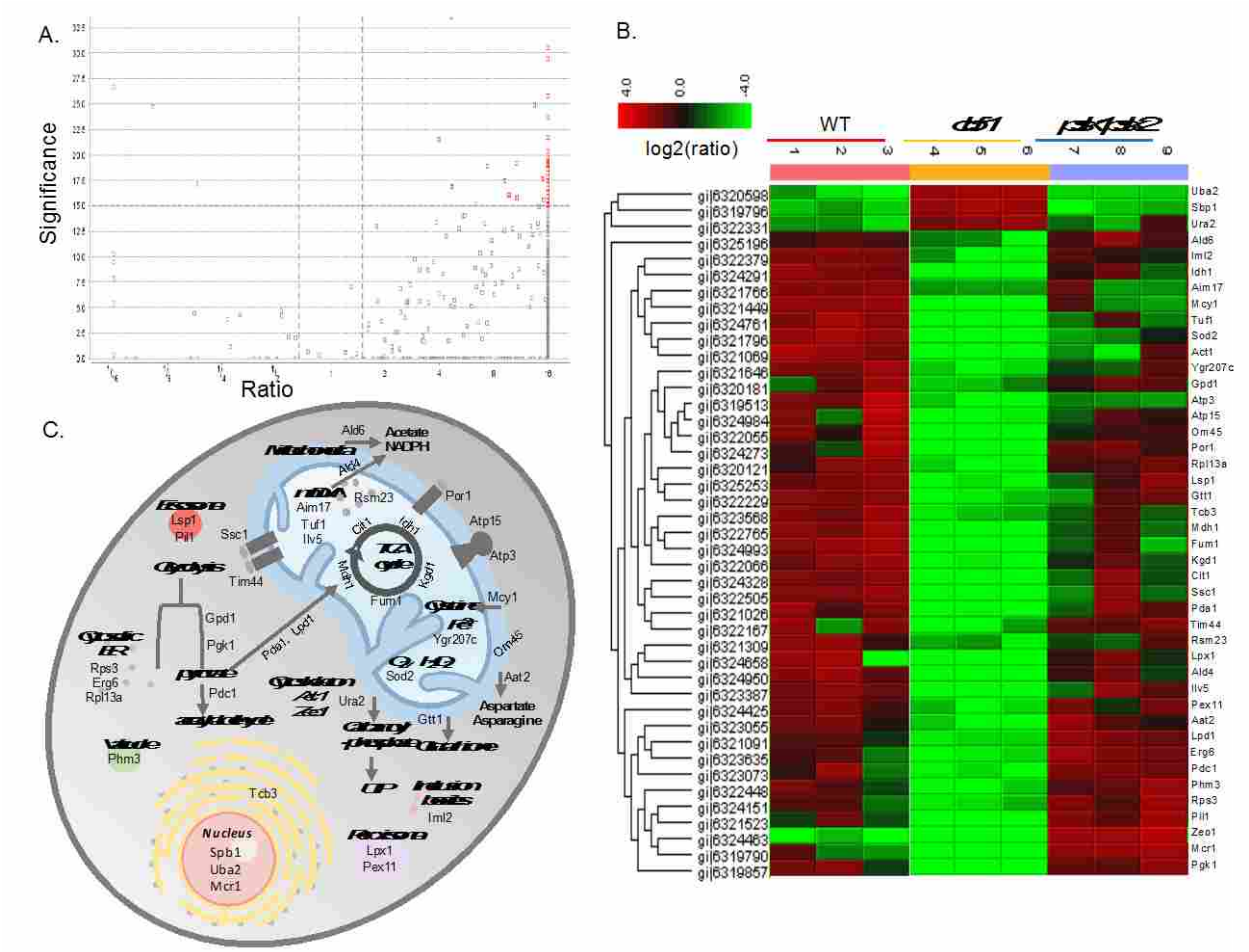

Figure 2.2 Comparison of the mitochondrial proteomes from WT, *cbf1* and *psk1psk2* yeast by mass spectrometry revealed 43 proteins with significantly altered expression (A) Volcano plot identified 43 proteins whose peptides were significantly different when quantified by LC-MS/MS of purified mitochondria extracted from three independent samples of wild type (WT), *CBF1*-deficient (*cbf1*) and PAS kinase-deficient (*psk1psk2*) yeast grown in S-glycerol/EtOH media. Significance determined by ANOVA is provided on the y-axis, while log2(ratio) is given on the x-axis of the volcano plot. (B) A heat map of the 43 proteins with the protein sequence GI number provided on the left and the *S. cerevisiae* common protein name provided on the right. C) A figure representing the cellular location, and in some cases the function, of each of these 43 significantly altered proteins. Function and cellular localization were obtained from the *Saccharyomyces* Genome Database.

Combined with the electron microscopy results, these results suggest that the respiration defect observed in *CBF1*-deficient yeast is in specific enzymes (such the TCA cycle and ATP synthase subunits) rather than in an equal reduction of total mitochondrial proteins. To verify these findings, we performed western blot analysis of several common mitochondrial proteins and compared this to the levels of Atp3 (the gamma subunit of the F_1 sector of the F_0F_1ATP synthase) and the porin protein, both predicted to have decreased expression from the mass spectrometry analysis. The western blot was normalized to total mitochondrial protein because mass spectrometry revealed many differences in proteins commonly used for normalization (such as porin). For each strain, the mitochondria was isolated (n>=4 independent isolations), total protein was quantified and the same amount of total protein was analyzed in technical duplicates to check loading. The Atp3 and porin protein levels appeared significantly reduced while electron transport proteins ubiquinol cytochrome-c reductase (Complex III) subunit 7 (Qcr7) and cytochrome c oxidase subunit VIa (Cox13) were not significantly altered (Figure 2.3). These results are consistent with the mass spectrometry analysis and suggest altered mitochondrial function rather than proportional reduction in mitochondrial area.

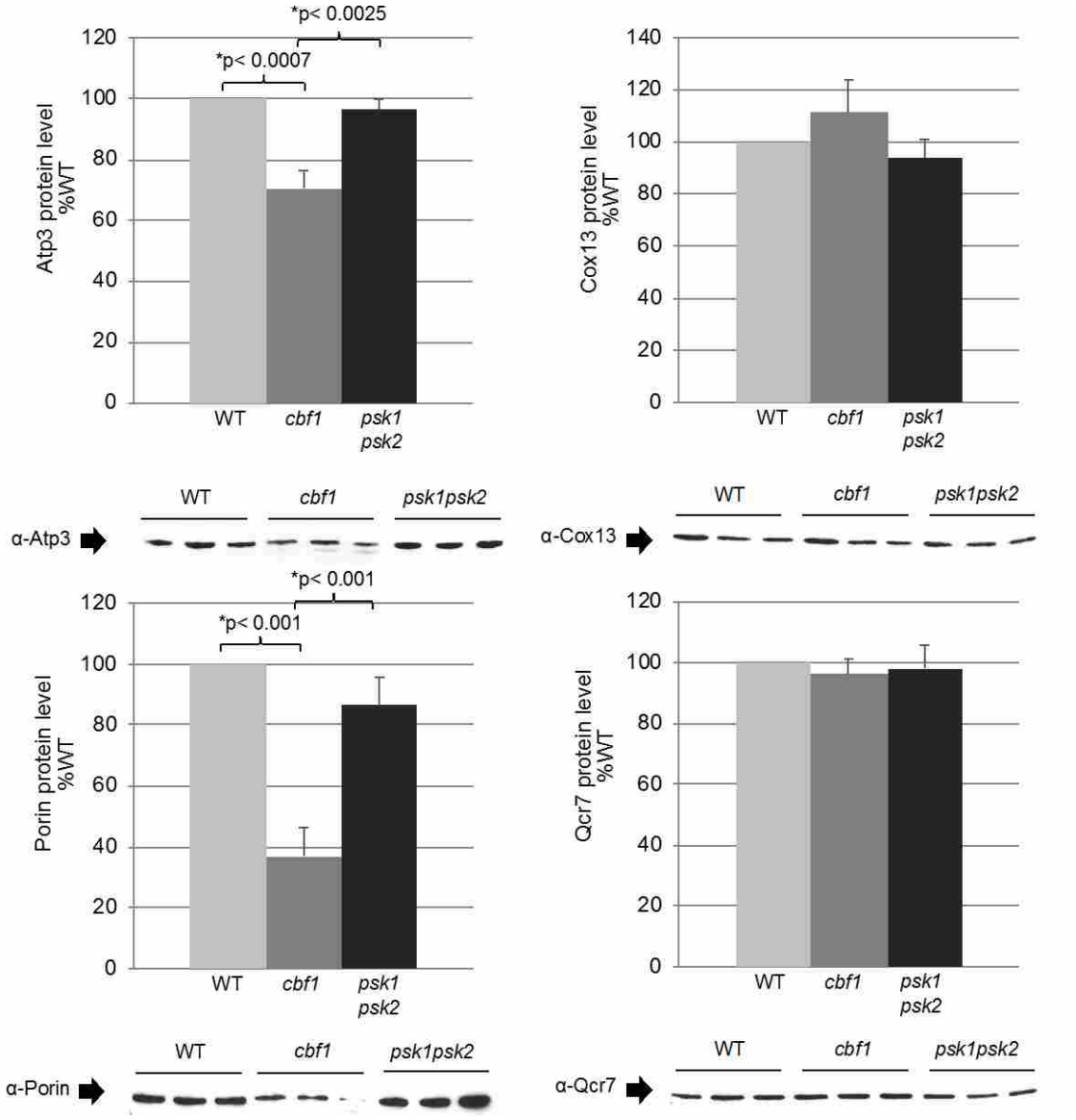

Figure 2.3 Quantification of Atp3, Qcr7, Cox13, and porin (Por1) protein in WT, cbf1, and psk1psk2 isolated mitochondria . Each biological replicate (n=>4) was run in duplicate to control for technical issues. Representative western blots for each protein are shown below each graph. An equal amount of protein was loaded per sample as determined by Bradford assay with bovine serum albumin as a protein standard. Error bars represent SEM. Data was analyzed using the one-way analysis of variance (ANOVA) with Tukey's HSD post hoc test. *P<0.05

2.4.5 Cbf1 regulates transcription of *ATP3* and *PSK1*

Large-scale transcription factor profiling [21, 34] has suggested Cbf1 as a potential player in respiratory control, potentially identifying the direct means by which Cbf1 controls respiration. We chose five of the respiration-associated genes reported as Cbf1-regulated in these large-scale transcriptome studies (*ATP3*, *COX4*, *HAP4*, *NDI1*, *QCR6)* and cloned their promoter regions into a LacZ fusion plasmid to test transcriptional control in vivo. Of the five genes tested, the gene encoding F_1-ATP synthase complex *(ATP3*) was the only one that appeared to have increased expression due to Cbf1 under these growth conditions (Figure 2.4A). Notably, this was also the only protein of the five previously reported respiration genes that was also retrieved from the mass spectrometry proteome analysis discussed above. As a control for the assays, two ceramide synthase promoters (*LAC1* and *LAG1*) that were previously shown through ß-galactosidase assays to be regulated by Cbf1 were also tested (Kolaczkowski et al., 2004). The *LAC1* and *LAG1* behaved similarly to what Kolaczkowski et al. have reported, giving support that the assays were working properly. However, the lack of observing effects on the other four putative targets (*COX4*, *HAP4*, *NDI1*, or *QCR6*) may be due to unforeseen issues with the constructs, the yeast strain used, or growth condition differences. Taken together, these results are consistent with Cbf1 upregulating respiration (through transcriptional regulation of genes such as ATP3) and downregulating lipid biosynthesis (through regulation of genes such as *LAC1* and *LAG1*).

In addition to these five genes involved in respiration, *PSK1* was identified as a putative Cbf1 target from among the hundreds of putative targets identified in the large-scale transcription factor studies (Petti et al., 2012). This suggested a feedback loop, where Psk1 phosphorylates and inhibits Cbf1, and Cbf1 in turn upregulates Psk1. The *PSK1* promoter was cloned into the LacZ fusion

plasmid and also displayed CBF1-dependent regulation (Figure 2.4A). These results support an important interplay between the *CBF1* and *PSK1* and solidifies the evolutionary link between them.

To test for direct binding of Cbf1 to the *ATP3* and *PSK1* promoters, gel shift assays were performed with purified promoters (DNA) and purified Cbf1 protein. As shown in Fig. 2.4C, Cbf1 appears to bind the *ATP3*, *PSK1*, and *LAC1* promoters, but not the control (*LAG1*, which was previously shown to be regulated by Cbf1 in an indirect manner [22]). The predicted Cbf1 consensus site (CACGTG) was then mutated as shown in Fig. 2.4B in order to confirm specificity of binding. Reduced binding was observed for both the mutated *ATP3* and *PSK1* promoters, supporting direct Cbf1 binding (Figure 2.4C).

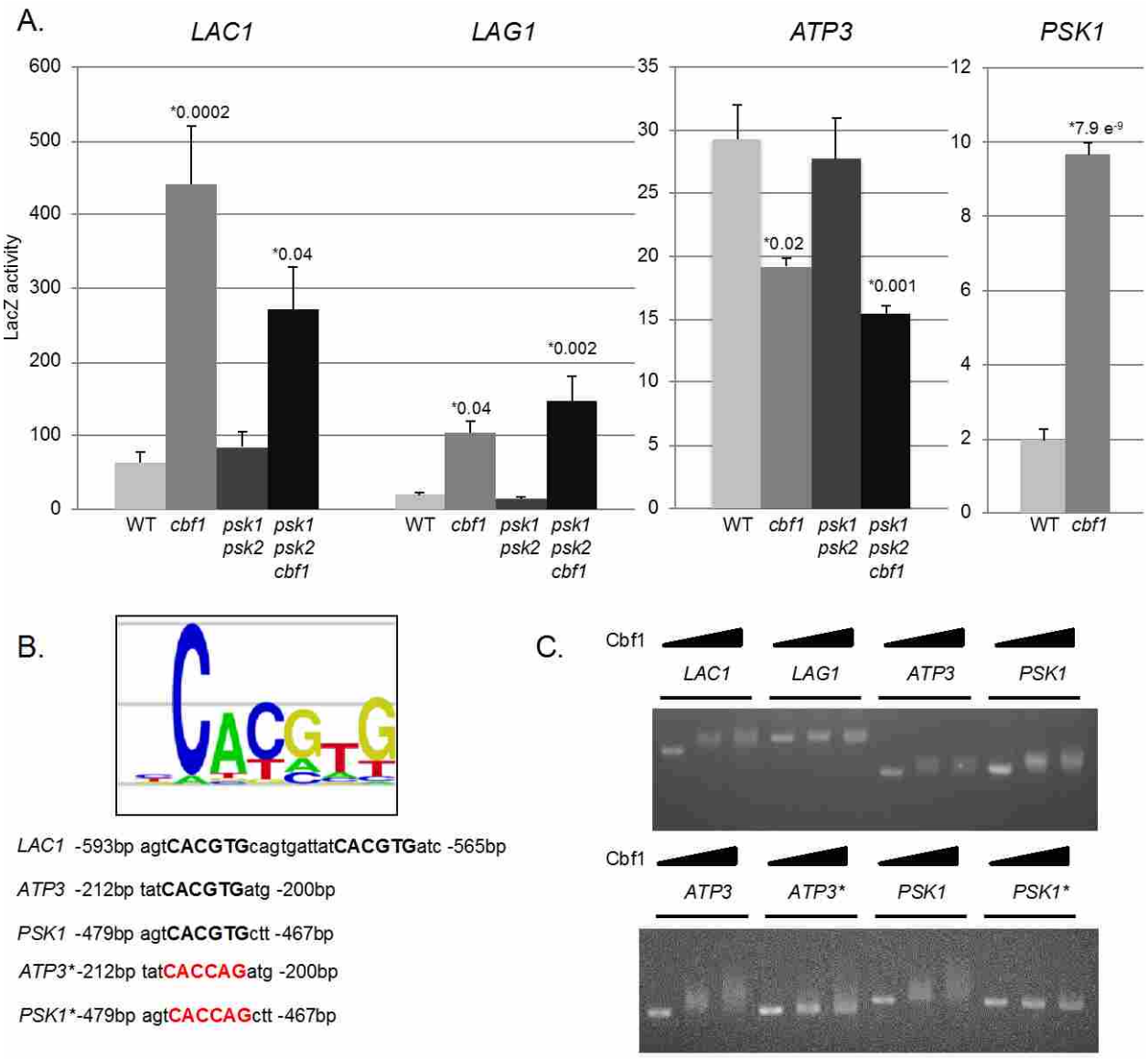

Figure 2.4 Evidence for the transcriptional regulation of *ATP3*, *LAC1*, *LAG1* and *PSK1* by Cbf1. (A) ß-galactosidase assays of yeast transformed with LacZ fusion plasmids (to the *ATP3, LAC1*, *LAG1* or *PSK1* promoters) grown in synthetic minimal media. LacZ activity was used as a readout of transcriptional regulation. (B) A diagram of the Cbf1 consensus binding site found in *LAC1*, *ATP3* and *PSK1* upstream regions. *LAG1* does not harbor a Cbf1 binding site, therefore, the sequence is not shown. Mutant versions of the Cbf1 consensus in the *ATP3* and *PSK1* promoters were created by site-directed mutagenesis and are shown in red. (C) Gel shifts were carried out by PCR amplifying the promoter regions of *LAC1*, *LAG1*, *ATP3* and *PSK1* (top), as well as promoter regions with Cbf1 binding site alterations as controls (*ATP3** and *PSK1**) (bottom), then incubated with either 0 ng, 3 ng, or 6 ng of purified Cbf1 protein followed by agarose gel electrophoresis. Error bars represent SEM. Significant p-values for condition versus WT are shown. Data was analyzed using one-way analysis of variance (ANOVA) and Tukey's HSD *post hoc* test. Each strain was tested six times and averaged for ß-galactosidase assays.

2.4.6 Altered ATP and ROS generation in *CBF1*-deficient cells

The transcriptional regulation results, in conjunction with the mass spectrometry findings, strongly suggest that Cbf1 upregulates *ATP3* to promote respiration. Therefore, we monitored ATP production in wild type, *CBF1*-deficient and *PSK1PSK2*-deficient yeast. Unexpectedly, the *CBF1*-deficient yeast displayed a drastically higher ATP level per cell when compared to the wild type or *PSK1PSK2*-deficient yeast when using OD600 to normalize the cell count (Figure 2.5A). This effect, however, appeared to be due to a large proportion of dead/unhealthy cells as seen with the mass spectrometry mitochondrial preparation above because there was no significant alteration in ATP when we normalized to total viable cell count determined by plating (Figure 2.5B). Next we investigated whether the altered respiratory metabolism of CBF1-deficient yeast resulted in reactive oxygen species (ROS) generation (Figure 2.5C & D). The *CBF1*-deficient strain appeared to have a lower level of ROS generation than wild type yeast, consistent with decreased respiration in these yeast and supporting the altered mitochondrial proteome discussed above.

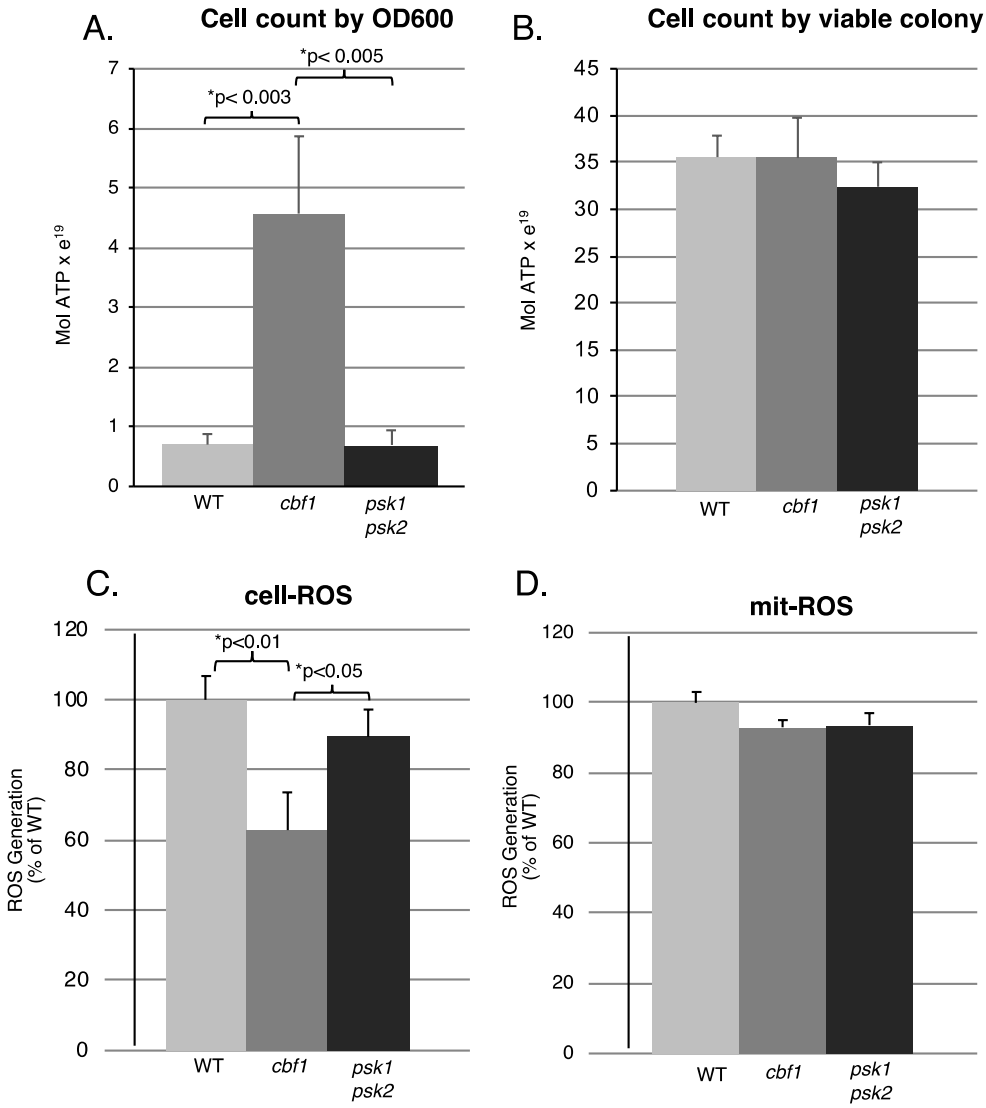

Figure 2.5 Cellular reactive oxygen species appeared to decrease in *CBF1*-deficient yeast while ATP assays revealed no significant change. ATP levels were measured in WT, cbf1, and psk1psk2 yeast strains grown under respiratory conditions (Gly/EtOH) using Promega's BactTiter-Glo Microbial Cell Viability Assay, a bioluminescent assay used for ATP quantification of bacterial or yeast cells. Yeast strains were normalized to either total cell count determine by OD600 (A) or by viable colonies from plating (B). Assays were run in technical duplicate and biological triplicate and results were averaged. Flow cytometry was utilized to quantify the (C) total intracellular reactive oxygen species (cell-ROS) and (D) mitochondrial reactive oxygen species (mit-ROS) in WT, cbf1, and psk1psk2 yeast strains. The fluorescence was monitored in the emission fluorescence channel FL1. Error bars represent SEM. Significant p-values for condition versus WT are shown with asterisks. *p-value was determined using one-way analysis of variance (ANOVA) and Tukey's HSD post hoc test.

2.4.7 Human USF1 protein is a conserved substrate of PAS kinase in vitro and affects respiration in vivo

Just as Cbf1 regulates lipids in yeast through transcriptional control of LAC1 and LAG1, it's human homolog Upstream transcription factor 1 (USF1) is a major contributor to familial combined hyperlipidemia (FCHL) [16-20, 35-46]. These studies have provided strong evidence for the role of USF1 in lipid regulation, but a role in respiratory regulation has not been shown. Cbf1 and USF1 have homology in the region of the PAS kinase phosphorylation site on Cbf1, just upstream of the conserved basic helix-loop-helix domain (Figure 2.6A). To determine if USF1 is a conserved substrate of human PAS kinase (hPASK) in vitro kinase assays were performed (Figure 2.6B). USF1 was phosphorylated in vitro a hPASK-dependent manner. The effects of USF1 on respiration were then assessed in yeast through both respiration chamber assays (Figure 2.6C) as well as plate assays (Figure 2.6D). The results from both assays gave supporting evidence that USF1 can complement the respiration phenotype of *CBF1*-deficiency in yeast, suggesting that Cbf1/USF1 play a conserved role in the partitioning of glucose towards respiration and away from lipid biogenesis.

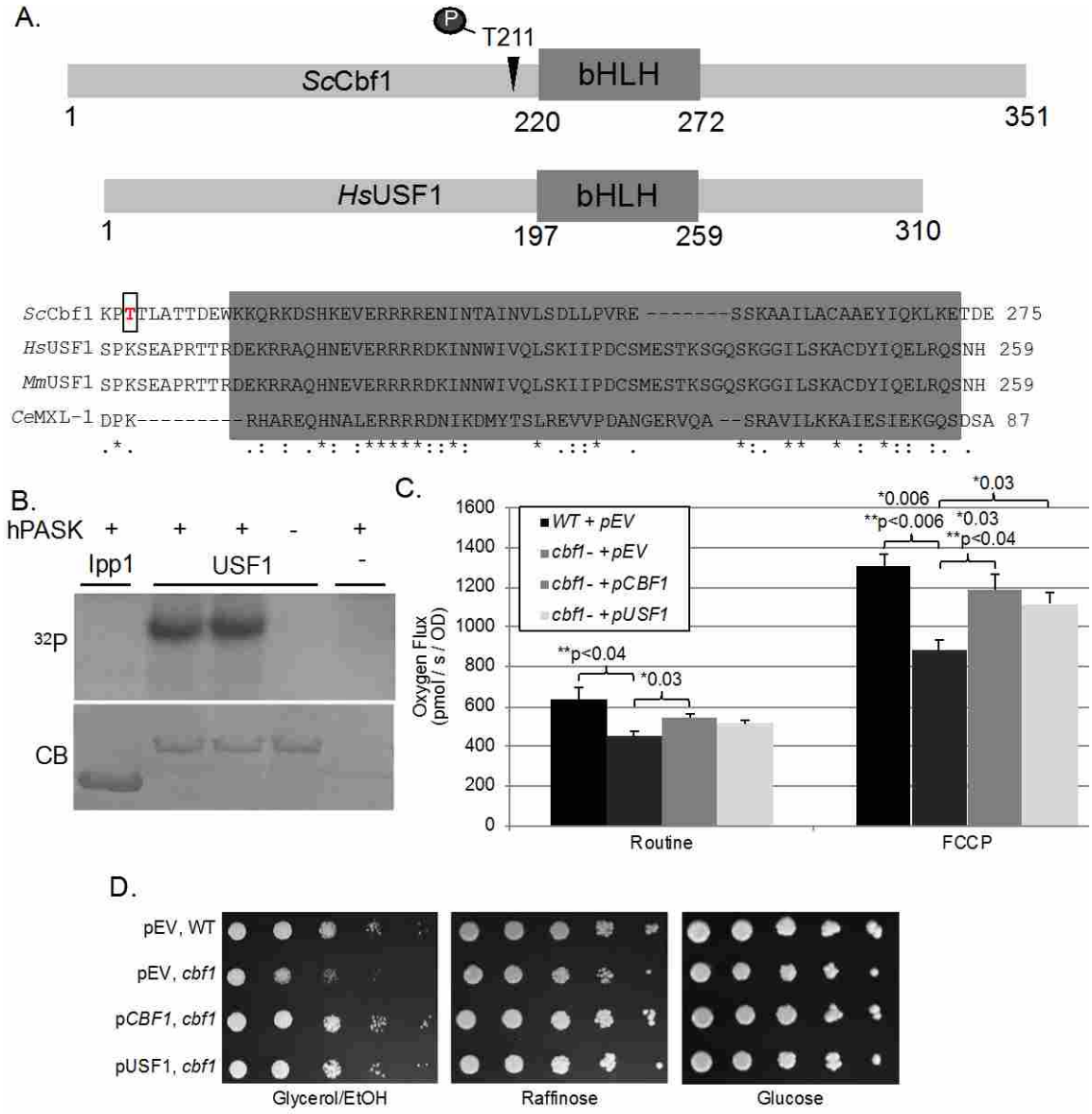

Figure 2.6 Evidence for the phosphorylation of human USF1 by hPASK and for a conserved role in the regulation of respiration. (A) Clustal Omega (Goujon et al., 2010; Sievers et al., 2011) alignment of the bHLH domain region for functional orthologs of Cbf1 obtained from the Isobase database (Liao et al., 2009; Park et al., 2011; Singh et al., 2008): *S. cerevisiae* (*Sc*Cbf1), *H. sapiens* (*Hs*USF1), *M. musculus* (*Mm*USF1), and *C. elegans* (*Ce*MXL-1). (B) Kinase assays using purified hPASK and USF1 proteins were run on 12% SDS page, stained with Coomassie Brilliant Blue (CB), then imaged using autoradiography (^{32}P). Ipp1, retrieved from a previous screen for PAS kinase interactors (DeMille et al., 2014), was used as a negative control. (C) For respiration assays, overnights in selective S-glucose media were switched to selective S-galactose media and respiration rates were measured using an Oroboros O_2K Oxygraph. (D) Wild type and *cbf1* yeast transformed with an empty vector, Cbf1 or USF1 were grown in selective S-glucose media. Overnights in selective S-glucose media were serially diluted in water (1:10) then plated to selective S-glycerol/EtOH, -raffinose, or -glucose plates and incubated for 2-3 days at 30°C. Significant p-values for data was analyzed using pair wise Student's T-Test (*) and one-way analysis of variance (ANOVA) with Tukey's HSD *post hoc* test (**) are shown.

2.5 Discussion

As the primary source of cellular energy, the regulation of mitochondrial metabolism is key in proper glucose allocation. As such, mitochondrial dysfunction has come to the forefront of a wide variety of disease, including diabetes, obesity, Alzheimer's and cancer [47-49]. Despite their clear importance, there is still much unknown about mitochondrial regulation. This study provides novel molecular mechanisms behind the regulation of mitochondrial metabolism by PAS kinase and its substrate Cbf1/USF1. Our results suggest that PAS kinase and Cbf1 function at a pivotal point for partitioning glucose to respiration or to lipid biosynthesis (Figure 2.7).

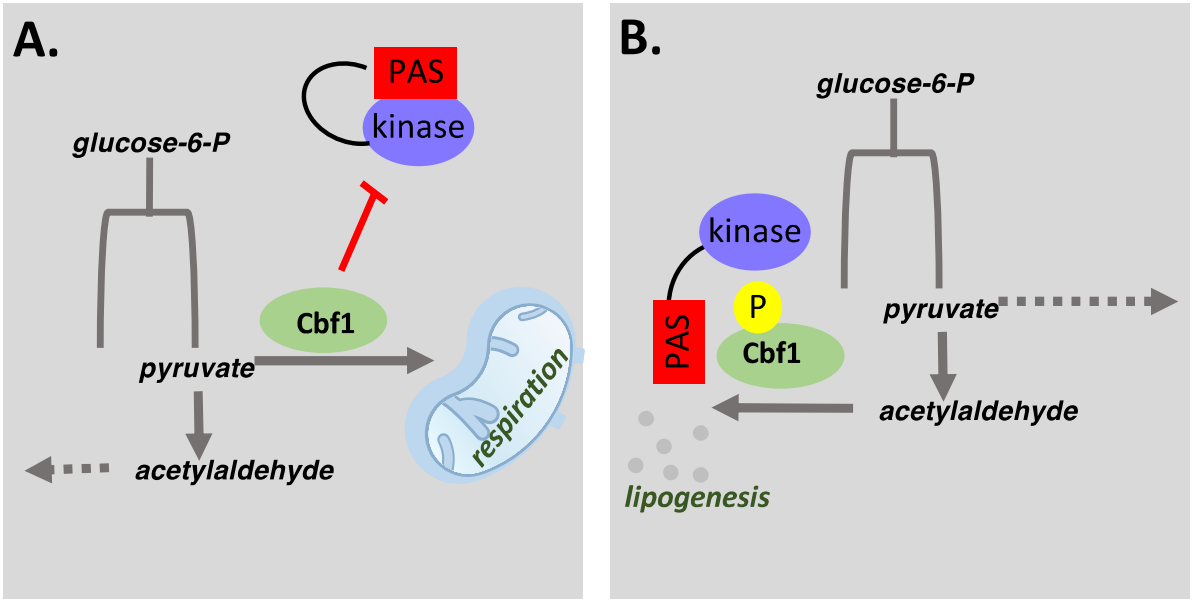

Figure 2.7 A model for function of Cbf1 and PAS kinase as a key point in the partitioning of glucose for respiration or for lipogenesis. (A) When PAS kinase is inactive, Cbf1 upregulates pathways involved in respiration and inhibits PAS kinase expression. (B) When PAS kinase is active, Cbf1 is phosphorylated at T211 and upregulates pathways involved in lipogenesis.

First, PAS kinase-dependent phosphorylation of Cbf1 at the critical threonine 211 site appears to reduce cellular respiration (Figure 2.1A-D). The mechanisms behind this respiratory phenotype were characterized by looking at mitochondrial area and the mitochondrial proteome. No significant decrease of mitochondrial area was observed by transmission electron microscopy of

CBF1-deficient yeast (Figure 2.1E & F), suggesting alternative methods for regulating respiration. In contrast, PAS kinase-deficient yeast did display an increased mitochondrial area, suggesting additional targets that may control mitochondrial biogenesis as supported by the additional affects observed in the respiration assays (Figure 2.1 and DeMille et al., 2014). This approximately one-third increase in area may help account for the increase in respiration, however it is difficult to know how much the mitochondrial area can directly correlate to function since the effects on mitochondrial proteins reported in this paper show that they may not be evenly regulated.

Although the effects of CBF1 on respiration did not appear to be on mitochondrial area, an apparent significant effect on the mitochondrial proteome was detected by mass spectrometry, with 43 proteins that appeared significantly altered in *CBF1*-deficient yeast (Figure 2.2). These results indicated altered levels of key electron transport chain proteins, including a decrease in Atp3 (F_1 ATP synthase) and porin levels which were confirmed by western blot (Figure 2.3).

Due to the presence of a conserved Cbf1-binding site in the ATP3 promoter, promoter ß-galactosidase and gel shift assays were performed in parallel with genes (*LAC1*, *LAG1*) involved in lipid biosynthesis previously shown to be CBF1-regulated [22, 50] . Atp3 appeared to have *CBF1*-dependent increased expression and Cbf1 bound the *ATP3* promoter in the in vitro gel shift assays (Figure 2.4). Thus, Cbf1 appears to upregulate respiration through *ATP3* (Figure 2.2-4), and to downregulate lipid biogenesis through *LAC1* and *LAG1* (Figure 2.4).

The *CBF1*-dependent increase of *ATP3* expression suggested that ATP levels may be lower in *CBF1*-deficient yeast. However, we found that while *CBF1*-deficient yeast had lower ROS generation consistent with decreased respiration, no significant difference in ATP levels were observed when levels were normalized to cell count (Figure 2.5). These results suggest that *CBF1*-deficient yeast may produce a majority of the ATP in alternative pathways. Since 40 of the 43 high

confidence hits from mass spectrometry displayed decreased expression in *CBF1*-deficient yeast, ATP could be produced by pathways not localized to the mitochondria (such as increased glycolysis).

In addition to Atp3, we confirmed PAS kinase 1 (*PSK1*) as a direct transcriptional target of Cbf1, solidifying the importance of their interaction (Figure 2.4). From promoter ß-galactosidase assays, *CBF1*-deficiency led to an almost five-fold increase in Psk1 expression, and Psk1 in turn inhibits Cbf1 activity through phosphorylation (DeMille et al., 2014). In addition, the activation of PAS kinase by respiratory growth conditions, and its subsequent inhibition of respiration appears contradictory. In each of these cases, PAS kinase and/or Cbf1 appears to be providing a feedback mechanism for delicately controlling metabolism, partitioning glucose to competing pathways and ensuring, for example, that some lipids are produced from glucose breakdown even during times when respiration is favored. This interplay between the two indicates a long evolutionary history, suggesting the pathway may be conserved in higher eukaryotes.

The human homolog of Cbf1, USF1, has been associated with lipid biogenesis and hyperlipidemia in many studies [16-20, 35-46]. Combined with our results herein Cbf1/USF1 may play a conserved role in partitioning glucose towards respiration at the expense of lipid metabolism. In support of this hypothesis, USF1 appears to regulate respiration in yeast (Figure 2.6C & D). The role of PAS kinase in inhibiting Cbf1 also appears to be conserved, in that hPASK can phosphorylate USF1 in vitro (Figure 2.6B). The conservation of the USF1/PAS kinase pathway may aid in explaining the most dramatic phenotypes reported for PAS kinase-deficient mice, namely an increased O_2 uptake and decreased liver triglyceride accumulation [11]. Further study of how PASK is regulating the many activities of USF1 may provide additional insight into the role of PAS kinase in human diseases including hyperlipidemia, obesity and diabetes.

2.6 Acknowledgements

We would like to thank Audrey Workman (Brigham Young University) for aid in analysis of mass spectrometry data. We thank Dr. Martin Ott (Stockholm University) for the generous gift of Qcr7 and Cox13 antibodies. We thank Michael Standing (Brigham Young University) who imaged our yeast for the electron micrographs and Dennis Winge (University of Utah, Salt Lake City, UT) for the porin antibodies. Funding for this work was supported by National Institutes of Health Grant R15 GM100376-01, a Brigham Young University Mentoring Environmental Grant to J.H.G, Brigham Young University Simmons Center for Cancer Research Fellowships to D.D and J.A.P, and the Brigham Young University Department of Microbiology and Molecular Biology and College of Life Sciences.

2.7 Supplementary materials

Table 2.S1 Mitochondrial proteins identified by mass spectrometry from mitochondrial extracts of wild type (JGY43) and PAS kinase-deficient yeast (JGY1244), but not CBF1-deficient yeast. Proteins are divided into functional categories and are listed by protein name, accession number, the number of times the protein was retrieved (out of three biological replicates), the average retrieval number of the protein as well as the standard deviation of the retrieval number for strains 43 and 1244, and the description of the protein. Retrieval numbers are included as an indication of confidence Protein functions were based off of their gi description in NCBI, or the description in the Saccharomyces Genome Database (Cherry et al., 2012; Engel et al., 2014).

Gene/ protein	Accession #	# strain 43	Ave. # strain 43	Std. dev. strain 43	# strain 1244	Ave. # strain 1244	Std. dev. strain 1244	Description
TCA/Respiration/Metabolism								
Idh2	gi|6324709	3	20.3	3.2	3	24.7	9.0	isocitrate dehydrogenase
Nde1	gi|6323794	3	56.0	31.5	3	64.0	18.4	Mito. external NADH dehydro.
Leu4	gi|6324225	3	26.3	7.2	3	43.3	20.6	α-isopropylmalate synthase
Pda1	gi|6321026	3	38.7	4.6	3	49.0	23.4	α-subunit pyruvate dehydro.
Kgd2	gi|6320352	3	35.0	10.8	3	50.3	8.4	α-ketoglutarate dehydro. subunit
Cyt1	gi|6324639	3	71.3	27.7	3	320.7	214.5	Cytochrome c1
Lat1	gi|6324258	3	61.3	28.0	3	80.7	20.5	pyruvate dehydro. component (E2)
Ald5	gi|6320917	3	55.7	3.5	3	71.3	18.6	Aldehyde dehydro.
Ilv1	gi|6320930	3	56.7	8.3	3	65.7	15.5	threonine deaminase
Alo1	gi|6323553	3	67.7	19.4	3	81.0	16.8	D-arabinono-1
Cdc19	gi|6319279	3	118.7	115.5	3	40.0	12.0	Pyruvate kinase
Fat2	gi|6319699	3	170.7	195.2	3	51.7	30.2	Probable AMP-binding protein
Ilv6	gi|6319837	3	53.0	11.5	3	76.3	28.3	Acetolactate synthase reg.subunit
Sdh2	gi|6322987	3	77.7	32.9	3	219.3	176.8	Succinate dehydro. subunit
Lys4	gi|6320440	3	88.3	20.6	3	192.0	96.1	homoaconitase
Adh1	gi|6324486	3	129.3	49.0	3	89.7	27.4	Alcohol dehydro.
Ccp1	gi|6322919	3	61.7	26.9	3	48.3	18.6	Cytochrome-c peroxidase
Pdc1	gi|6323073	3	132.0	101.8	3	88.3	48.2	pyruvate decarboxylase
Gpd1	gi|6320181	3	151.7	131.9	3	64.3	22.2	glycerol-3-phosphate dehydro.
Pdh1	gi|6325258	3	94.7	8.1	2	203.0	0.0	putative 2-methylcitrate dehydratase
Eno2	gi|6321968	2	201.0	120.2	3	72.0	32.9	enolase
Aim45	gi|6325261	3	99.7	35.9	1	69.0	0.0	putative mammalian ETF-α ortholog

Cdc48	gi|6320077	2	167.0	0.0	3	71.0	26.5	microsomal ATPase
Gpm1	gi|6322697	3	158.0	80.9	3	81.0	48.9	Phosphoglycerate mutase
Gsy2	gi|6323287	2	139.0	99.0	2	57.0	26.9	Glycogen synthase
Cyb2	gi|6323587	2	79.0	8.5	2	97.0	0.0	Cytochrome b2
Protein Expression								
Mss51	gi|6323232	3	91.3	18.5	2	128.5	75.6	involved mRNA maturation of COX1
Rps3	gi|6324151	3	103.3	43.2	3	74.3	13.3	Ribosomal protein S3
Eft1	gi|6324707	3	108.3	81.1	3	49.0	14.7	translation elongation factor2
Eft2	gi|6320593	3	108.3	81.1	3	49.0	14.7	translation elongation factor 2
Ssb1	gi|6319972	3	90.7	21.2	3	62.3	15.5	cytoplasmic HSP70 family member
Scp160	gi|6322381	2	408.5	122.3	2	99.0	17.0	G-protein receptor of mating
Mrpl1	gi|6320321	1	72.0	0.0	1	394.0	0.0	Mito.large subunit ribosomal protein
Secretion/Export/Import								
Mic60	gi|6322868	3	99.7	70.1	2	172.0	0.0	Component of the MICOS complex
Kar2	gi|6322426	3	89.0	30.3	3	188.7	118.3	mammalian BiP (GPR78) homolog
Tom70	gi|6324208	3	60.7	11.9	3	45.3	8.1	mito. specialized import receptor
Tim44	gi|6322167	3	96.0	14.2	3	188.7	96.5	48.8 kDa mito. import protein
Yeast Growth/Division								
Mmd1	gi|6322138	3	51.7	14.4	3	78.3	33.4	Deoxyhypusine hydroxylase
Cdc12	gi|6321899	2	87.0	1.4	3	133.3	103.9	10nm filaments of septin component
Structural								
Om45	gi|6322055	3	29.0	18.0	3	64.7	20.6	mito. outer membrane protein
Pex11	gi|6324425	2	67.5	7.8	3	150.7	95.8	Peroxisomal membrane protein
Stress Response/Sporulation								
Ssb2	gi|6324120	3	90.7	21.2	2	70.0	11.3	Heat shock protein of HSP70 family
Hsp82	gi|6325016	3	207.3	224.0	3	60.0	8.9	82 kDa heat shock protein
Hsc82	gi|6323840	3	207.3	224.0	3	60.0	8.9	constitutive heat shock protein
Ssa1	gi|6319314	3	93.7	41.8	3	30.0	21.8	Heat shock protein of HSP70 family
Signal Transduction								
Rho1	gi|6325423	2	99.5	36.1	3	85.3	51.0	GTP-binding ras-like protein
Amino Acid Synthesis								
Erg6	gi|6323635	3	86.3	41.6	3	52.0	10.1	Delta(24)-sterol C-methyltransferase

Bat1	gi|6322002	3	81.0	7.8	3	135.0	73.0	branched-chain amino acid trans.
DNA Replication/Recombination								
Abf2	gi|6323717	1	94.0	0.0	1	189.0	0.0	HMG-1 homolog
Unknown								
Aim9	gi|6320924	3	60.3	11.5	3	85.0	48.5	Yer080wp

Abbreviations include dehydrogenase (dehydro.), regulatory (reg.), mitochondrial (mito), transaminase (trans.), methyltransferase (methyl.).

Table 2.S2 Mitochondrial proteins identified by mass spectrometry from mitochondrial extracts of CBF1-deficient yeast but not wild type (JGY43) and PAS kinase-deficient yeast (JGY1244). Proteins are divided into functional categories and are listed by protein name, accession number, the number of times the protein was retrieved (out of three biological replicates), the average retrieval number of the protein as well as the standard deviation of the retrieval number, and the description of the protein. Retrieval numbers are included as an indication of confidence. Protein functions were based off of their gi description in NCBI, or the description in the Saccharomyces Genome Database (Cherry et al., 2012; Engel et al., 2014).

Gene/ Protein	Accession #	#	Ave. #	Std. dev.	Description
TCA/Respiration/Metabolism					
Ale1	gi|6324749	1	63	0	Lysophospholipid acyltransferase
Sdh1	gi|6322416	1	24	0	Succinate dehydrogenase
Pgi1	gi|6319673	1	85	0	Glucose-6-phosphoate isomerase
Glt1	gi|6320030	1	95	0	Glutamate synthase
Protein Expression					
Aim10	gi|6320931	1	40	0	protein with similarity to tRNA synthetases
Rps25b	gi|6323365	1	89	0	Ribosomal protein S25B (S31B) (rp45) (YS23)
Rps25a	gi|6321464	1	89	0	Ribosomal protein S25A (S31A) (rp45) (YS23
Hsh155	gi|6323944	1	90	0	U2-snRNP associated splicing factor
Secretion/Export/Import					
Sna1	gi|6320482	3	53	0.7	Hypothetical transmembrane protein
Structural					
Mas6	gi|6324344	1	40	0	Mitochondrial inner membrane protein of the Tim23 complex
Mdm20	gi|6324497	1	96	0	Subunit of the NatB N-terminal acetyltransferase
Stress Response/Sporulation					
Ynl194cp	gi|6324135	2	60	0	sporulation and plasma membrane sphingolipid content
Signal Transduction					
Yel043wp	gi|6320792	1	98	0	Cytoskeleton protein involved in intracellular signaling
Ypr097wp	gi|6325354	1	94	0	Contains a PX domain and binds phoshoinositides
Vesicles/Endocytosis					
Pal1	gi|6320555	1	91	0	Protein of unknown function maybe involved in endocytosis

Table 2.S3 Mitochondrial proteins identified by mass spectrometry from mitochondrial extracts of wild type (JGY43) yeast but not CBF1-deficient (JGY1277) or PAS kinase-deficient yeast (JGY1244). Proteins are divided into functional categories and are listed by protein name, accession number, the number of times the protein was retrieved (out of three biological replicates), the average retrieval number of the protein as well as the standard deviation of the retrieval number, and the description of the protein. Retrieval numbers are included as an indication of confidence. Protein functions were based off of their gi description in NCBI, or the description in the Saccharomyces Genome Database (Cherry et al., 2012; Engel et al., 2014).

Gene/ Protein	Accession #	#	Ave. #	Std. dev.	Description
TCA/Respiration/Metabolism					
Mcx1	gi|6319704	2	331.5	6.4	mitochondrial ClpX
Oac1	gi|6322729	2	346.0	162.6	mitochondrial oxaloacetate transport protein
Afg1	gi|6320783	2	353.5	252.4	ATPase family gene
Leu9	gi|6324682	2	357.0	7.1	isopropylmalate synthase
Pos5	gi|6325068	2	371.5	2.1	mitochondrial NADH kinase
Pex22	gi|6319263	2	386.0	36.8	peroxisomal membrane protein
Wbp1	gi|6320835	3	387.3	22.4	oligosaccharyl transferase glycoprotein complex
Ecm31	gi|6319653	2	402.0	106.1	3-methyl-2-oxobutanoate hydroxymethyltransferase
Oar1	gi|6322795	2	414.0	7.1	3-oxoacyl-[acyl-carrier-protein] reductase
Rpn7	gi|6325365	2	415.5	106.8	subunit of the regulatory particle of the proteasome
Coa1	gi|6322034	2	419.5	38.9	assembly of the cytochrome c oxidase complex
Gif1	gi|6322215	2	430.0	26.9	(putative) involved in cell cycle control; Gif1p
Lip5	gi|6324770	2	448.5	122.3	lipoic acid synthase
Pkp1	gi|6322147	2	457.5	99.7	mitochondrial protein kinase
Protein expression					
Cbp6	gi|6319596	2	205.0	48.1	translational activator of COB mRNA
Mrp20	gi|6320613	2	244.0	169.7	mitochondrial ribosomal large subunit protein
Mrpl22	gi|6324152	3	271.3	127.2	mitochondrial ribosomal large subunit protein
Mrpl49	gi|6323472	3	297.7	123.1	mitochondrial 60S ribosomal protein L4
Mrpl31	gi|6322711	2	298.0	130.1	15.5 kDa mitochondrial ribosomal protein YmL31
Pet54	gi|6321661	2	310.0	198.0	translational activator of cytochrome c oxidase subunit III
Nuc1	gi|6322253	2	320.0	168.3	mitochondrial nuclease
Gas1	gi|6323967	2	341.0	200.8	cell surface glycoprotein 115-120 kDa
Mrpl36	gi|6319598	3	369.0	171.5	mitochondrial ribosomal protein MRPL36 (YmL36)
Rml2	gi|6320785	2	375.0	120.2	mitochondrial protein of the large ribosomal subunit
Cox11	gi|6325125	2	403.5	105.4	required for delivery of copper to Cox1p
Msw1	gi|6320474	3	404.7	134.8	mitochondrial tryptophanyl-tRNA synthetase
Mtf2	gi|6320160	2	429.5	64.3	involved in mRNA splicing
Ydr370c	gi|6320578	2	505.5	21.9	mRNA 5'-end-capping quality-control protein
Secretion/Export/Import					
Mdl2	gi|6324985	2	309.5	70.0	ATP-binding cassette (ABC) transporter family member
Tim21	gi|6321470	2	348.0	80.6	component of the TIM23 complex
Cpr6	gi|6323246	2	362.0	223.4	cyclophilin related to the mammalian CyP-40
Bfr1	gi|6324772	2	421.0	110.3	involved in secretion
Spc3	gi|6323095	3	433.0	46.4	signal peptidase subunit
Structural					
Aim24	gi|6322540	2	288.0	162.6	functions in determining mitochondrial architecture
Prp12	gi|6323960	2	363.0	4.2	Integral membrane mitochondrial protein
Snl1	gi|6322173	2	403.5	82.7	18.3 kD integral membrane protein

Signal transduction					
Srp54	gi|6325345	2	490.0	9.9	Signal recognition particle subunit
Endocytosis					
Erv25	gi|6323630	2	391.5	119.5	vesicle coat component
Unknown					
Ypr063c	gi|6325320	2	379.0	43.8	ER-localized protein of unknown function
Ydl157c	gi|6320044	2	395.0	228.1	unknown function
Ykl053c-a	gi|6322797	2	399.0	4.2	dubious ORF
Yil077c	gi|6322113	2	425.5	53.0	unknown function

REFERENCES

1. Rutter J, Michnoff CH, Harper SM, Gardner KH, McKnight SL. PAS kinase: an evolutionarily conserved PAS domain-regulated serine/threonine kinase. Proc Natl Acad Sci U S A. 2001;98(16):8991-6. Epub 2001/07/19. doi: 10.1073/pnas.161284798161284798 [pii]. PubMed PMID: 11459942; PMCID: 55361.

2. DeMille D, Grose JH. PAS kinase: a nutrient sensing regulator of glucose homeostasis. IUBMB Life. 2013;65(11):921-9. Epub 2013/11/23. doi: 10.1002/iub.1219. PubMed PMID: 24265199.

3. Cardon CM, Rutter J. PAS kinase: integrating nutrient sensing with nutrient partitioning. Semin Cell Dev Biol. 2012;23(6):626-30. Epub 2012/01/17. doi: 10.1016/j.semcdb.2011.12.007S1084-9521(12)00003-1 [pii]. PubMed PMID: 22245833; PMCID: 3331943.

4. Grose JH, Rutter J. The role of PAS kinase in PASsing the glucose signal. Sensors (Basel). 2010;10(6):5668-82. Epub 2010/01/01. doi: 10.3390/s100605668sensors-10-05668 [pii]. PubMed PMID: 22219681; PMCID: 3247726.

5. Hao HX, Rutter J. The role of PAS kinase in regulating energy metabolism. IUBMB Life. 2008;60(4):204-9. Epub 2008/03/18. doi: 10.1002/iub.32. PubMed PMID: 18344204.

6. Schlafli P, Borter E, Spielmann P, Wenger RH. The PAS-domain kinase PASKIN: a new sensor in energy homeostasis. Cell Mol Life Sci. 2009;66(5):876-83. Epub 2009/02/04. doi: 10.1007/s00018-009-8699-0. PubMed PMID: 19189049.

7. Smith TL, Rutter J. Regulation of glucose partitioning by PAS kinase and Ugp1 phosphorylation. Mol Cell. 2007;26(4):491-9. Epub 2007/05/29. doi: S1097-2765(07)00228-6 [pii]10.1016/j.molcel.2007.03.025. PubMed PMID: 17531808.

8. Zhang DD, Zhang JG, Wang YZ, Liu Y, Liu GL, Li XY. Per-Arnt-Sim Kinase (PASK): An Emerging Regulator of Mammalian Glucose and Lipid Metabolism. Nutrients. 2015;7(9):7437-50. Epub 2015/09/16. doi: 10.3390/nu7095347nu7095347 [pii]. PubMed PMID: 26371032; PMCID: 4586542.

9. Grose JH, Smith TL, Sabic H, Rutter J. Yeast PAS kinase coordinates glucose partitioning in response to metabolic and cell integrity signaling. EMBO J. 2007;26(23):4824-30. Epub 2007/11/09. doi: 7601914 [pii]10.1038/sj.emboj.7601914. PubMed PMID: 17989693; PMCID: 2099474.

10. da Silva Xavier G, Rutter J, Rutter GA. Involvement of Per-Arnt-Sim (PAS) kinase in the stimulation of preproinsulin and pancreatic duodenum homeobox 1 gene expression by glucose. Proc Natl Acad Sci U S A. 2004;101(22):8319-24. Epub 2004/05/19. doi: 10.1073/pnas.0307371010307737101 [pii]. PubMed PMID: 15148392; PMCID: 420392.

11. Hao HX, Cardon CM, Swiatek W, Cooksey RC, Smith TL, Wilde J, Boudina S, Abel ED, McClain DA, Rutter J. PAS kinase is required for normal cellular energy balance. Proc Natl Acad Sci U S A. 2007;104(39):15466-71. Epub 2007/09/20. doi: 0705407104 [pii]10.1073/pnas.0705407104. PubMed PMID: 17878307; PMCID: 2000499.

12. DeMille D, Bikman BT, Mathis AD, Prince JT, Mackay JT, Sowa SW, Hall TD, Grose JH. A comprehensive protein-protein interactome for yeast PAS kinase 1 reveals direct inhibition of respiration through the phosphorylation of Cbf1. Mol Biol Cell. 2014;25(14):2199-215. Epub 2014/05/23. doi: 10.1091/mbc.E13-10-0631mbc.E13-10-0631 [pii]. PubMed PMID: 24850888; PMCID: 4091833.

13. Baker RE, Fitzgerald-Hayes M, O'Brien TC. Purification of the yeast centromere binding protein CP1 and a mutational analysis of its binding site. J Biol Chem. 1989;264(18):10843-50. Epub 1989/06/25. PubMed PMID: 2543684.

14. Bram RJ, Kornberg RD. Isolation of a Saccharomyces cerevisiae centromere DNA-binding protein, its human homolog, and its possible role as a transcription factor. Mol Cell Biol. 1987;7(1):403-9. Epub 1987/01/01. PubMed PMID: 3550420; PMCID: 365082.

15. Cai M, Davis RW. Yeast centromere binding protein CBF1, of the helix-loop-helix protein family, is required for chromosome stability and methionine prototrophy. Cell. 1990;61(3):437-46. Epub 1990/05/04. doi: 0092-8674(90)90525-J [pii]. PubMed PMID: 2185892.

16. Pajukanta P, Lilja HE, Sinsheimer JS, Cantor RM, Lusis AJ, Gentile M, Duan XJ, Soro-Paavonen A, Naukkarinen J, Saarela J, Laakso M, Ehnholm C, Taskinen MR, Peltonen L. Familial combined hyperlipidemia is associated with upstream transcription factor 1 (USF1). Nat Genet. 2004;36(4):371-6. Epub 2004/03/03. doi: 10.1038/ng1320ng1320 [pii]. PubMed PMID: 14991056.

17. Naukkarinen J, Ehnholm C, Peltonen L. Genetics of familial combined hyperlipidemia. Curr Opin Lipidol. 2006;17(3):285-90. Epub 2006/05/09. doi: 10.1097/01.mol.0000226121.27931.3f00041433-200606000-00013 [pii]. PubMed PMID: 16680034.

18. Auer S, Hahne P, Soyal SM, Felder T, Miller K, Paulmichl M, Krempler F, Oberkofler H, Patsch W. Potential role of upstream stimulatory factor 1 gene variant in familial combined hyperlipidemia and related disorders. Arterioscler Thromb Vasc Biol. 2012;32(6):1535-44. Epub 2012/03/31. doi: 10.1161/ATVBAHA.112.245639ATVBAHA.112.245639 [pii]. PubMed PMID: 22460558.

19. Di Taranto MD, Staiano A, D'Agostino MN, D'Angelo A, Bloise E, Morgante A, Marotta G, Gentile M, Rubba P, Fortunato G. Association of USF1 and APOA5 polymorphisms with familial combined hyperlipidemia in an Italian population. Mol Cell Probes. 2015;29(1):19-24. Epub 2014/10/14. doi: 10.1016/j.mcp.2014.10.002S0890-8508(14)00048-6 [pii]. PubMed PMID: 25308402.

20. Laurila PP, Soronen J, Kooijman S, Forsstrom S, Boon MR, Surakka I, Kaiharju E, Coomans CP, Van Den Berg SA, Autio A, Sarin AP, Kettunen J, Tikkanen E, Manninen T, Metso J, Silvennoinen R, Merikanto K, Ruuth M, Perttila J, Makela A, Isomi A, Tuomainen AM, Tikka A, Ramadan UA, Seppala I, Lehtimaki T, Eriksson J, Havulinna A, Jula A, Karhunen PJ, Salomaa V, Perola M, Ehnholm C, Lee-Rueckert M, Van Eck M, Roivainen A, Taskinen MR, Peltonen L, Mervaala E, Jalanko A, Hohtola E, Olkkonen VM, Ripatti S, Kovanen PT, Rensen PC, Suomalainen A, Jauhiainen M. USF1 deficiency activates brown adipose tissue and improves cardiometabolic health. Sci Transl Med. 2016;8(323):323ra13. Epub 2016/01/29. doi: 10.1126/scitranslmed.aad00158/323/323ra13 [pii]. PubMed PMID: 26819196.

21. Lin Z, Wang TY, Tsai BS, Wu FT, Yu FJ, Tseng YJ, Sung HM, Li WH. Identifying cis-regulatory changes involved in the evolution of aerobic fermentation in yeasts. Genome Biol Evol. 2013;5(6):1065-78. Epub 2013/05/08. doi: 10.1093/gbe/evt067evt067 [pii]. PubMed PMID: 23650209; PMCID: 3698916.

22. Kolaczkowski M, Kolaczkowska A, Gaigg B, Schneiter R, Moye-Rowley WS. Differential regulation of ceramide synthase components LAC1 and LAG1 in Saccharomyces cerevisiae. Eukaryot Cell. 2004;3(4):880-92. Epub 2004/08/11. doi: 10.1128/EC.3.4.880-892.20043/4/880 [pii]. PubMed PMID: 15302821; PMCID: 500886.

23. Mymrikov EV, Seit-Nebi AS, Gusev NB. Large potentials of small heat shock proteins. Physiol Rev. 2011;91(4):1123-59. Epub 2011/10/21. doi: 10.1152/physrev.00023.201091/4/1123 [pii]. PubMed PMID: 22013208.

24. DeMille D, Badal BD, Evans JB, Mathis AD, Anderson JF, Grose JH. PAS kinase is activated by direct SNF1-dependent phosphorylation and mediates inhibition of TORC1 through the phosphorylation and activation of Pbp1. Mol Biol Cell. 2015;26(3):569-82. Epub 2014/11/28. doi: 10.1091/mbc.E14-06-1088mbc.E14-06-1088 [pii]. PubMed PMID: 25428989.

25. Shevchenko A, Wilm M, Vorm O, Mann M. Mass spectrometric sequencing of proteins silver-stained polyacrylamide gels. Anal Chem. 1996;68(5):850-8. Epub 1996/03/01. PubMed PMID: 8779443.

26. McCormack AL, Schieltz DM, Goode B, Yang S, Barnes G, Drubin D, Yates JR, 3rd. Direct analysis and identification of proteins in mixtures by LC/MS/MS and database searching at the low-femtomole level. Anal Chem. 1997;69(4):767-76. Epub 1997/02/15. PubMed PMID: 9043199.

27. Guttman M, Betts GN, Barnes H, Ghassemian M, van der Geer P, Komives EA. Interactions of the NPXY microdomains of the low density lipoprotein receptor-related protein 1. Proteomics. 2009;9(22):5016-28. Epub 2009/09/23. doi: 10.1002/pmic.200900457. PubMed PMID: 19771558; PMCID: 2862490.

28. Rutter J, Probst BL, McKnight SL. Coordinate regulation of sugar flux and translation by PAS kinase. Cell. 2002;111(1):17-28. Epub 2002/10/10. doi: S0092867402009741 [pii]. PubMed PMID: 12372297.

29. Byrne KP, Wolfe KH. Consistent patterns of rate asymmetry and gene loss indicate widespread neofunctionalization of yeast genes after whole-genome duplication. Genetics. 2007;175(3):1341-50. Epub 2006/12/30. doi: genetics.106.066951 [pii]10.1534/genetics.106.066951. PubMed PMID: 17194778; PMCID: 1840088.

30. Conant GC, Wolfe KH. Increased glycolytic flux as an outcome of whole-genome duplication in yeast. Mol Syst Biol. 2007;3:129. Epub 2007/08/02. doi: msb4100170 [pii]10.1038/msb4100170. PubMed PMID: 17667951; PMCID: 1943425.

31. Grassi L, Fusco D, Sellerio A, Cora D, Bassetti B, Caselle M, Lagomarsino MC. Identity and divergence of protein domain architectures after the yeast whole-genome duplication event. Mol Biosyst. 2010;6(11):2305-15. Epub 2010/09/08. doi: 10.1039/c003507f. PubMed PMID: 20820472.

32. Maclean CJ, Greig D. Reciprocal gene loss following experimental whole-genome duplication causes reproductive isolation in yeast. Evolution. 2011;65(4):932-45. Epub 2010/12/01. doi: 10.1111/j.1558-5646.2010.01171.x. PubMed PMID: 21114494.

33. Sugino RP, Innan H. Estimating the time to the whole-genome duplication and the duration of concerted evolution via gene conversion in yeast. Genetics. 2005;171(1):63-9. Epub 2005/06/24. doi: genetics.105.043869 [pii]10.1534/genetics.105.043869. PubMed PMID: 15972458; PMCID: 1456531.

34. MacIsaac KD, Wang T, Gordon DB, Gifford DK, Stormo GD, Fraenkel E. An improved map of conserved regulatory sites for Saccharomyces cerevisiae. BMC Bioinformatics. 2006;7:113. Epub 2006/03/09. doi: 1471-2105-7-113 [pii]10.1186/1471-2105-7-113. PubMed PMID: 16522208; PMCID: 1435934.

35. Coon H, Xin Y, Hopkins PN, Cawthon RM, Hasstedt SJ, Hunt SC. Upstream stimulatory factor 1 associated with familial combined hyperlipidemia, LDL cholesterol, and triglycerides. Hum Genet. 2005;117(5):444-51. Epub 2005/06/17. doi: 10.1007/s00439-005-1340-x. PubMed PMID: 15959806.

36. Holzapfel C, Baumert J, Grallert H, Muller AM, Thorand B, Khuseyinova N, Herder C, Meisinger C, Hauner H, Wichmann HE, Koenig W, Illig T, Klopp N. Genetic variants in the USF1 gene are associated with low-density lipoprotein cholesterol levels and incident type 2 diabetes mellitus in women: results from the MONICA/KORA Augsburg case-cohort study, 1984-2002. Eur J Endocrinol. 2008;159(4):407-16. Epub 2008/07/03. doi: 10.1530/EJE-08-0356EJE-08-0356 [pii]. PubMed PMID: 18593823.

37. Huertas-Vazquez A, Aguilar-Salinas C, Lusis AJ, Cantor RM, Canizales-Quinteros S, Lee JC, Mariana-Nunez L, Riba-Ramirez RM, Jokiaho A, Tusie-Luna T, Pajukanta P. Familial combined hyperlipidemia in Mexicans: association with upstream transcription factor 1 and

linkage on chromosome 16q24.1. Arterioscler Thromb Vasc Biol. 2005;25(9):1985-91. Epub 2005/06/25. doi: 01.ATV.0000175297.37214.a0 [pii]10.1161/01.ATV.0000175297.37214.a0. PubMed PMID: 15976322.

38. Komulainen K, Alanne M, Auro K, Kilpikari R, Pajukanta P, Saarela J, Ellonen P, Salminen K, Kulathinal S, Kuulasmaa K, Silander K, Salomaa V, Perola M, Peltonen L. Risk alleles of USF1 gene predict cardiovascular disease of women in two prospective studies. PLoS Genet. 2006;2(5):e69. Epub 2006/05/16. doi: 10.1371/journal.pgen.0020069. PubMed PMID: 16699592; PMCID: 1458962.

39. Lee JC, Weissglas-Volkov D, Kyttala M, Sinsheimer JS, Jokiaho A, de Bruin TW, Lusis AJ, Brennan ML, van Greevenbroek MM, van der Kallen CJ, Hazen SL, Pajukanta P. USF1 contributes to high serum lipid levels in Dutch FCHL families and U.S. whites with coronary artery disease. Arterioscler Thromb Vasc Biol. 2007;27(10):2222-7. Epub 2007/08/04. doi: ATVBAHA.107.151530 [pii]10.1161/ATVBAHA.107.151530. PubMed PMID: 17673701.

40. Meex SJ, van Vliet-Ostaptchouk JV, van der Kallen CJ, van Greevenbroek MM, Schalkwijk CG, Feskens EJ, Blaak EE, Wijmenga C, Hofker MH, Stehouwer CD, de Bruin TW. Upstream transcription factor 1 (USF1) in risk of type 2 diabetes: association study in 2000 Dutch Caucasians. Mol Genet Metab. 2008;94(3):352-5. Epub 2008/05/01. doi: 10.1016/j.ymgme.2008.03.011S1096-7192(08)00084-X [pii]. PubMed PMID: 18445538.

41. Naukkarinen J, Gentile M, Soro-Paavonen A, Saarela J, Koistinen HA, Pajukanta P, Taskinen MR, Peltonen L. USF1 and dyslipidemias: converging evidence for a functional intronic variant. Hum Mol Genet. 2005;14(17):2595-605. Epub 2005/08/04. doi: ddi294 [pii]10.1093/hmg/ddi294. PubMed PMID: 16076849.

42. Naukkarinen J, Nilsson E, Koistinen HA, Soderlund S, Lyssenko V, Vaag A, Poulsen P, Groop L, Taskinen MR, Peltonen L. Functional variant disrupts insulin induction of USF1: mechanism for USF1-associated dyslipidemias. Circ Cardiovasc Genet. 2009;2(5):522-9. Epub 2009/12/25. doi: 10.1161/CIRCGENETICS.108.840421CIRCGENETICS.108.840421 [pii]. PubMed PMID: 20031629.

43. Ng MC, Miyake K, So WY, Poon EW, Lam VK, Li JK, Cox NJ, Bell GI, Chan JC. The linkage and association of the gene encoding upstream stimulatory factor 1 with type 2 diabetes and metabolic syndrome in the Chinese population. Diabetologia. 2005;48(10):2018-24. Epub 2005/09/01. doi: 10.1007/s00125-005-1914-0. PubMed PMID: 16132950.

44. Plaisier CL, Horvath S, Huertas-Vazquez A, Cruz-Bautista I, Herrera MF, Tusie-Luna T, Aguilar-Salinas C, Pajukanta P. A systems genetics approach implicates USF1, FADS3, and other causal candidate genes for familial combined hyperlipidemia. PLoS Genet. 2009;5(9):e1000642. Epub 2009/09/15. doi: 10.1371/journal.pgen.1000642. PubMed PMID: 19750004; PMCID: 2730565.

45. Reiner AP, Carlson CS, Jenny NS, Durda JP, Siscovick DS, Nickerson DA, Tracy RP. USF1 gene variants, cardiovascular risk, and mortality in European Americans: analysis of two US

cohort studies. Arterioscler Thromb Vasc Biol. 2007;27(12):2736-42. Epub 2007/09/22. doi: ATVBAHA.107.154559 [pii]10.1161/ATVBAHA.107.154559. PubMed PMID: 17885212.

46. van der Vleuten GM, Isaacs A, Hijmans A, van Duijn CM, Stalenhoef AF, de Graaf J. The involvement of upstream stimulatory factor 1 in Dutch patients with familial combined hyperlipidemia. J Lipid Res. 2007;48(1):193-200. Epub 2006/10/27. doi: M600184-JLR200 [pii]10.1194/jlr.M600184-JLR200. PubMed PMID: 17065663.

47. Cardoso S, Santos R, Correia S, Carvalho C, Zhu X, Lee HG, Casadesus G, Smith MA, Perry G, Moreira PI. Insulin and Insulin-Sensitizing Drugs in Neurodegeneration: Mitochondria as Therapeutic Targets. Pharmaceuticals (Basel). 2009;2(3):250-86. Epub 2009/12/23. doi: ph2030250 [pii]10.3390/ph2030250. PubMed PMID: 27713238; PMCID: 3978547.

48. Chow J, Rahman J, Achermann JC, Dattani MT, Rahman S. Mitochondrial disease and endocrine dysfunction. Nat Rev Endocrinol. 2016. Epub 2016/11/04. doi: 10.1038/nrendo.2016.151nrendo.2016.151 [pii]. PubMed PMID: 27716753.

49. Hu H, Tan CC, Tan L, Yu JT. A Mitocentric View of Alzheimer's Disease. Mol Neurobiol. 2016. Epub 2016/10/04. doi: 10.1007/s12035-016-0117-710.1007/s12035-016-0117-7 [pii]. PubMed PMID: 27696116.

50. Petti AA, McIsaac RS, Ho-Shing O, Bussemaker HJ, Botstein D. Combinatorial control of diverse metabolic and physiological functions by transcriptional regulators of the yeast sulfur assimilation pathway. Mol Biol Cell. 2012;23(15):3008-24. Epub 2012/06/15. doi: 10.1091/mbc.E12-03-0233mbc.E12-03-0233 [pii]. PubMed PMID: 22696679; PMCID: 3408426.

51. Winzeler EA, Shoemaker DD, Astromoff A, Liang H, Anderson K, Andre B, Bangham R, Benito R, Boeke JD, Bussey H, Chu AM, Connelly C, Davis K, Dietrich F, Dow SW, El Bakkoury M, Foury F, Friend SH, Gentalen E, Giaever G, Hegemann JH, Jones T, Laub M, Liao H, Liebundguth N, Lockhart DJ, Lucau-Danila A, Lussier M, M'Rabet N, Menard P, Mittmann M, Pai C, Rebischung C, Revuelta JL, Riles L, Roberts CJ, Ross-MacDonald P, Scherens B, Snyder M, Sookhai-Mahadeo S, Storms RK, Veronneau S, Voet M, Volckaert G, Ward TR, Wysocki R, Yen GS, Yu K, Zimmermann K, Philippsen P, Johnston M, Davis RW. Functional characterization of the S. cerevisiae genome by gene deletion and parallel analysis. Science. 1999;285(5429):901-6. Epub 1999/08/07. doi: 7737 [pii]. PubMed PMID: 10436161.

CHAPTER 3: Per-Arnt-Sim Kinase (PASK) Deficiency Increases Cellular Respiration on a Standard Diet and Decreases Liver Triglyceride Accumulation on a Western High-Fat High-Sugar Diet

The following chapter is taken from an article published in Nutrients Journal. All content and figures have been formatted for this dissertation but it is otherwise unchanged.

3.1 Abstract

Diabetes and the related disease metabolic syndrome are epidemic in the United States, in part due to a shift in diet and decrease in physical exercise. PAS kinase is a sensory protein kinase associated with many of the phenotypes of these diseases, including hepatic triglyceride accumulation and metabolic dysregulation in male mice placed on a high-fat diet. Herein we provide the first characterization of the effects of western diet (high-fat high-sugar, HFHS) on Per-Arnt-Sim kinase mice ($PASK^{-/-}$) and the first characterization of both male and female $PASK^{-/-}$ mice. Soleus muscle from the $PASK^{-/-}$ male mice displayed a 2-fold higher oxidative phosphorylation capacity than wild type (WT) on the normal chow diet. $PASK^{-/-}$ male mice were also resistant to hepatic triglyceride accumulation on the HFHS diet, displaying a 2.7-fold reduction in hepatic triglycerides compared to WT mice on the HFHS diet. These effects on male hepatic triglyceride were further explored through mass spectrometry-based lipidomics. The absence of PAS kinase was found to affect many of the 44 triglycerides analyzed, preventing hepatic triglyceride accumulation in response to the HFHS diet. In contrast, the female mice showed resistance to hepatic triglyceride accumulation on the HFHS diet regardless of genotype, suggesting the effects of PAS kinase may be masked.

3.2 Introduction

Diabetes and the related disease metabolic syndrome are an ever-increasing epidemic in today's society. In 2015, 9.4% of the United States population had diabetes and the estimate for metabolic syndrome was much higher at 30% [1,2,3]. Characterized by having a combination of increased blood pressure, high blood sugar, excess body fat around the waist, and abnormal triglyceride levels, metabolic syndrome increases one's risk for heart disease, stroke, and diabetes [1]. The increasing rates of these diseases are in part due to a global shift toward energy-dense, high-fat, low nutrient foods, combined with a decrease in physical activity [4]. As these changes affect the body as a whole, they also challenge the cellular processes in the body as it attempts to adapt to the new nutrient and activity levels. Nutrient sensors play a critical role in adapting to these new levels by constantly monitoring cellular nutrients and regulating cellular pathways to maintain homeostasis [5,6]. When dysregulation in nutrient-sensing pathways occurs, many human diseases such as diabetes and metabolic syndrome develop.

PAS kinase is a nutrient-sensing protein kinase that is conserved from yeast to man [7]. It has been reported to regulate many of the phenotypes associated with metabolic syndrome and/or diabetes. PAS kinase deficiency decreases insulin production, insulin resistance, body weight, and hepatic triglyceride accumulation, while leading to increased glycogen storage as well as metabolic rate (for research articles and associated recent reviews see [8,9,10,11,12,13,14,15,16,17,18,19,20,21]). For example, PAS kinase-deficient ($PASK^{-/-}$) male mice are resistant to weight gain, hepatic triglyceride accumulation and insulin resistance when placed on a high-fat (HF) diet [18]. Without a change in food-intake or exercise, these $PASK^{-/-}$ male mice also exhibit a hypermetabolic phenotype, giving off more CO_2 and taking in more O_2. In addition, several mRNA's involved in lipid biosynthesis are downregulated in $PASK^{-/-}$ male mice such as stearoyl-

CoA desaturase 1 (SCD1), long-chain fatty-acid elongase, fatty-acid transporter (CD36) and the lipid-responsive nuclear hormone receptor peroxisome proliferator-activated receptor γ. This PAS kinase-dependent decrease in hepatic triglycerides on a HF diet has been confirmed in Sprague-Dawley rats treated with pharmacological inhibitors [13]. Furthermore, the genetic and pharmacological inhibition of PAS kinase in cultured cells suggests that these effects are in part due to the inhibition of SREBP-1c proteolytic maturation [13]. PAS kinase itself is also regulated by cellular nutrient status. PAS kinase activity and/or mRNA expression increases under conditions of increasing nutrients, specifically upon feeding in mice [13] or at high glucose concentrations in mammalian cells [14].

Herein we characterize the molecular effects of PAS kinase on respiration and triglyceride metabolism, as well as how PAS kinase alters these pathways in response to diet and sex. This study utilized cellular respiration assays, western blots for electron transport chain protein abundance, and triglyceride metabolomics approaches. To determine the effect of diet in $PASK^{-/-}$ mice, we investigated the addition of sugar to the previously reported HF diet (a high-fat high-sugar diet, HFHS diet). This diet provides conditions where PAS kinase may be more active (high-sugar) while also more accurately reflecting the Western Diet of today's society (high-sugar and high-fat [22]). In addition, we consider sex (female versus male mice) when characterizing the molecular effects of PAS kinase, which has been not been previously reported. These findings will aid in understanding the effects of PAS kinase as well as a HFHS diet on metabolism, shedding light on the pathways that contribute to diseases such as metabolic syndrome and diabetes.

3.3 Materials and methods

3.3.1 Animals

C57BL/6 (Charles River Laboratories Wilmington, MA, USA) PASK$^{-/-}$ mice were generously donated by Jared Rutter (University of Utah) and were described previously [18]. Wild type C57BL/6 were obtained from Charles River Laboratories Wilmington, MA. Age-matched male and female wild type and PASK$^{-/-}$ mice, generated by breeding PASK$^{+/-}$ mice, were placed on a HFHS diet (D12266Bi Condensed Milk Diet from Research Diets—16.8% kcal protein, 31.8% kcal fat, 51.4% kcal carbs—primarily sucrose, lactic casein and corn starch) or normal chow (NC) diet (Teklad Rodent Diet 8604 from Envigo—32% protein, 14% fat, 54% carbs—primarily dehulled soybean meal) at 12 weeks old and maintained on the diet for a total of 25 weeks. Mice were co-housed at no more than 5 mice/cage according to sex, genotype and assigned diet in a conventional animal house. Food and water were freely available, and mice were on a 12-h light/dark cycle. All procedures were approved by the Brigham Young University Institutional Animal Care and Use Committee (protocol numbers 13-1003 submitted by L.C.B.).

3.3.2 Study design

The design was based on the characterization of PASK$^{-/-}$ male mice on the HF diet wherein mice were placed on the HF diet at 12 weeks, and 12–24 mice of each group were used to obtain statistical significance of several phenotypes including body weight [18]. The study herein contains 8 experimental groups including male and female WT NC diet, WT HFHS diet, PASK$^{+/-}$ NC diet, PASK$^{+/-}$ HFHS diet that were kept on the HFHS diet for 25 weeks prior to tissue harvest. More male then female mice were required due to limited tissues (such as liver tissue for triglyceride assay versus oxygen consumption assay). An account of all animals used in this study is provided in Figure S1.

3.3.3 Respiration assays

Liver tissue and soleus muscle was harvested and immediately used for respiration assays. O_2 consumption was determined using an O2K oxygraph (Oroboros Instruments Corp, Innsbruck, Austria) as previously described [23]. Tissues were minced with a scalpel and permeabilized with saponin (50 ug/ml). A baseline respiration rate was determined in each respiration chamber and then the samples were added. Respiration was measured by following the substrate-uncoupler-inhibitor-titration (SUIT) protocol: glutamate, malate, and succinate (GMS) were added to assess complex I and II electron flow. ADP (2.5 mM) was then added to determine oxidative phosphorylation capacity (GMSD). Following data collection, three-factor Analysis of Variance (ANOVA) was performed using JMP Pro14 software with Tukey post-hoc test for three-factor and two-factor comparisons and students t-test for one-factor comparisons.

3.3.4 Western blot analysis

Muscle tissue was homogenized using the Bullet Blender Storm 24 (Next Advance) in RIPA Lysis and Extraction buffer (ThermoFisher Scientific, Waltham, MA, USA catalog number 89900) with Halt Protease Inhibitor Cocktail (ThermoFisher Scientific, Waltham, MA, USA, catalog number 78438) using 2 mm Zirconium oxide beads. Protein concentration was determined using the Pierce Coomassie Plus (Bradford) Assay Reagent (ThermoFisher Scientific, Waltham, MA, USA). An equal amount of protein (2 ug) was loaded on a 12% SDS-PAGE gel, separated, then transferred onto a nitrocellulose membrane. After incubation with 5% nonfat milk in tris-buffered saline with Tween 20 (TBST), the membrane was rinsed 2 times with tris-buffered saline (TBS) and then probed with the OxPhosBlue Native WB Antibody Cocktail (ThermoFisher Scientific, Waltham, MA, USA) containing mouse monoclonal NDUFA9, SDHA, UQCRC2, COX IV, and ATP5A antibodies for 2 days (these correspond to subunits of complex I, II, III, IV and V). Membranes were rinsed twice

with TBST, once with TBS then incubated with a 1:1000 dilution of horseradish peroxidase-conjugated anti-mouse antibodies for 2 h. Blots were rinsed and then developed using the WesternBright ECL HRP substrate (Advansta Inc., San Jose, CA, USA, catalog number K-12045-D50) according to the manufacturer's protocol. Bands were quantified using the ImageJ software version 1.50i (National Institute of Health, Bethesda, MD, USA) [24]. Two-factor ANOVA was performed using JMP Pro14 (version 14.0) software (SAS Institute, Cary, NC, USA) with student's t-test for one-factor analysis.

3.3.5 Triglyceride assays

Mouse liver samples were homogenized in 110 µL of PBS-Triton. Hepatic triglyceride levels were measured using the BioVision (Milpitas, CA, USA) Triglyceride Quantification Colorimetric/Fluorometric Kit (K622) according to manufacturer's protocol, and absorbance was measured at 530–590 nm. Protein concentration was determined using the Pierce Coomassie Plus (Bradford) Assay Reagent (ThermoFisher Scientific, Waltham, MA, USA). Three-factor ANOVA was performed using JMP Pro14 software with Tukey post-hoc test for three-factor and two-factor interaction analysis and students t-test for one-factor analysis.

3.3.6 Liquid chromatography-mass spectrometry (LC/MS) lipidomics

Forty-four triglycerides were analyzed by LC/MS at the University of Utah Metabolomics Core Facility. Triglycerides were extracted from frozen tissue in 225 µL ice-cold MeOH containing internal standards (Avanti 860902 TG (16:0/18:1/16:0-d5) 100 µg/mL, 10 µL each/sample; cholesterol-d7, 100 µg/mL, 20 µL each/sample) 750 µL of ice-cold MTBE (methyl tert-butyl ether) in bead mill tubes (1.4 mm ceramic, QIAGEN, Venlo, Netherlands, catalog number 13113-50). The sample was homogenized in one 30 s cycle, rested on ice for 15 min, then 300 µL of water was added to induce phase separation. Samples were then centrifuged at 20,000 g for 5 min at 4 °C, the

upper phases are collected separately and evaporated to dryness under vacuum. Triglyceride samples are reconstituted in 200 µL ACN:H2O:IPA (1:1:2) + 0.1% formic acid and transferred to an LC/MS vial with insert for analysis. A pooled QC sample were prepared by taking 40 µL aliquots from each sample. Concurrently a process blank sample was brought forward. Triglyceride extracts were separated on a Waters (Milford, MA, USA) Acquity UPLC CSH C18 1.7 µm 2.1 × 100 mm column maintained at 60 °C connected to an Agilent (Santa Clara, CA, USA) HiP 1290 Sampler, Agilent 1290 Infinity pump, equipped with an Agilent 1290 Flex Cube and Agilent 6530 Accurate Mass Q-TOF dual ESI mass spectrometer. For positive mode, the source gas temperature was set to 200 °C, with a gas flow of 11 L/min and a nebulizer pressure of 50 psig. VCap voltage was set at 5000 V, fragmentor at 100 V, skimmer at 85 V and Octopole RF peak at 750 V. For negative mode, the source gas temperature was set to 270 °C, with a drying gas flow of 8.5 L/min and a nebulizer pressure of 40 psig. VCap voltage is set at 3000 V, fragmentor at 247.5 V, skimmer at 57.5 V and Octopole RF peak at 750 V. Reference masses in positive mode (m/z 121.0509 and 922.0098) were infused with nebulizer pressure at 2 psig, and in negative mode (1033.988, 966.0007, 112.9856 and 68.9958) were infused with a nebulizer pressure at 5 psig. Samples were analyzed in a randomized order in both positive and negative ionization mode in separate experiments acquiring with the scan range between m/z 100 and 1700. Mobile phase A consisted of ACN:H2O (60:40 v/v) in 10 mM ammonium formate and 0.1% formic acid, and mobile phase B consisted of IPA:ACN:H2O (90:9:1 v/v) in 10 mM ammonium formate and 0.1% formic acid. The chromatography gradient for both positive and negative modes started at 15% mobile phase B then increased to 30% B over 2 min, it then increased to 52% B from 2 to 2.5 min, then increased to 82% B from 2.5 to 11 min, then increased to 95% B from 11 to 11.5 min, then increased to 99% B from 11.5 to 13.5 min. From 13.5 to 20 min it was held at 99% B, then decreased to 15% B from 20 to 20.2 min and held there from

20.2 to 25 min. Flow was 0.35 mL/min throughout, injection volume was 1 µL for positive mode and 5 µL for negative mode. Tandem mass spectrometry was conducted using the same LC gradient at a collision energy of 40 V. Results from LC/MS QQQ experiments were collected using Agilent Mass Hunter Workstation and analyzed using the software packages Mass Hunter Qual and Mass Hunter Quant. Results from MHQuant were exported to Excel, then normalized to internal standard, background subtracted and divided by the tissue mass.

3.3.7 Statistical analysis

Three-factor ANOVA was used throughout the study to analyze the effects of sex, genotype, and diet, with specific differences listed for each method. Where only male mice were use, two-factor ANOVA was used to analyze the effects of genotype and diet. Factorial ANOVA was performed using JMP Pro14 (version 14.0) software with Tukey post-hoc test used for three-factor (sex, genotype, and diet) and two-factor (sex and genotype, sex and diet, genotype and diet) analysis and students t-test used for one-factor (sex, genotype, or diet) analysis. Analysis of combined factors is indicated by "*". For example, "sex and genotype" is written is sex*genotype.

3.4 Results

3.4.1 PAS kinase-deficient mice exhibit increased respiration when on a normal chow (NC) diet

Previous studies have reported a hypermetabolic phenotype for $PASK^{-/-}$ mice on a HF diet, including increased whole-animal O_2 intake and CO_2 output [9]. This phenotype may be due to increased respiration in peripheral tissues. Therefore, we measured cellular oxygen consumption rates in female and male soleus muscle, a muscle primarily composed of slow oxidative fibers, as well as in female and male liver tissue (Figure 3.1). The soleus tissue of both female and male $PASK^{-/-}$ mice displayed a trending increase in basal respiration rate on the NC diet when compared to WT mice upon three-factor (sex, diet, genotype) analysis. Two-factor and one-factor analysis were

used to determine if any factors were significantly contributing to this trending increase. Two-factor analysis using combined factors such as sex and genotype (sex*genotype, sex*diet, or genotype*diet) revealed no significant interaction of factors, but further one-factor analysis revealed that the PASK$^{-/-}$ genotype was mainly responsible for significantly increasing respiration (a ~1.5-fold increase), with sex or diet having no significant effect (Figure 1A,D, GMS). In addition, a dramatic effect in oxidative phosphorylation capacity (GMSD) was observed in soleus tissue of the male NC diet PASK$^{-/-}$ mice, which showed a 2-fold increase when compared to the WT in soleus tissue (Figure 3.1A, GMSD). A three-factor ANOVA followed by two-factor analysis indicate sex*genotype as well as genotype*diet as the main contributing factors to this increase, suggesting a complex interaction of these factors (Figure 1C,D). Combined, the soleus muscle results are consistent with whole-body oxygen consumption increases in PASK$^{-/-}$ mice reported for the whole-animal on a HF diet [9]. In comparison, the liver oxygen consumption rates displayed small differences when compared to the soleus. The WT mice showed decreased basal respiration in response to the HFHS diet, with main dependence on the genotype*diet interaction in the two-factor analysis (Figure 3.1E). In addition, there were main dependences on sex (an increase in male) and diet (a decrease on HFHS) in the one-factor analysis for liver oxidative phosphorylation capacity (Figure 3.1F).

Adenosine triphosphate (ATP) assays were performed to determine if the increased capacity for oxidative phosphorylation observed in the soleus tissue of PASK$^{-/-}$ mice translates to increased ATP (Figure 3S.2). Soleus tissue from male mice was used due to the increased respiration rates observed in this tissue on the NC diet; however, no significant differences were observed. This inability to observe a difference may in part be due to the necessity to use mice from a later cohort of the same breeding colony (see Figure 3S.2 legend).

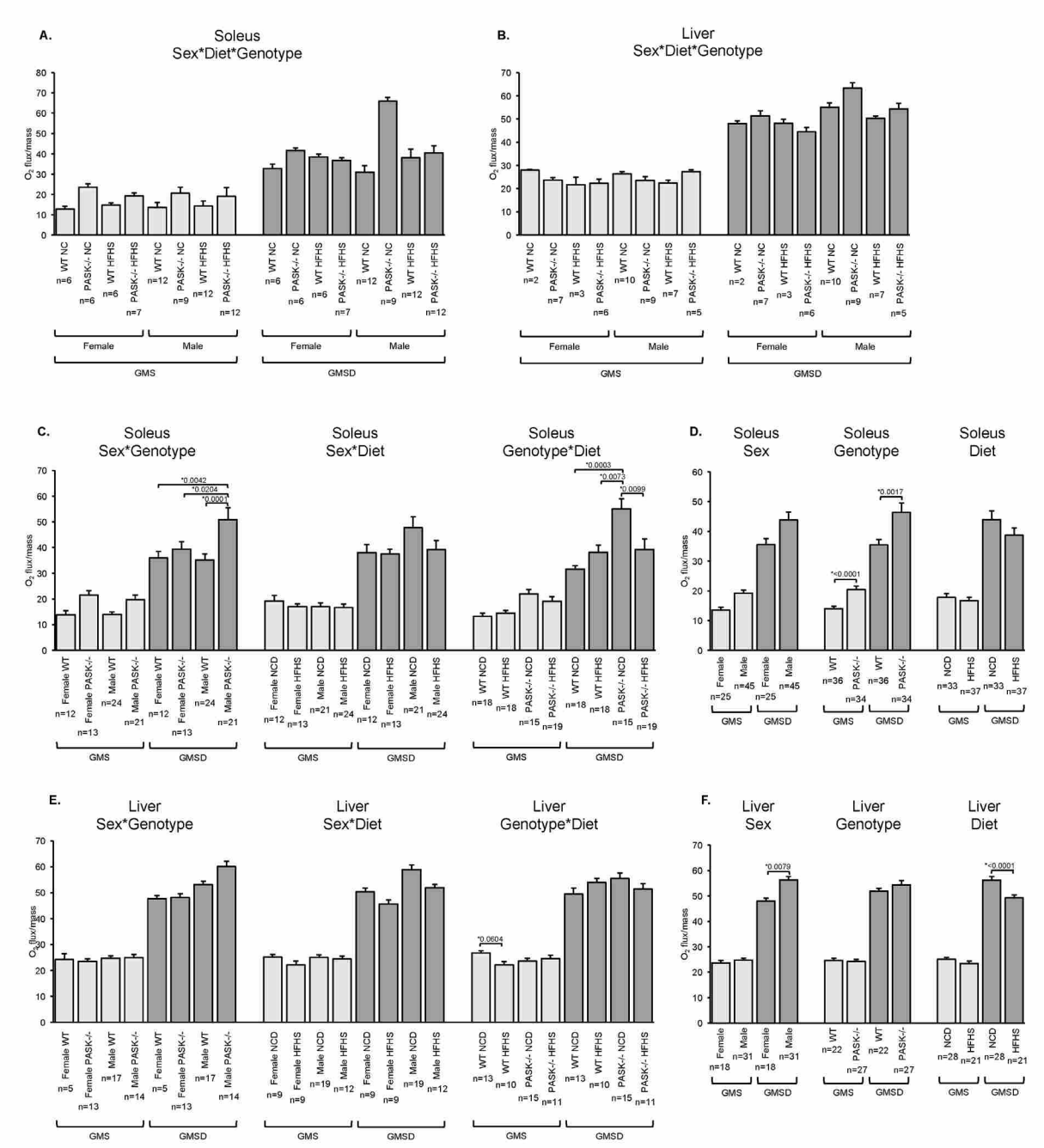

Figure 3.1 PAS kinase-deficient mice (PASK$^{-/-}$) exhibit increased respiration on a normal chow diet. (A–F) Soleus muscle and liver tissue mitochondrial O_2 consumption determined according to the protocol in Materials and Methods. Results shown are a basal respiration rate (GMS) and oxidative phosphorylation capacity (GMSD). (A,B) three-factor analysis (sex, genotype, and diet) for (A) soleus and (B) liver tissue. (C,E) two-factor analysis (sex and genotype, sex and diet or genotype and diet) for (C) soleus and (E) liver tissue. (D,F) one-factor analysis (sex, genotype, or diet) for (D) soleus and (F) liver tissue. NC is Normal Chow, HFHS is High-Fat High-Sugar diet. For all figures, error bars represent standard error of the mean (SEM). Three-factor ANOVA was performed using JMP Pro14 software. Significant differences were further analyzed by Tukey post-hoc test for three-factor and two-factor comparisons and students t-test for one-factor comparisons. *$p < 0.05$ are reported.

3.4.2 Decreased complex I protein is observed on the HFHS diet

To investigate the molecular mechanisms behind the increased basal and oxidative phosphorylation capacity in PASK$^{-/-}$ mice soleus tissue, western blot analysis was used to quantify central electron transport chain protein subunits including NDUFA9 (complex I), SDHA (complex II, 70), UQCRC2 (complex III, core II), COX IV (complex IV, subunit IV), and ATP5A (complex V alpha subunit) (Figure 2). Male mice were used due to the increased magnitude of respiration effects observed (see Figure 3.1). Quantification of these 5 electron transport chain complexes reveals one significant difference in the HFHS PASK$^{-/-}$ mice compared to the NC WT for complex I (Figure 3.2A). Further one-factor ANOVA analysis revealed that this difference is due to diet and not genotype, with the HFHS diet decreasing complex I (Figure 3.2B). Thus, the effects of PAS kinase on basal respiration or oxidative phosphorylation capacity in the male mice may not be detectable by our western blot assay. For example, the effects may be on other subunits of these complexes or in other pathways, or they may be post-translational modifications as can often be expected for a protein kinase.

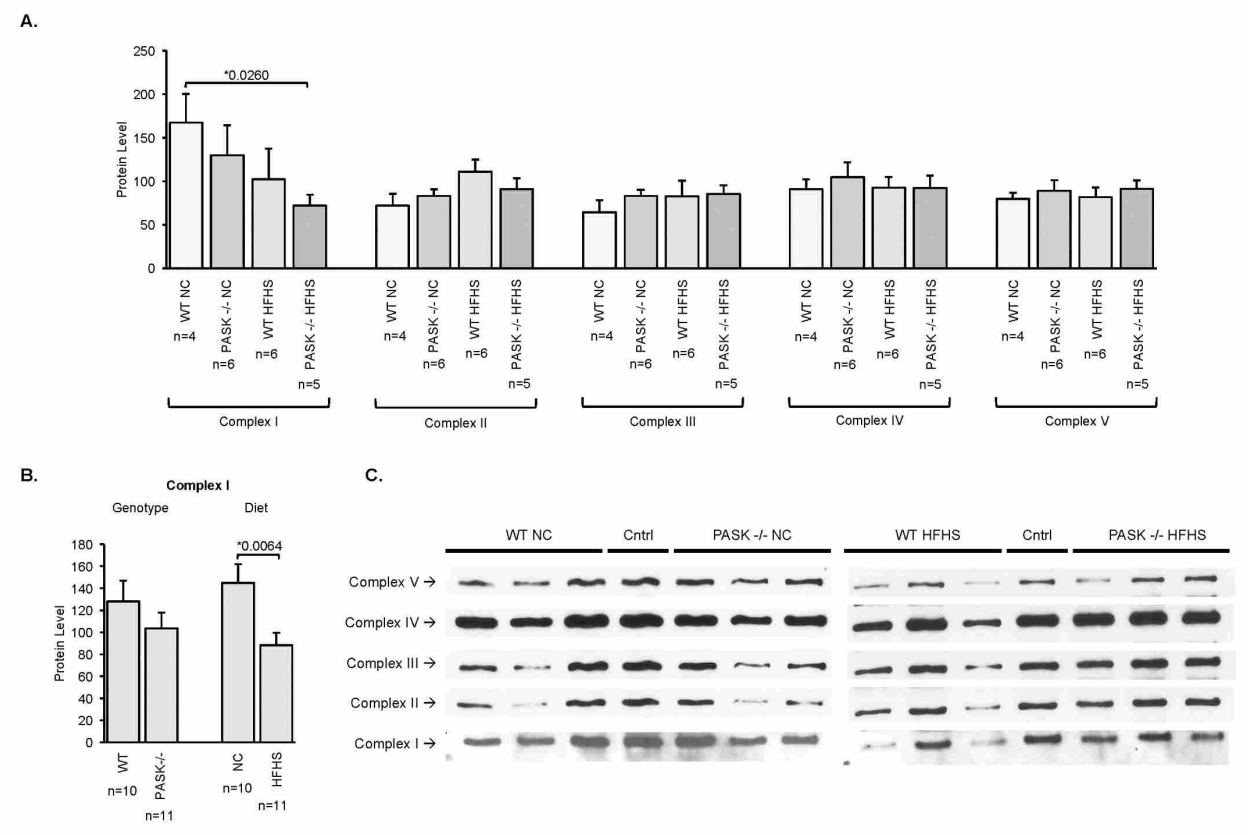

Figure 3.2 Quantification of 5 electron transport chain complexes using homogenized soleus muscle reveals no significant differences in the PAS kinase-deficient male ($PASK^{-/-}$) mice compared to the WT. (A) Soleus tissue was homogenized and analyzed by western blot using the OxPhosBlue Native WB Antibody Cocktail (ThermoFisher Scientific, Waltham, MA, USA) containing mouse monoclonal NDUFA9 (complex I), SDHA (complex II), UQCRC2 (complex III, core II), COX IV (complex IV, subunit IV) and ATP5A (complex V alpha subunit) antibodies. Protein concentration was determined before loading using the Pierce Coomassie Plus (Bradford) Assay Reagent (ThermoFisher Scientific, Waltham, MA, USA). The same control sample (cntrl) was loaded on each gel for normalization between gels. (B) Plots of one-factor (genotype or diet) analysis of complex I. (C) Representative western blots for each complex are shown. Each biological replicate $n > 4$ was run in duplicate. Error bars represent SEM. Two-factor (genotype and diet) ANOVA was performed using JMP Pro14 software with students t-test performed on significant differences, * $p < 0.05$ is shown.

3.4.3 Male PASK$^{-/-}$ mice displayed resistance to accumulation of hepatic triglyceride when placed on a HFHS diet

Total body weight was measured over 25 weeks, with fat pads measured at week 25 (Figure 3.3A–C). Female PASK$^{-/-}$ mice displayed a trend for decreased starting weight (Figure 3.3A, week 1 of diet) on the standard diet. Further factorial ANOVA analysis revealed the decreased female PASK$^{-/-}$ starting weight was mainly due to independent effects of sex, genotype, and diet (Figure 3.3F, Figure 3.S3A–C). Male mice weighed significantly more than the female mice after 25 weeks on the HFHS diet. The two-factor interaction analysis suggested these effects were due to interactions between sex*diet and genotype*diet (Figure 3.3F and Figure 3.S3A–C). No significant difference in weight was observed at 25 weeks when comparing the WT and PASK$^{-/-}$mice on the HFHS diet. This result is contrary to the resistance to weight gain on a HF diet reported for PASK$^{-/-}$ male mice [9]. These differences could be due to the HF versus HFHS diet, statistical analysis differences, or experimental differences since these were not performed on the same cohort. In male HFHS mice, there was a higher percentage of both retroperitoneal and gonadal fat that was not seen in female mice (Figure 3.3B,C). The two-factor interaction analysis suggested the main contributing factors to be a significant interaction between sex*diet for both retroperitoneal and gonadal fat, but not sex*genotype or genotype*diet (Figure 3.3F and Figure 3.S3D–I). Thus, no significance was seen for the PASK$^{-/-}$ genotype. When liver weight was measured as a percentage of body weight, a trending decrease in weight was seen in both male and female mice on a HFHS diet regardless of genotype (Figure 3.3D). The two-factor interaction revealed no major contributions from interaction, while the one-factor interaction analysis revealed diet as the only main contributing factor (Figure 3.3F and Figure 3.S3J–L). In summary, the most significant effects on weight due to PAS kinase deficiency appear to be decreased starting weights of female mice. Additionally, females

do not display the same magnitude of body weight difference on the HFHS diet compared to the NC diet as the males do, while both male and female on the HFHS diet have decreased relative liver weight.

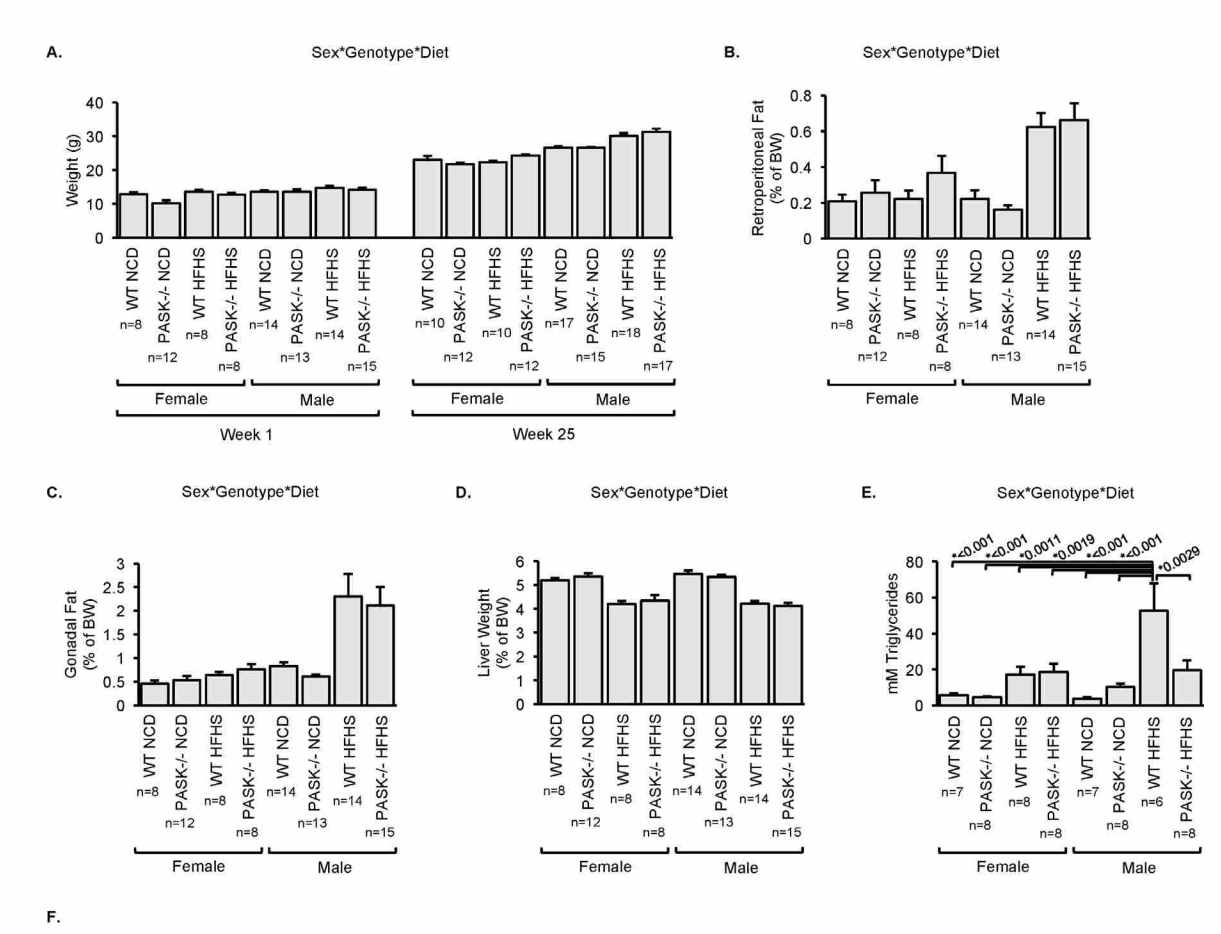

F.

	Start Weight	Final Weight	Retroperitoneal Fat (% of BW)	Gonadal Fat (% of BW)	Liver weight (% of BW)	mM Triglycerides
Source	**Prob > F**	**Prob > F**	**Prob > F**	**Prob > F**	**Prob > F**	**Prob > F**
Sex	0.0022*	<.0001*	0.0042*	<.0001*	0.927	0.0112*
Genotype	0.0457*	0.3653	0.4144	0.7963	0.8266	0.0924
Diet	0.0165*	<.0001*	<.0001*	0.0001*	<.0001*	<.0001*
Sex*Genotype	0.1727	0.9497	0.2985	0.459	0.1627	0.082
Sex*Diet	0.4994	0.0039*	0.0003*	0.0030*	0.2658	0.0378*
Genotype*Diet	0.5982	0.0320*	0.3484	0.9239	0.9834	0.0186*
Sex*Genotype*Diet	0.2324	0.5064	0.9901	0.9667	0.9641	0.0089*

Figure 3.3 PAS kinase deficiency protects against HFHS-induced accumulation of hepatic triglycerides. (A) Body weight of male and female mice at the start of the diet (week 1, 12-week-old mice) and the end of the diet (week 25). (B) Retroperitoneal fat, (C) gonadal fat and (D) liver weight as a percentage of Body Weight (BW). (E) Hepatic triglyceride quantification for female and male mice using BioVision Triglyceride Quantification kit. (F) Factorial ANOVA analysis (sex, genotype, and diet) results for the data presented in (A–E). NC is Normal Chow diet, HFHS is High-Fat High-Sugar diet. For all figures, error bars represent SEM. Three-factor ANOVA was performed using JMP Pro14 software with Tukey post-hoc test for three-factor and two-factor (sex and genotype, sex and diet, or genotype and diet) comparisons and students t-test for one-factor (sex, genotype, or diet) comparisons. * $p < 0.05$ are shown in (A–E) for the three-factor analysis.

Both PASK$^{-/-}$ male mice [18] and rats [13] were previously shown to be resistant to hepatic triglyceride accumulation when placed on a HF diet. The effect of PAS kinase in male mice on the HFHS diet appeared to be similar when we assayed total hepatic triglycerides with an enzymatic kit (Figure 3.3E). Hepatic triglycerides increased in WT male mice placed on the HFHS diet, while no significant increase occurred in PASK$^{-/-}$ male mice on the same diet (there was a 2.7-fold reduction in total triglycerides when compared to the WT mice on the HFHS diet). This trend was not reflected in the female mice, as they appeared to be resistant to hepatic triglyceride accumulation on a HFHS diet. Factorial ANOVA revealed that male WT HFHS mice had elevated triglycerides when compared to all other mouse groups, and indicated this difference was due to a complex, three-factor interaction between sex, genotype, and diet (Figure 3.3F and Figure 3.S3M–O).

3.4.4 Male PASK$^{-/-}$ mice resist hepatic triglyceride accumulation in a relatively non-specific manner

To determine if the PAS kinase-associated protection from triglyceride accumulation was specific for particular triglycerides, LC/MS lipidomic analysis was performed on 6 male mice from each of the 4 mouse groups by the University of Utah Metabolomics Core Facility. When all 44 of the triglycerides analyzed were totaled the mice displayed a similar pattern to the enzymatic total triglyceride quantification performed in our laboratory (which may represent far more than 44 triglycerides). An analysis of each of the triglycerides quantified in the LC/MS lipidomic study is presented in a heat map (Figure 3.4A). PAS kinase appears to regulate triglycerides almost indiscriminately, with the pattern of most triglycerides mimicking that which was seen in the total triglycerides. Twenty-five triglycerides were significantly elevated in the WT mice ($p < 0.05$) but not the PASK$^{-/-}$ mice in response to HFHS diet, 10 others are close to significance ($p < 0.1$). Examples of 2 of these 25 triglycerides are shown (Figure 3.5A). The false discovery rate (FDR) q-value was

less than 8.22% for all these 25 indicating that ~2 (2.05) may be false positives. To achieve a predicted rate of only one false positive, a FDR *q*-value of <0.06 must be chosen, leaving 18 triglycerides as significant. A few triglycerides were not elevated in WT HFHS mice, suggesting that diet did not affect the accumulation of these triglycerides. Examples from 2 of these non-affected triglycerides are shown (Figure 3.5B). One triglyceride to note is TG (15:0_18.2_18.2) (Figure 3.5C). This triglyceride is elevated in the WT HFHS as can be expected, but it is also significantly elevated in the PASK$^{-/-}$ HFHS. When the side chains of the 44 triglycerides were analyzed and quantified as saturated fatty acid (SFA), monounsaturated fatty acid (MUFA), and polyunsaturated fatty acid (PUFA), PAS kinase appeared to more specifically regulate SFA (Figure 3.5D–I). The two-factor interaction analysis indicated that the SFA significance was mainly due to an interaction between diet and genotype. In support of this effect, the 25 PAS kinase-dependent triglycerides (*q*-value < 0.0822%) represented 90% of the 44 triglycerides by abundance.

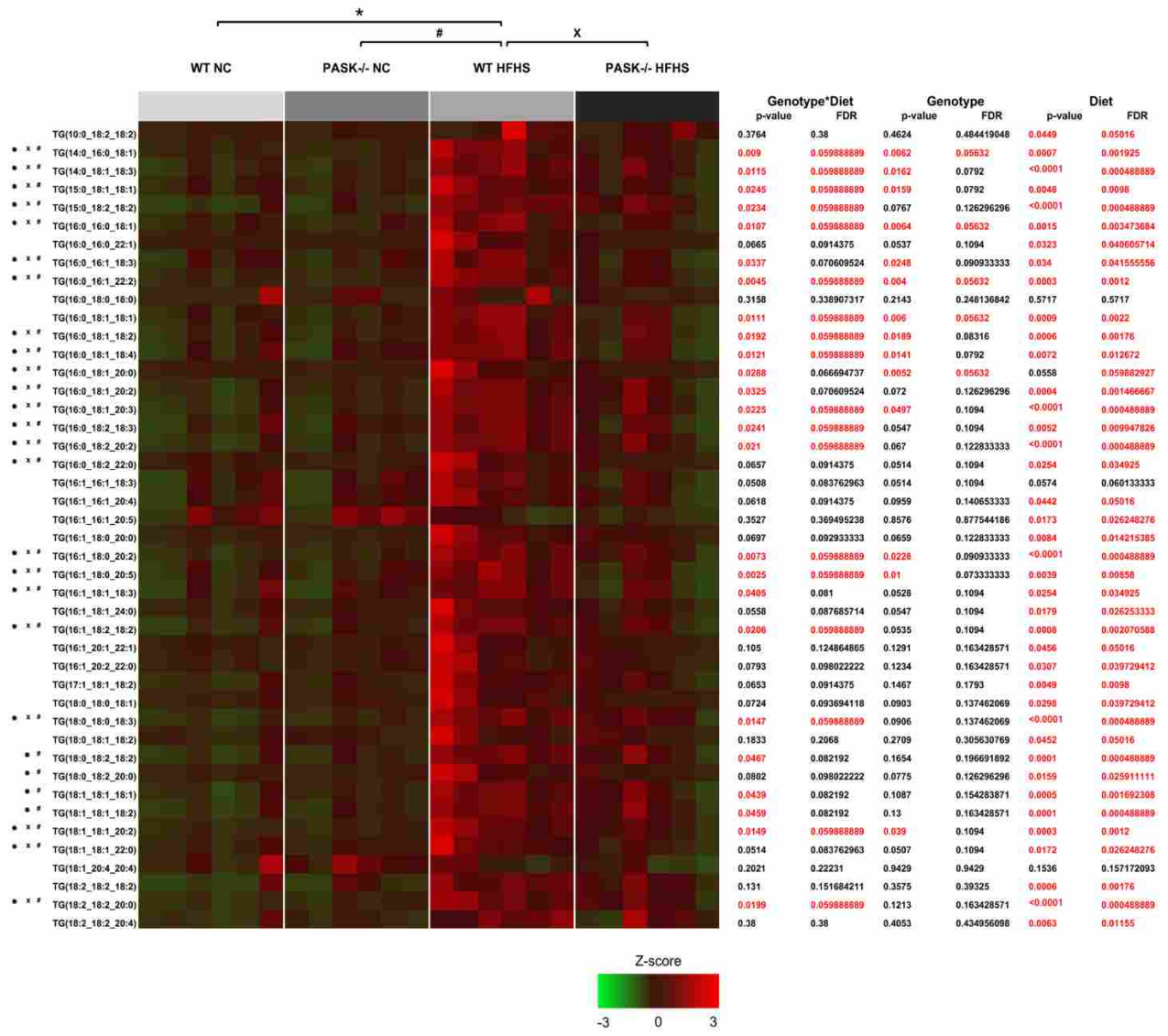

Figure 3.4 LC/MS triglyceride analysis of WT and PASK$^{-/-}$ male mice on NC and HFHS reveal significant changes in individual triglycerides. A heat map LC/MS triglyceride analysis from male WT and PASK$^{-/-}$ mice placed on a NC and HFHS diet (n = 6 for each of 4 sample groups) *, #, or X, $p < 0.05$ when analyzed by two-factor ANOVA and Tukey post-hoc test. Two-factor (genotype and diet) and one-factor (genotype or diet) interaction analysis is provided in a table on the right with p-values and false discovery rates (FDR) given. Significant p-values ($p < 0.05$) are shown in red, with alternative FDR q-value cutoff ($p < 0.0599$) provided in red for comparison.

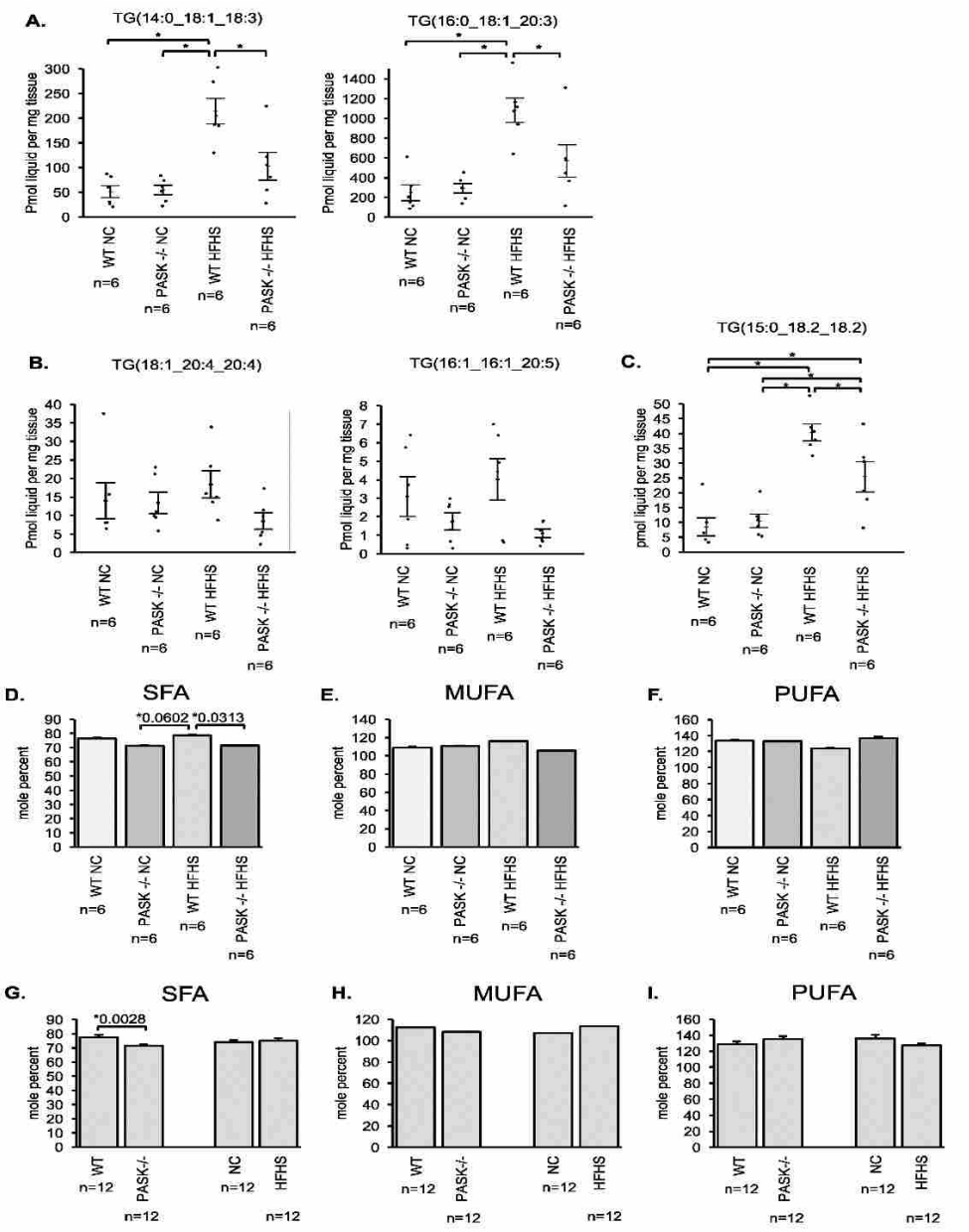

Figure 3.5 Saturated fatty-acid side chains are elevated in WT male mice on the HFHS diet but not PASK−/− male mice on the HFHS diet . (A) Examples of PAS kinase-dependent protection from triglyceride accumulation. (B) Examples of triglycerides that were not significantly affected by the HFHS diet. (C) One triglyceride that increased in response to the HFHS diet in the PASK$^{-/-}$ mouse. Bars represent SEM. * $p <$ 0.05 when analyzed by two-factor ANOVA and Tukey post-hoc test. (D–F) Data in Figure 4 was analyzed for saturated fatty acid (SFA), monounsaturated fatty acid (MUFA), and polyunsaturated fatty acid (PUFA) side chains within each triglyceride. Side-chain abundance was calculated using mole percent ratio (percentage of moles of each fatty-acid side chain compared to total mole concentration). $p < 0.1$ when analyzed by two-factor ANOVA and Tukey post-hoc test. (G–I) One-factor (genotype or diet) analysis of (D–F). $p < 0.05$ when analyzed by student's t-test.

3.5 Discussion

The regulation of respiratory and triglyceride metabolism lies at the center of several prevalent diseases including heart disease, obesity, diabetes, metabolic syndrome, and cancer. Previous studies have shown PASK$^{-/-}$ mice to be resistant to hepatic triglyceride accumulation and to have a whole-body hypermetabolic phenotype when placed on a HF diet [18]. In support of these observations, we have shown PAS kinase to play a pivotal role in regulating cellular respiration in yeast as well [25,26]. Herein we build upon these studies by performing the first characterization of cellular respiration, quantification and analysis of hepatic triglyceride accumulation, and body weight changes in both male and female PASK$^{-/-}$ mice (previous reports were solely in male mice). Furthermore, this is the first report of these mice on a HFHS diet, a diet that may more accurately reflect the western diet [22]. PAS kinase has been previously shown to be activated by high glucose in mammalian tissue [14]. Due to the presence of sugar in this HFHS diet, we expected PAS kinase to be more active and the related phenotypes to be more pronounced.

We observed increased oxygen consumption rates in PASK$^{-/-}$ mice in soleus muscle tissue that was dependent on genotype (Figure 3.1). This is consistent with the whole-body hypermetabolism (increased O_2uptake and CO_2 output) in PASK$^{-/-}$ mice placed on a HF diet [18] as well as the increased cellular respiration rate in PAS kinase-deficient yeast [25,26]. This increase, however, was often seen on the NC diet and was blunted on HFHS (Figure 1). Male PASK$^{-/-}$ mice also displayed significant increases in the oxidative phosphorylation capacity in soleus tissue. ANOVA analysis revealed this difference to be mainly due to complex interactions between sex*genotype as well as genotype*diet. Overall, the effects of PAS kinase on respiratory function were detectable on the NC diet but not the HFHS, in contrast to the whole-body hypermetabolic phenotype reported on the HF diet [18]. This result is opposite of what we expected due to previous

reports of PAS kinase activation by high glucose [14]. These differences may be due to many experimental variables including single cell respiration versus whole-animal metabolism, feed and the metabolism of feed, age of animal, in vitro versus in vivo respiration assay conditions, generations from F0 parent, compensation by alternate pathways, etc. However, the trend of $PASK^{-/-}$ displaying increased metabolism is conserved wherever we do see a difference in respiration.

In contrast to the respiratory function, the role of PAS kinase in regulating hepatic triglyceride accumulation is most evident in male mice on the HFHS diet (Figure 3.3E). The WT male mice displayed a dramatic increase in hepatic triglyceride levels when placed on the HFHS diet, whereas the $PASK^{-/-}$ male mice did not show any appreciable increase. This effect was similar to that reported for the $PASK^{-/-}$ mice on the HF diet [18]. The female mice, in contrast, appeared to be more resistant to liver triglyceride accumulation in response to the HFHS diet (Figure 3.3E). Our results are consistent with previous reports that female WT mice are more resistant to triglyceride accumulation on the HFHS diet [27]. This suggests that sex differences may be overshadowing the role of PAS kinase in females.

LC/MS lipidomic analysis of 44 hepatic triglycerides from male mice revealed that almost all (40/44) were elevated in response to the HFHS diet in WT mice ($p < 0.05$). $PASK^{-/-}$ mice were resistant to accumulation of 25 of these 40 triglycerides ($p < 0.05$, FDR q-value < 0.0822), with another 10 close to significance. ANOVA analysis revealed that this resistance was mainly due to the interaction of genotype*diet rather than sex*diet or diet*genotype. Further analysis of these 44 triglycerides revealed that PAS kinase preferentially regulates saturated fatty-acid side chains (SFA) (Figure 3.5D–I). The 25 PAS kinase-dependent triglycerides represented 90% of the 44 triglycerides by abundance, indicating the side-chain analysis of all 44 may reveal PAS kinase-dependent effects.

As predicted from the triglyceride data, male mice displayed an increase in total body weight as well as retroperitoneal and gonadal fat pad (% of body weight) on the HFHS diet, while we saw no significant increase in female mice (Figure 3.3). However, PAS kinase deficiency did not affect body weight or fat pad weight as it did triglyceride accumulation. When looking at the combined data for female mice (which displayed only very small changes in total body mass, fat accumulation, or hepatic triglyceride accumulation) it appears that the HFHS diet is having a very limited effect on female metabolism. This study highlights how diet and genetic effects may be masked by sex differences, making it critical to continue studies of PAS kinase in both male and female mice to truly understand how it is functioning in both sexes.

PAS kinase has been shown to be activated by high glucose in cultured human pancreatic islet cells [14] and to be regulated by glucose levels in yeast as well [28], stimulating our interest in the HFHS diet which more closely approximates the western diet and tends to abundant in high fructose corn-syrup and milk products [22]. In this study, the respiratory effects observed in $PASK^{-/-}$ versus WT mice occurred on the NC diet, whereas the triglyceride effects were most significant on the HFHS diet. In addition to the experimental variabilities discussed above, these results may indicate differential regulation of PAS kinase functions, consistent with protein kinases regulating tens of substrates with alternate functions. They may also reflect redundant pathways that mask PAS kinase deficiency, or genetic adaptations that have occurred in these knockout mice [29,30,31]. Such adaptations are less likely to be obscuring our triglyceride data because pharmacological PAS kinase inhibition has also been shown to protect against HF diet-inducted hepatic triglyceride accumulation in rats [13].

The molecular substrates of PAS kinase that elicit the effects on respiration and triglyceride accumulation are just beginning to be uncovered. Wu et al. recently reported PAS kinase as essential

for SREBP-1c maturation in cultured hepatic cells [13]. SREBP-1 is clearly an important transcription factor that drives hepatic fatty acid and triglyceride biosynthesis (for reviews see [32,33,34] and articles therein); however, it is not the only one. Upstream stimulation factors (USFs) are bHLH-leucine zipper transcription factors that bind as homo- or heterodimers to promoter E boxes with the DNA sequence CANNTG and have been associated with hyperlipidemia in many studies [35,36,37,38,39,40,41,42,43,44,45,46,47,48]. Several studies have provided evidence for the direct regulation of fatty-acid synthase expression by USF1 and USF2 [49,50,51]. We have recently provided evidence that PAS kinase phosphorylates and inhibits the yeast homolog of USF1 (Cbf1), which in turn controls both cellular respiration and lipid biosynthesis in yeast [25,26]. Its mammalian homolog, USF1, complements the respiratory defect of CBF1-deficient yeast and is phosphorylated by hPASK in vitro [26]. USF1 and SREBP-1 have been reported to have both synergistic, direct binding [52,53] and independent modes of action [51,54], thus PAS kinase may control triglyceride biosynthesis through the regulation of both proteins. Our ongoing studies are focused on the role of PAS kinase in regulating USF1 function in mammalian cells, including both respiratory and lipid roles.

3.6 Conclusions

Herein we investigated the effects of a HFHS diet, sex and PAS kinase-deficiency on respiratory metabolism, body, fat and liver weight, as well as hepatic triglyceride accumulation. PAS kinase-deficiency resulted in increased basal respiration (~1.5-fold) in soleus tissue, and for male mice, an increased oxidative phosphorylation capacity (2-fold) when on a NC diet. For WT mice, the HFHS diet decreased basal respiration in liver tissue. Although PAS kinase-deficiency did not appear to protect male mice from weight gain, it did decrease hepatic triglyceride accumulation significantly on the HFHS diet, with $PASK^{-/-}$ male mice having a 2.7-fold decrease when compared to the WT

mice. Female mice appeared to be protected from both weight gain and liver triglyceride accumulation on the HFHS diet, which may mask the effects of PAS kinase in these pathways. These results solidify PAS kinase as a regulator of cellular respiration and hepatic triglyceride accumulation, phenotypes associated with diabetes and metabolic syndrome.

3.7 Supplementary materials

Mouse #	Sex	Genotype	Diet	OCR Soleus	OCR Liver	ETC WB	Week 1 BW	Week 25 BW	Retro Fat	Gonadal Fat	Liver Weight	Total TG	TG MS
4-3	F	WT	NC	+	-	-	-	+	-	-	-	-	-
9-3	F	WT	NC	+	-	-	-	+	-	-	-	-	-
32-7	F	WT	NC	+	-	-	+	+	+	+	+	-	-
44-5	F	WT	NC	+	+	-	+	+	+	+	+	+	-
46-1	F	WT	NC	+	-	-	+	+	+	+	+	+	-
46-6	F	WT	NC	+	-	-	+	+	+	+	+	+	-
60-1	F	WT	NC	-	-	-	+	+	+	+	+	+	-
60-6	F	WT	NC	-	-	-	+	+	+	+	+	+	-
71-2	F	WT	NC	-	+	-	+	+	+	+	+	+	-
84-4	F	WT	NC	-	-	-	+	+	+	+	+	+	-
20-4	F	PASK -/-	NC	+	-	-	+	+	+	+	+	-	-
25-2	F	PASK -/-	NC	+	-	-	+	+	+	+	+	+	-
25-3	F	PASK -/-	NC	+	-	-	+	+	+	+	+	-	-
34-5	F	PASK -/-	NC	+	-	-	+	+	+	+	+	-	-
41-3	F	PASK -/-	NC	+	+	-	+	+	+	+	+	+	-
45-8	F	PASK -/-	NC	+	+	-	+	+	+	+	+	+	-
46-8	F	PASK -/-	NC	-	-	-	+	+	+	+	+	+	-
68-1	F	PASK -/-	NC	-	+	-	+	+	+	+	+	-	-
71-7	F	PASK -/-	NC	-	+	-	+	+	+	+	+	+	-
76-3	F	PASK -/-	NC	-	+	-	+	+	+	+	+	+	-
77-1	F	PASK -/-	NC	-	+	-	+	+	+	+	+	+	-
77-4	F	PASK -/-	NC	-	+	-	+	+	+	+	+	+	-
13-4	F	WT	HFHS	+	-	-	-	+	-	-	-	-	-
28-6	F	WT	HFHS	+	-	-	+	+	+	+	+	+	-
32-4	F	WT	HFHS	+	-	-	-	+	-	-	-	-	-
33-7	F	WT	HFHS	+	-	-	+	+	+	+	+	+	-
41-1	F	WT	HFHS	+	+	-	+	+	+	+	+	+	-
44-3	F	WT	HFHS	+	+	-	+	+	+	+	+	+	-
53-6	F	WT	HFHS	-	-	-	+	+	+	+	+	+	-
57-2	F	WT	HFHS	-	+	-	+	+	+	+	+	+	-
86-3	F	WT	HFHS	-	-	-	+	+	+	+	+	+	-

88-4	F	WT	HFHS	-	-	-	+	+	+	+	+	+	-
7-7	F	PASK -/-	HFHS	+	-	-	-	+	-	-	-	-	-
19-3	F	PASK -/-	HFHS	+	-	-	-	+	-	-	-	-	-
21-6	F	PASK -/-	HFHS	+	-	-	-	+	-	-	-	-	-
44-7	F	PASK -/-	HFHS	+	+	-	+	+	+	+	+	+	-
45-6	F	PASK -/-	HFHS	+	+	-	-	+	-	-	-	-	-
45-9	F	PASK -/-	HFHS	+	+	-	+	+	+	+	+	+	-
46-4	F	PASK -/-	HFHS	+	-	-	+	+	+	+	+	+	-
53-3	F	PASK -/-	HFHS	-	-	-	+	+	+	+	+	+	-
54-5	F	PASK -/-	HFHS	-	+	-	+	+	+	+	+	+	-
57-1	F	PASK -/-	HFHS	-	+	-	+	+	+	+	+	+	-
76-1	F	PASK -/-	HFHS	-	+	-	+	+	+	+	+	+	-
98-7	F	PASK -/-	HFHS	-	-	-	+	+	+	+	+	+	-
4-4	M	WT	NC	+	-	-	-	+	-	-	-	+	-
8-3	M	WT	NC	+	-	-	-	+	-	-	-	+	+
9-2	M	WT	NC	+	-	-	-	+	-	-	-	+	-
17-2	M	WT	NC	+	-	+	+	+	+	+	+	+	-
18-1	M	WT	NC	+	-	-	+	+	+	+	+	+	-
21-2	M	WT	NC	+	-	-	+	+	+	+	+	+	+
31-6	M	WT	NC	+	-	-	+	+	+	+	+	+	+
40-4	M	WT	NC	+	-	-	+	+	+	+	+	-	-
42-7	M	WT	NC	+	+	+	+	+	+	+	+	-	+
43-7	M	WT	NC	+	+	-	+	+	+	+	+	-	-
46-3	M	WT	NC	+	+	-	+	+	+	+	+	-	-
46-7	M	WT	NC	+	+	-	+	+	+	+	+	-	+
55-5	M	WT	NC	-	+	-	+	+	+	+	+	-	-
58-1	M	WT	NC	-	+	+	+	+	+	+	+	-	-
59-4	M	WT	NC	-	+	-	-	-	-	-	-	-	-
63-1	M	WT	NC	-	+	+	+	+	+	+	+	-	-
76-2	M	WT	NC	-	+	-	+	+	+	+	+	-	+
77-2	M	WT	NC	-	+	-	+	+	+	+	+	-	-
5-9	M	PASK -/-	NC	+	-	-	-	+	-	-	-	+	-
9-5	M	PASK -/-	NC	+	-	-	-	+	-	-	-	-	+
32-1	M	PASK -/-	NC	+	-	-	+	+	+	+	+	+	-
34-4	M	PASK -/-	NC	+	-	+	+	+	+	+	+	-	-
36-1	M	PASK -/-	NC	+	-	-	+	+	+	+	+	-	-
38-5	M	PASK -/-	NC	+	-	-	+	+	+	+	+	-	+
41-5	M	PASK -/-	NC	+	+	-	+	+	+	+	+	-	-
43-2	M	PASK -/-	NC	+	+	+	+	+	+	+	+	-	+
44-4	M	PASK -/-	NC	+	+	+	+	+	+	+	+	-	-
55-6	M	PASK -/-	NC	-	+	-	+	+	+	+	+	+	+
62-1	M	PASK -/-	NC	-	+	+	+	+	+	+	+	+	-
68-5	M	PASK -/-	NC	-	+	+	+	+	+	+	+	+	-
75-1	M	PASK -/-	NC	-	+	+	+	+	+	+	+	+	-

75-3	M	PASK -/-	NC	-	+	-	+	+	+	+	+	+	+
75-6	M	PASK -/-	NC	-	+	-	+	+	+	+	+	+	+
7-1	M	WT	HFHS	+	-	-	-	+	-	-	-	+	-
8-1	M	WT	HFHS	+	-	-	-	+	-	-	-	+	+
8-4	M	WT	HFHS	+	-	-	-	+	-	-	-	+	-
12-1	M	WT	HFHS	+	-	+	-	+	-	-	-	+	-
14-1	M	WT	HFHS	+	-	-	+	+	+	+	+	-	+
18-4	M	WT	HFHS	+	-	-	+	+	+	+	+	+	-
21-4	M	WT	HFHS	+	-	-	+	+	+	+	+	+	+
22-1	M	WT	HFHS	-	-	-	+	+	+	+	+	-	-
23-3	M	WT	HFHS	+	-	-	+	+	+	+	+	-	-
28-7	M	WT	HFHS	+	-	-	+	+	+	+	+	-	+
41-2	M	WT	HFHS	+	+	+	+	+	+	+	+	-	-
42-3	M	WT	HFHS	+	+	-	+	+	+	+	+	-	-
45-4	M	WT	HFHS	+	+	-	+	+	+	+	+	-	+
61-1	M	WT	HFHS	-	-	+	+	+	+	+	+	-	-
63-3	M	WT	HFHS	-	+	+	+	+	+	+	+	-	-
69-2	M	WT	HFHS	-	+	+	+	+	+	+	+	-	-
71-6	M	WT	HFHS	-	+	-	+	+	+	+	+	-	-
77-6	M	WT	HFHS	-	+	+	+	+	+	+	+	-	+
5-2	M	PASK -/-	HFHS	+	-	-	-	+	-	-	-	+	-
5-5	M	PASK -/-	HFHS	+	-	-	-	+	-	-	-	+	+
14-2	M	PASK -/-	HFHS	+	-	-	+	+	+	+	+	+	+
19-2	M	PASK -/-	HFHS	+	-	+	+	+	+	+	+	+	-
21-3	M	PASK -/-	HFHS	+	-	+	+	+	+	+	+	-	-
21-7	M	PASK -/-	HFHS	+	-	+	+	+	+	+	+	-	-
23-1	M	PASK -/-	HFHS	+	-	+	+	+	+	+	+	-	-
31-5	M	PASK -/-	HFHS	+	-	-	+	+	+	+	+	-	-
35-1	M	PASK -/-	HFHS	+	-	-	+	+	+	+	+	-	-
36-2	M	PASK -/-	HFHS	+	-	-	+	+	+	+	+	-	-
38-6	M	PASK -/-	HFHS	+	-	-	+	+	+	+	+	-	-
43-8	M	PASK -/-	HFHS	+	+	-	+	+	+	+	+	-	-
59-3	M	PASK -/-	HFHS	-	+	+	+	+	+	+	+	-	-
62-6	M	PASK -/-	HFHS	-	+	-	+	+	+	+	+	+	+
72-6	M	PASK -/-	HFHS	-	+	-	+	+	+	+	+	+	+
75-2	M	PASK -/-	HFHS	-	-	-	+	+	+	+	+	+	+
75-7	M	PASK -/-	HFHS	-	+	-	+	+	+	+	+	+	+

Figure 3.S1 An account of all mice used in this study. Includes mouse number for this study, genotype, sex, diet, Oxygen Consumption Rates in soleus tissue (OCR soleus), Oxygen Consumption Rates in liver tissue (OCR liver), electron chain western blot (ETC WB), week 1 and week 25 BW (Body Weight), Liver Weight, Retroperitoneal Fat weight (RetroFat), Gonadal Fat weight, total triglycerides (Total TG), triglyceride mass spectrometry (TG MS). Mice from supplementary Figure 2 are not included because they are not otherwise used in the study.

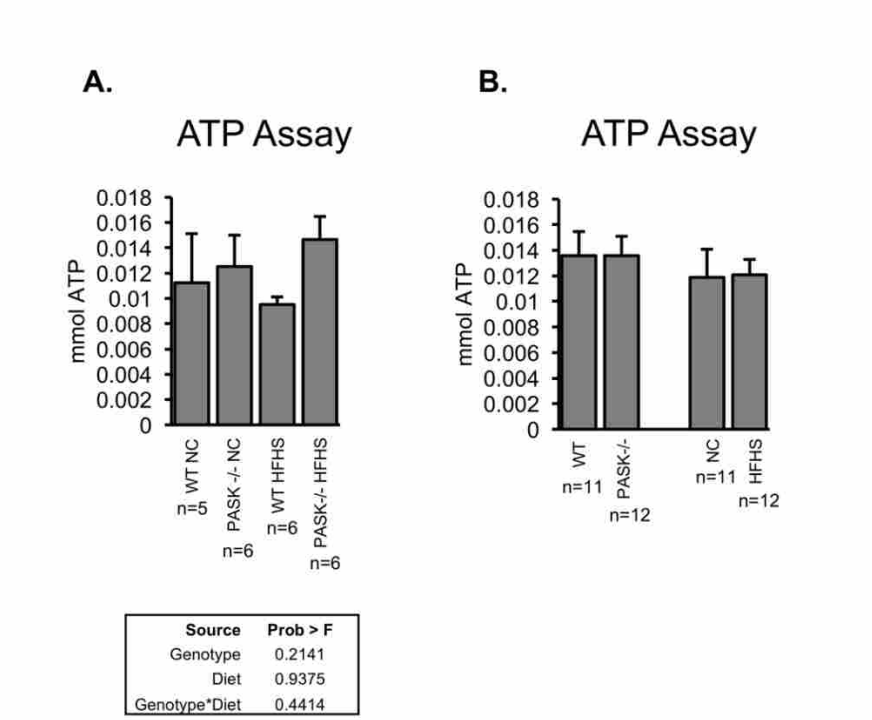

Figure 3.S2 ATP levels of soleus tissue isolated from WT and PASK-/- mice on a normal chow (NC) or high fat high sugar (HFHS) diet suggest no significant differences. Mice were from the same breading colony but an alternate immunology study that had the same genotypes and treatments due to technical difficulties with variability in the flash frozen samples (samples were originally flash frozen for use in both western blot or ATP assay). To overcome these technical variabilities, soleus muscle was harvested and stored at -80°C in ATP Assay buffer (Sigma-Aldrich Adenosine 5'-triphosphate (ATP) Bioluminescent Assay Kit (FLAA-1KT)) prior to the assay. Soleus muscle was homogenized using the Bullet Blender Storm 24 (Next Advance) with 2mm Zirconium oxide beads then deproteinized using the BioVision Deproteinizing Sample Preparation Kit (K808). Due to small amount of protein (0.01ug/ul) the PCA and neutralization buffer in the kit were diluted (1:10 and 1:20 respectively) to prevent excessive PCA or neutralization buffer being added. ATP assays were run using the Sigma-Aldrich Adenosine 5'- triphosphate (ATP) Bioluminescent assay kit (FLAA-1KT) according to manufacturer's protocol. Luminescence was measured using the BioTek Synergy HT Multi-mode microplate reader. Protein concentration was determined using the Pierce Coomassie Plus (Bradford) Assay Reagent (ThermoFisher Scientific, catalog number 23236).

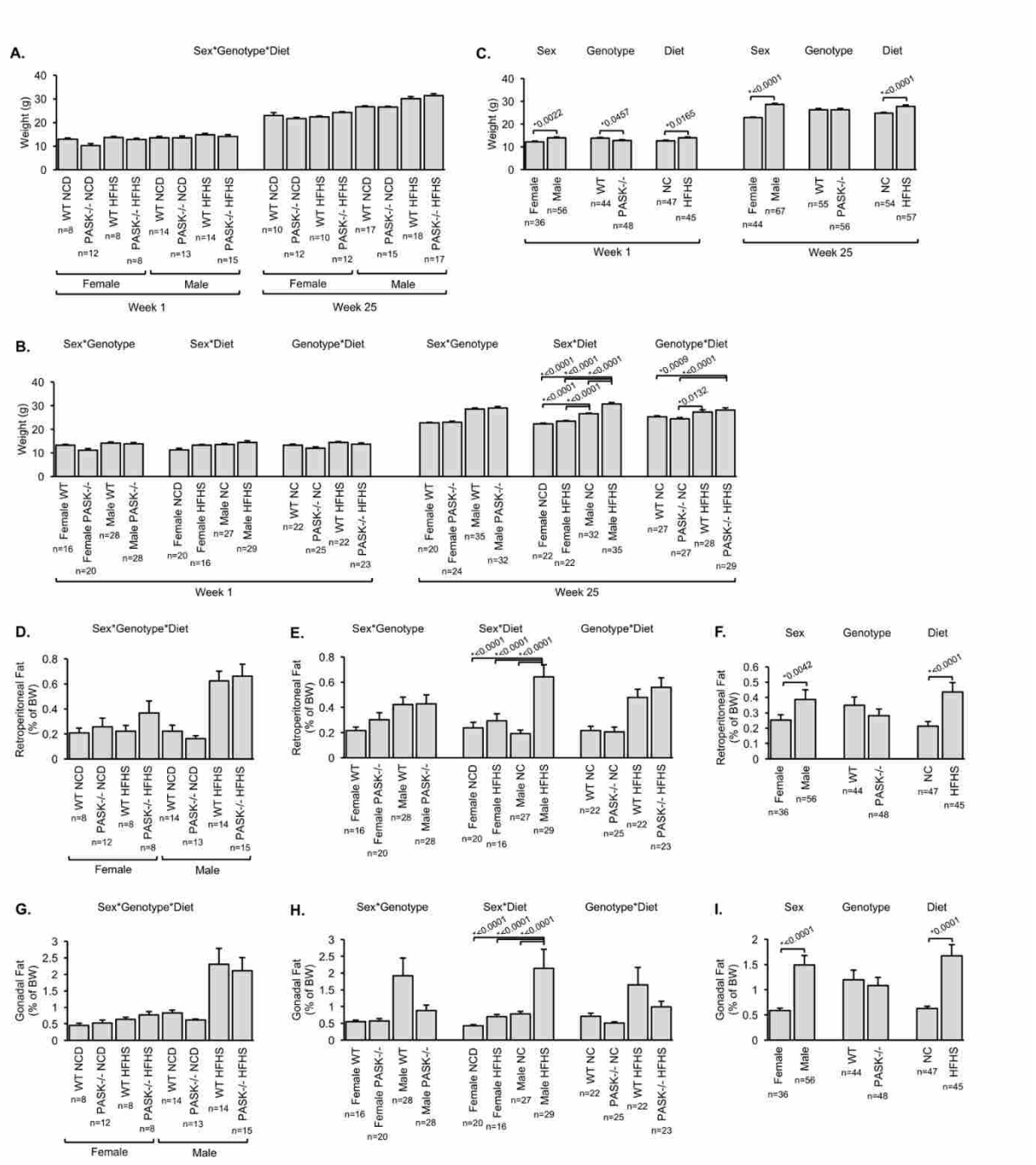
A.
Sex*Genotype*Diet
Weight (g)
WT NCD
PASK-/- NCD
WT HFHS
PASK-/- HFHS
Female
Male
Week 1
Week 25
C.
Sex
Genotype
Diet
Week 1
Week 25
B.
Sex*Genotype
Sex*Diet
Genotype*Diet
Female WT
Female PASK-/-
Male WT
Male PASK-/-
Female NCD
Female HFHS
Male NC
Male HFHS
WT NC
PASK-/- NC
WT HFHS
PASK-/- HFHS
D.
Retroperitoneal Fat (% of BW)
E.
F.
G.
Gonadal Fat (% of BW)
H.
I.

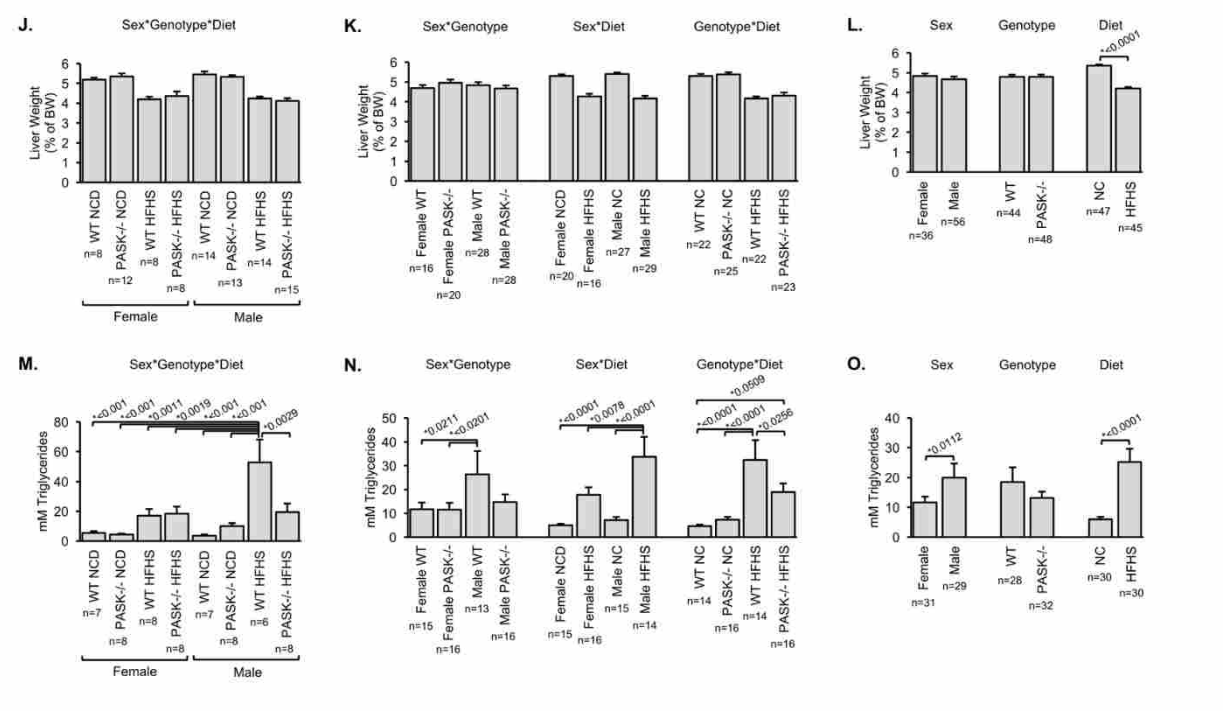

Figure 3.S3 Figures of analysis for three-factor ANOVA of mouse body weights and triglycerides. (A) Body weight of male and female mice at the start of the diet (week 1, 12-week-old mice) and the end of the diet (week 25). Retroperitoneal fat (D), Gonadal fat (G) and Liver weight (J) as a percentage of body weight (BW). (M) Hepatic triglyceride quantification for male and female mice using BioVision Triglyceride Quantification kit. (B, E, H, K, N) two-way interaction analysis of (A, D, G, J, M) respectively. (C, F, I, L,O) one-factor analysis of (A,D, G,J, M). NC is Normal Chow diet, HFHS is High-Fat High-Sugar diet. For all figures, error bars represent SEM. Three-factor ANOVA was performed using JMP Pro14 software with Tukey post-hoc test for three-factor and two-factor comparisons and students t-test for onefactor comparisons. *p < 0.05 is shown.

REFERENCES

1. Alberti, K.G.; Eckel, R.H.; Grundy, S.M.; Zimmet, P.Z.; Cleeman, J.I.; Donato, K.A.; Fruchart, J.C.; James, W.P.; Loria, C.M.; Smith, S.C., Jr.; et al. Harmonizing the metabolic syndrome: A joint interim statement of the International Diabetes Federation Task Force on Epidemiology and Prevention; National Heart, Lung, and Blood Institute; American Heart Association; World Heart Federation; International Atherosclerosis Society; and International Association for the Study of Obesity. *Circulation* 2009, *120*, 1640–1645.

2. Ford, E.S.; Giles, W.H.; Dietz, W.H. Prevalence of the metabolic syndrome among US adults: Findings from the third National Health and Nutrition Examination Survey. *JAMA* 2002, *287*, 356–359.

3. Mokdad, A.H.; Serdula, M.K.; Dietz, W.H.; Bowman, B.A.; Marks, J.S.; Koplan, J.P. The spread of the obesity epidemic in the United States, 1991–1998. *JAMA* 1999, *282*, 1519–1522.

4. Mendoza, J.A.; Drewnowski, A.; Christakis, D.A. Dietary energy density is associated with obesity and the metabolic syndrome in U.S. adults. *Diabetes Care* 2007, *30*, 974–979.

5. Lindsley, J.E.; Rutter, J. Nutrient sensing and metabolic decisions. *Comp. Biochem. Physiol. B Biochem. Mol. Biol.* 2004, *139*, 543–559.

6. Efeyan, A.; Comb, W.C.; Sabatini, D.M. Nutrient-sensing mechanisms and pathways. *Nature* 2015, *517*, 302–310.

7. Rutter, J.; Michnoff, C.H.; Harper, S.M.; Gardner, K.H.; McKnight, S.L. PAS kinase: An evolutionarily conserved PAS domain-regulated serine/threonine kinase. *Proc. Natl. Acad. Sci. USA* 2001, *98*, 8991–8996.

8. Cardon, C.M.; Rutter, J. PAS kinase: Integrating nutrient sensing with nutrient partitioning. *Semin. Cell Dev. Biol.* 2012, *23*, 626–630.

9. DeMille, D.; Grose, J.H. PAS kinase: A nutrient sensing regulator of glucose homeostasis. *IUBMB Life*2013, *65*, 921–929.

10. Sabatini, P.V.; Lynn, F.C. All-encomPASsing regulation of beta-cells: PAS domain proteins in beta-cell dysfunction and diabetes. *Trends Endocrinol. Metab.* 2015, *26*, 49–57.

11. Schlafli, P.; Borter, E.; Spielmann, P.; Wenger, R.H. The PAS-domain kinase PASKIN: A new sensor in energy homeostasis. *Cell Mol. Life Sci.* 2009, *66*, 876–883.

12. Zhang, D.D.; Zhang, J.G.; Wang, Y.Z.; Liu, Y.; Liu, G.L.; Li, X.Y. Per-Arnt-Sim Kinase (PASK): An Emerging Regulator of Mammalian Glucose and Lipid Metabolism. *Nutrients* 2015, *7*, 7437–7450.

13. Wu, X.; Romero, D.; Swiatek, W.I.; Dorweiler, I.; Kikani, C.K.; Sabic, H.; Zweifel, B.S.; McKearn, J.; Blitzer, J.T.; Nickols, G.A.; et al. PAS kinase drives lipogenesis through SREBP-1 maturation. *Cell Rep.*2014, *8*, 242–255.

14. Da Silva Xavier, G.; Farhan, H.; Kim, H.; Caxaria, S.; Johnson, P.; Hughes, S.; Bugliani, M.; Marselli, L.; Marchetti, P.; Birzele, F.; Sun, G.; et al. Per-arnt-sim (PAS) domain-containing protein kinase is downregulated in human islets in type 2 diabetes and regulates glucagon secretion. *Diabetologia* 2011, *54*, 819–827.

15. Semplici, F.; Vaxillaire, M.; Fogarty, S.; Semache, M.; Bonnefond, A.; Fontes, G.; Philippe, J.; Meur, G.; Diraison, F.; Sessions, R.B.; et al. Human mutation within Per-Arnt-Sim (PAS) domain-containing protein kinase (PASK) causes basal insulin hypersecretion. *J. Biol. Chem.* 2011, *286*, 44005–44014.

16. Semplici, F.; Mondragon, A.; Macintyre, B.; Madeyski-Bengston, K.; Persson-Kry, A.; Barr, S.; Ramne, A.; Marley, A.; McGinty, J.; French, P.; et al. Cell type-specific deletion in mice reveals roles for PAS kinase in insulin and glucagon production. *Diabetologia* 2016, *59*, 1938–1947.

17. Wilson, W.A.; Skurat, A.V.; Probst, B.; de Paoli-Roach, A.; Roach, P.J.; Rutter, J. Control of mammalian glycogen synthase by PAS kinase. *Proc. Natl. Acad. Sci. USA* 2005, *102*, 16596–16601.

18. Hao, H.X.; Cardon, C.M.; Swiatek, W.; Cooksey, R.C.; Smith, T.L.; Wilde, J.; Boudina, S.; Abel, E.D.; McClain, D.A.; Rutter, J. PAS kinase is required for normal cellular energy balance. *Proc. Natl. Acad. Sci. USA* 2007, *104*, 15466–15471.

19. An, R.; da Silva Xavier, G.; Hao, H.X.; Semplici, F.; Rutter, J.; Rutter, G.A. Regulation by Per-Arnt-Sim (PAS) kinase of pancreatic duodenal homeobox-1 nuclear import in pancreatic beta-cells. *Biochem. Soc. Trans.* 2006, *34*, 791–793.

20. Fontes, G.; Semache, M.; Hagman, D.K.; Tremblay, C.; Shah, R.; Rhodes, C.J.; Rutter, J.; Poitout, V. Involvement of Per-Arnt-Sim Kinase and extracellular-regulated kinases-1/2 in palmitate inhibition of insulin gene expression in pancreatic beta-cells. *Diabetes* 2009, *58*, 2048–2058.

21. Hurtado-Carneiro, V.; Roncero, I.; Blazquez, E.; Alvarez, E.; Sanz, C. PAS kinase as a nutrient sensor in neuroblastoma and hypothalamic cells required for the normal expression and activity of other cellular nutrient and energy sensors. *Mol. Neurobiol.* 2013, *48*, 904–920.

22. Cordain, L.; Eaton, S.B.; Sebastian, A.; Mann, N.; Lindeberg, S.; Watkins, B.A.; O'Keef, J.H.; Brand-Miller, J. Origins and evolution of the Western diet: Health implications for the 21st century. *Am. J. Clin. Nutr.* 2005, *81*, 341–354.

23. Reynolds, M.S.; Hancock, C.R.; Ray, J.D.; Kener, K.B.; Draney, C.; Garland, K.; Hardman, J.; Bikman, B.T.; Tessem, J.S. B-Cell deletion of Nr4a1 and Nr4a3 nuclear receptors impedes mitochondrial respiration and insulin secretion. *Am. J. Physiol. Endocrinol. Metab.* 2016, *311*, E186–E201.

24. Schneider, C.A.; Rasband, W.S.; Eliceiri, K.W. NIH Image to ImageJ: 25 years of image analysis. *Nat. Methods* 2012, *9*, 671–675.

25. DeMille, D.; Bikman, B.T.; Mathis, A.D.; Prince, J.T.; Mackay, J.T.; Sowa, S.W.; Hall, T.D.; Grose, J.H. A comprehensive protein-protein interactome for yeast PAS kinase 1 reveals direct inhibition of respiration through the phosphorylation of Cbf1. *Mol. Biol. Cell* 2014, *25*, 2199–2215.

26. DeMille, D.; Pape, J.A.; Bikman, B.T.; Ghassemian, M.; Grose, J.H. The regulation of Cbf1 by PAS kinase is a pivotal control point for lipogenesis versus respiration in *Saccharomyces cerevisiae*. *G3* 2018.

27. Ballestri, S.; Nascimbeni, F.; Baldelli, E.; Marrazzo, A.; Romagnoli, D.; Lonardo, A. NAFLD as a Sexual Dimorphic Disease: Role of Gender and Reproductive Status in the Development and Progression of Nonalcoholic Fatty Liver Disease and Inherent Cardiovascular Risk. *Adv. Ther.* 2017, *34*, 1291–1326.

28. Grose, J.H.; Smith, T.L.; Sabic, H.; Rutter, J. Yeast PAS kinase coordinates glucose partitioning in response to metabolic and cell integrity signaling. *EMBO J.* 2007, *26*, 4824–4830.

29. Morley, B.J.; Dolan, D.F.; Ohlemiller, K.K.; Simmons, D.D. Generation and Characterization of α9 and α10 Nicotinic Acetylcholine Receptor Subunit Knockout Mice on a C57BL/6J Background. *Front. Neurosci.*2017, *11*, 516.

30. Ji, H.; Pai, A.V.; West, C.A.; Wu, X.; Speth, R.C.; Sandberg, K. Loss of Resistance to Angiotensin II-Induced Hypertension in the Jackson Laboratory Recombination-Activating Gene Null Mouse on the C57BL/6J Background. *Hypertension* 2017, *69*, 1121–1127.

31. Zurita, E.; Chagoyen, M.; Cantero, M.; Alonso, R.; González-Neira, A.; López-Jiménez, A.; López-Moreno, J.A.; Landel, C.P.; Benítez, J.; Pazos, F.; et al. Genetic polymorphisms among C57BL/6 mouse inbred strains. *Transgenic Res.* 2011.

32. Shimano, H.; Sato, R. SREBP-regulated lipid metabolism: Convergent physiology-divergent pathophysiology. *Nat. Rev. Endocrinol.* 2017, *13*, 710–730.

33. Rosen, E.D.; Walkey, C.J.; Puigserver, P.; Spiegelman, B.M. Transcriptional regulation of adipogenesis. *Genes Dev.* 2000, *14*, 1293–1307.

34. Horton, J.D.; Goldstein, J.L.; Brown, M.S. SREBPs: Activators of the complete program of cholesterol and fatty acid synthesis in the liver. *J. Clin. Invest.* 2002, *109*, 1125–1131.

35. Auer, S.; Hahne, P.; Soyal, S.M.; Felder, T.; Miller, K.; Paulmichl, M.; Krempler, F.; Oberkofler, H.; Patsch, W. Potential role of upstream stimulatory factor 1 gene variant in familial combined hyperlipidemia and related disorders. *Arterioscler. Thromb. Vasc. Biol.* 2012, *32*, 1535–1544.

36. Naukkarinen, J.; Ehnholm, C.; Peltonen, L. Genetics of familial combined hyperlipidemia. *Curr. Opin. Lipidol.* 2006, *17*, 285–290.

37. Coon, H.; Xin, Y.; Hopkins, P.N.; Cawthon, R.M.; Hasstedt, S.J.; Hunt, S.C. Upstream stimulatory factor 1 associated with familial combined hyperlipidemia, LDL cholesterol, and triglycerides. *Hum. Genet.* 2005, *117*, 444–451.

38. Holzapfel, C.; Baumert, J.; Grallert, H.; Muller, A.M.; Thorand, B.; Khuseyinova, N.; Herder, C.; Meisinger, C.; Hauner, H.; Wichmann, H.E.; et al. Genetic variants in the USF1 gene are associated with low-density lipoprotein cholesterol levels and incident type 2 diabetes mellitus in women: Results from the MONICA/KORA Augsburg case-cohort study, 1984–2002. *Eur. J. Endocrinol.* 2008, *159*, 407–416.

39. Huertas-Vazquez, A.; Aguilar-Salinas, C.; Lusis, A.J.; Cantor, R.M.; Canizales-Quinteros, S.; Lee, J.C.; Mariana-Nuñez, L.; Riba-Ramirez, R.M.; Jokiaho, A.; Tusie-Luna, T.; et al. Familial combined hyperlipidemia in Mexicans: Association with upstream transcription factor 1 and linkage on chromosome 16q24.1. *Arterioscler. Thromb. Vasc. Biol.* 2005, *25*, 1985–1991.

40. Komulainen, K.; Alanne, M.; Auro, K.; Kilpikari, R.; Pajukanta, P.; Saarela, J.; Ellonen, P.; Salminen, K.; Kulathinal, S.; Kuulasmaa, K.; et al. Risk alleles of USF1 gene predict cardiovascular disease of women in two prospective studies. *PLoS Genet.* 2006, *2*, e69.

41. Lee, J.C.; Weissglas-Volkov, D.; Kyttala, M.; Sinsheimer, J.S.; Jokiaho, A.; de Bruin, T.W.; Lusis, A.J.; Brennan, M.L.; van Greevenbroek, M.M.; van der Kallen, C.J.; et al. USF1 contributes to high serum lipid levels in Dutch FCHL families and U.S. whites with coronary artery disease. *Arterioscler. Thromb. Vasc. Biol.* 2007, *27*, 2222–2227.

42. Naukkarinen, J.; Gentile, M.; Soro-Paavonen, A.; Saarela, J.; Koistinen, H.A.; Pajukanta, P.; Taskinen, M.R.; Peltonen, L. USF1 and dyslipidemias: Converging evidence for a functional intronic variant. *Hum. Mol. Genet.* 2005, *14*, 2595–2605.

43. Naukkarinen, J.; Nilsson, E.; Koistinen, H.A.; Soderlund, S.; Lyssenko, V.; Vaag, A.; Poulsen, P.; Groop, L.; Taskinen, M.R.; Peltonen, L. Functional variant disrupts insulin induction of USF1: Mechanism for USF1-associated dyslipidemias. *Circ. Cardiovasc. Genet.* 2009, *2*, 522–529.

44. Ng, M.C.; Miyake, K.; So, W.Y.; Poon, E.W.; Lam, V.K.; Li, J.K.; Cox, N.J.; Bell, G.I.; Chan, J.C. The linkage and association of the gene encoding upstream stimulatory factor 1 with type 2 diabetes and metabolic syndrome in the Chinese population. *Diabetologia* 2005, *48*, 2018–2024.

45. Plaisier, C.L.; Horvath, S.; Huertas-Vazquez, A.; Cruz-Bautista, I.; Herrera, M.F.; Tusie-Luna, T.; Aguilar-Salinas, C.; Pajukanta, P. A systems genetics approach implicates USF1, FADS3, and other causal candidate genes for familial combined hyperlipidemia. *PLoS Genet.* 2009, *5*, e1000642.

46. Reiner, A.P.; Carlson, C.S.; Jenny, N.S.; Durda, J.P.; Siscovick, D.S.; Nickerson, D.A.; Tracy, R.P. USF1 gene variants, cardiovascular risk, and mortality in European Americans: Analysis of two US cohort studies. *Arterioscler. Thromb. Vasc. Biol.* 2007, *27*, 2736–2742.

47. Van der Vleuten, G.M.; Isaacs, A.; Hijmans, A.; van Duijn, C.M.; Stalenhoef, A.F.; de Graaf, J. The involvement of upstream stimulatory factor 1 in Dutch patients with familial combined hyperlipidemia. *J. Lipid Res.* 2007, *48*, 193–200.

48. Laurila, P.P.; Soronen, J.; Kooijman, S.; Forsstrom, S.; Boon, M.R.; Surakka, I.; Kaiharju, E.; Coomans, C.P.; Van Den Berg, S.A.; Autio, A.; et al. USF1 deficiency activates brown adipose tissue and improves cardiometabolic health. *Sci. Transl. Med.* 2016, *8*, 323ra13.

49. Wang, D.; Sul, H.S. Upstream stimulatory factors bind to insulin response sequence of the fatty acid synthase promoter. USF1 is regulated. *J. Biol. Chem.* 1995, *270*, 28716–28722.

50. Casado, M.; Vallet, V.S.; Kahn, A.; Vaulont, S. Essential role in vivo of upstream stimulatory factors for a normal dietary response of the fatty acid synthase gene in the liver. *J. Biol. Chem.* 1999, *274*, 2009–2013.

51. Wang, D.; Sul, H.S. Upstream stimulatory factor binding to the E-box at -65 is required for insulin regulation of the fatty acid synthase promoter. *J. Biol. Chem.* 1997, *272*, 26367–26374.

52. Griffin, M.J.; Wong, R.H.; Pandya, N.; Sul, H.S. Direct interaction between USF and SREBP-1c mediates synergistic activation of the fatty-acid synthase promoter. *J. Biol. Chem.* 2007, *282*, 5453–5467.

53. Griffin, M.J.; Sul, H.S. Insulin regulation of fatty acid synthase gene transcription: Roles of USF and SREBP-1c. *IUBMB Life* 2004, *56*, 595–600.

54. Latasa, M.J.; Griffin, M.J.; Moon, Y.S.; Kang, C.; Sul, H.S. Occupancy and function of the -150 sterol regulatory element and -65 E-box in nutritional regulation of the fatty acid synthase gene in living animals. *Mol. Cell. Biol.* 2003, *23*, 5896–5907.

CHAPTER 4: The Effect of Diet, Metabolic Health, and Sex in Amyotrophic Lateral Sclerosis

The following chapter is taken from an article submitted to Nutrients Journal. All content and figures have been formatted for this dissertation but it is otherwise unchanged.

4.1 Abstract

Amyotrophic lateral sclerosis (ALS) is a devastating neurodegenerative disease with no known cure. Being as 90% of ALS cases are sporadic, there are many behavioral factors hypothesized to affect ALS onset, progression, and survival. These behavioral factors include but are not limited to cannabis use, acupuncture, functional therapy, diet, and nutritional supplements. Many metabolic alterations occur during ALS progression including hypermetabolism, lowered BMI, and hyperlipidemia making diet and nutritional supplements attractive treatments. Taken together, the implications of diet and metabolic health are important to understand in ALS as these are behavioral factors that may be modified. Interestingly, as these factors have been studied sex-dependent differences have also been discovered, shedding light on the importance of not only understanding the molecular pathways altered by diet and metabolic health, but understanding how sex can influence these pathways, particularly through endogenous and exogenous sex hormones. This will provide more effective therapeutic targets for both males and females. This review will highlight how diet, metabolic health, and sex affect the risk and progression of ALS.

4.2 Introduction

Amyotrophic lateral sclerosis (ALS) is a devastating neurodegenerative disease, with approximately fifteen new cases being diagnosed every day [1]. ALS is caused by progressive degeneration of the motor neurons in the brain and spinal cord. This degeneration eventually leads to

an inability to perform voluntary movements and typically leads to death by respiratory paralysis within 2 to 5 years. ALS gained attention in the early 1940's when legendary Yankee baseball player Lou Gehrig was diagnosed and eventually succumbed to the disease. As such, ALS is often referred to as Lou Gehrig's disease. Although ALS has been an important topic of scientific research for almost a century, few advancements have been made in terms of treatment. In fact, only one drug has been FDA approved for ALS patients (Riluzole) and it has the potential to extend life by only a few months [2]. This speaks to the complexities of the disease as safe and effective therapies are slow in the making.

Approximately 10% of ALS cases are familial while the remaining 90% of cases are sporadic. This means that there is likely not a single causative genetic mutation of the disease. In 1993, a mutation in superoxide dismutase 1 (SOD1) was identified in about 20% of familial ALS cases, allowing for the development of a model to represent the disease [3]. Since its discovery, many other genes associated with ALS have been identified, including but not limited to TARDBP, FUS, and ATXN2. These genes have been shown to display functional overlap with mutations in sporadic cases of ALS, making work in disease models applicable to both sporadic and familial forms of the disease. Disease models are a breakthrough in ALS research, allowing for the study of many factors that contribute to ALS.

Due to the largely sporadic nature of most ALS cases, behavioral factors have been considered in ALS risk, age of onset, progression and survival time. These factors include but are not limited to cannabis, acupuncture, diet, and nutritional supplements [for further information regarding behavioral factors that may affect ALS, see [4]]. Diet and nutritional supplements are particularly interesting because many ALS patients struggle to sustain a healthy weight, leading to exacerbated disease symptoms and shorter lifespans [5]. By implementing specific dietary programs, ALS

patients can possibly slow disease progression and improve their quality of life. Furthermore, altered metabolic states have been detected in ALS mouse models before physical symptoms are noticeable [6]. This has led to many studies focused on understanding how the patient's metabolic health before and after disease onset affects ALS and what alterations are taking place on a molecular level. Researches have set out to identify therapies to ameliorate these metabolic alterations and restore healthy metabolism. These studies are not only highlighting potential therapies for ALS patients, but also how other therapies may prove detrimental to ALS patients if they negatively alter metabolism.

As diet and metabolic health have been more extensively studied, sex-specific differences have been noticed with certain therapies. This isn't too surprising as men are reported to be 2-3 times more susceptible to ALS [74-77]. However, it wasn't until 2016 that the NIH established a requirement for sex to be reported as an important biological variable. This has led to many prior studies being conducted in only one gender, more often males than females, potentially overshadowing important findings that may only be present in one gender. It is important not only to understand why ALS presents differently between the sexes, but also how different therapies may be working between the sexes to establish a treatment that is most beneficial for each patient. This review is focused on highlighting how diet, metabolic health, and sex factor into the risk, onset, progression, and survival time of ALS patients and why each of these factors should be considered when designing and analyzing therapies for ALS.

4.3 The effect of diet in ALS (summary in Table 1)

4.3.1 High-fat diet

ALS patients often present with metabolic abnormalities that increase the energy required for their body to function. This combined with physical changes, including the inability to swallow and changes in appetite, can lead to malnutrition as the body attempts to maintain healthy energy

balance. Diet is a behavioral factor that can potentially compensate for the irregular energy homeostasis and influence how the disease progresses in the individual. Diets high in fat have been widely studied as this type of diet typically causes weight gain in healthy individuals. To determine the benefits of a high-fat diet, a study done with over three-hundred participants revealed that a high intake of PUFAs decreased the risk of ALS development by 50-60% [7]. A later study with over one million participants revealed that a diet high in PUFAs decreased the risk of ALS development by 34% and suggested that it may be protective against ALS onset [8].

Beyond decreasing the risk of ALS, it is thought that a high-fat diet is beneficial in ALS patients because it can help negate the effects of hypermetabolism, a trait prevalent in 25-68% of sporadic ALS cases [9]. The source of hypermetabolism is largely unknown, but results suggest an increased resting energy expenditure in ALS patients contributes to the decline in patient health [10, 11]. In TDP-43A315T and SOD-G93A ALS mouse models it has been shown that a high-fat diet can extend lifespan by increasing fat stores and improving motor function [12, 13]. In agreement, low-fat diets and caloric restriction hasten clinical onset and shorten lifespan [12]. One report did find that caloric restriction improved motor function in SOD-G93A mice [14], but it also hastened clinical onset. The contrasting diets and the resulting lifespan show that a high-fat diet can act as an essential element in relieving hypermetabolic stress in ALS mouse models.

It is possible that hypermetabolism presents in ALS patients before neurodegeneration. In a $SOD1^{G86R}$ mouse model, it was suggested that before neurodegeneration begins skeletal muscles are in a hypermetabolic state, and they remain in a hypermetabolic state after neurodegeneration occurs [6]. To offset this energy imbalance, a fat-enriched high-energy diet was fed to the mice after disease onset, effectively increasing body mass and adipose tissue and extending the mean survival time by

20% [6]. Thus, most studies support the idea of caloric supplementation rather than restriction in ALS patients.

However, this simple statement must be taken with caution because different fats may have different effects in ALS patients. A study done in a $SOD1^{G93A}$ transgenic mouse model showed exposure to the omega-3 polyunsaturated fatty acid eicosapentaenoic acid upon onset of disease did not affect the progression or presentation of the disease. In fact, pre-symptomatic exposure to eicosapentaenoic acid significantly decreased lifespan [15]. This suggests further studies are needed to understand how different fatty acids are working in these metabolic pathways of ALS and which ones will be most beneficial for ALS patients. It also suggests the need for careful understanding of how different diets are affecting ALS patients before disease onset so as not to hasten symptoms.

A deeper understanding of the molecular mechanisms behind a high fat diet may provide for effective combination with drug therapies. One study reported benefits when using a calorie energy supplemented diet (CED, a normal chow diet supplemented with fat and cholesterol) combined with a multifunctional monoamine oxidase (MAO). The effects were additive and positively affected motor performance as well as mouse survival in a $SOD1^{G93A}$ model [16]. This study suggests that an optimized diet may be combined with a drug therapy to significantly improve patient life.

4.3.2 Glucose, sucrose, and phenols

In addition to diets focused on fats, other energy sources have been shown to improve ALS symptoms. One study including 24 ALS patients used both a high-fat hypercaloric diet (HF/HC) and a high-carbohydrate hypercaloric diet (HC/HC) [22]. Their results indicated that patients on a HF/HC diet were unable to gain weight, even when consuming 174% of their estimated energy requirements. In addition, patients on the HF/HC diet noticed uncomfortable gastrointestinal side-effects. In contrast, patients on a HC/HC diet gained weight. Overall, they suggested a HC/HC diet as a safe

and beneficial diet for ALS patients over a HF/HC diet [17]. Due to the small sample size, this study would need to be replicated to confirm their results. However, the data is promising and suggests that a high carbohydrate diet may be even more beneficial than a high fat diet and bring with it fewer negative side-effects.

The molecular mechanisms behind the role of carbohydrates in ALS remain largely unstudied. C. elegans models of neurodegeneration, including mutant polyglutamine, TDP-43, FUS, and amyloid-β toxicity have been developed to study both glucose and sucrose function. It was found that glucose and sucrose could extend lifespan of C. elegans in a dose-dependent manner by reducing the amount of misfolded proteins. Importantly, excessive glucose in healthy controls still exhibited its typical negative effects on lifespan, fertility, and dauer formation, highlighting the necessity of applying the aforementioned diets only in regards to ALS therapy [18]. Furthermore, study done in a mutant TDP-43 C. elegans model observed the effect of maple syrup on TDP-43 proteotoxicity. Maple syrup was chosen because it was a natural product that had a very high sugar content along with other compounds such as antioxidants and phenols. Their study showed that maple syrup could in fact protect against TDP-43 proteotoxicity and that two specific phenols were protective in addition to sucrose [19]. These phenols protected against hypoxic stress was well as amyloid-B and alpha-synuclein proteotoxicity and are found in other natural products in addition to maple syrup. This suggests that supplementation of these phenols in the diet of those with ALS may help protect against TDP-43 proteotoxicity and extend lifespan.

A known diet that is high in phenols is the Mediterranean diet, which has also been shown to reduce neurodegeneration through its high olive oil content [20]. $SOD1^{G93A}$ mice exposed to a diet high in extra virgin olive oil showed an extended lifespan and increased motor performance [21]. A second supportive study showed that an extra virgin olive oil extract acted as a neuroprotective agent

in cultures obtained from a $SOD1^{G93A}$ mouse model [22]. The extract reduced neurodegeneration by downregulating the amount of nitric oxide released from activated glia stimulated by the SOD1 mutation. In addition, the TLR4 signaling pathway, a known pathogenic pathway in ALS, was inhibited by the olive oil extract. These advances in understanding may allow for extraction of beneficial phenols from natural products such as maple syrup and olive oil that can then be easily added to complement ALS patient's diets, instead of replacing their preferred dietary regiment.

4.3.3 Ketogenic diet

The ketogenic diet has been considered for ALS patients as a high-fat, low-carb diet that works to mimic carbohydrate starvation, replacing carbohydrates with ketone bodies as the main source of energy. Initially, the ketogenic diet was employed to help those with pharmacoresistant epilepsy. It was later applied to neurodegenerative diseases like ALS due to common metabolic abnormalities seen in the diseases [23]. Typically, when the SOD1 mutation is present, complex I activity of the electron transport chain and ATP production are decreased [24]. When on a ketogenic diet, the principle ketone body, D-β-hydroxybutyrate (DBH) can prevent rotenone mediated inhibition of complex I in a $SOD1^{G93A}$ transgenic mouse model [25]. Furthermore, the diet was shown to increase total body weight and spinal cord motor neurons. This suggests that a ketogenic diet may be working to protect against ALS by restoring the function of complex I and promoting ATP synthesis.

A second study performed by the same group was conducted using caprylic triglyceride, also known as fractioned coconut oil, a substance metabolized into ketone bodies. This is an attractive substance because it could be used as an easily distributed supplement for ALS patients. They found that caprylic triglyceride restored healthy energy metabolism, thus improving motor function in $SOD1^{G93A}$ ALS mice [26]. Combined, these studies suggest that a ketogenic diet may be beneficial to

patients with a SOD1 mutation. However, there is little data exploring how the ketogenic diet could affect other forms of the disease, such as patients with FUS or ATXN2 mutations.

4.3.4 The Deanna Protocol

The Deanna Protocol is a nutritional supplement reported to prevent glutamate excitotoxicity and preserve healthy metabolic function. The supplement is essentially composed of arginine-alpha-ketoglutarate, gamma-aminobutyric acid, a medium chain triglyceride high in caprylic acid and Coenzyme Q10. In a $SOD1^{G93A}$ mouse model, mice with Deanna Protocol supplementation exhibited improved neurological function, improved motor performance, and extended survival time when compared to controls [27]. This suggests that using the Deanna Protocol may extend patient lifespan as well as improve their quality of life. However, this is the only study published on the Deanna Protocol in an ALS model, and has yet to be replicated by another group.

4.3.5 Fruits and vegetables

Fruits and vegetables have a long history of being beneficial to health, so it comes as no surprise that they are proving to be beneficial to ALS patients as well. In a study including over 302 ALS patients, antioxidants, carotenes, fruits, and vegetables were associated with increased ALS function [28]. When looking at the benefits of fruits and beta-carotenes specifically, increased intake was associated with a decreased risk of sporadic ALS in a study done with seventy-seven Koreans. Furthermore, they identified that intake of beef, fish, and fast food were associated with an increased risk of ALS [29]. However, this is a small study and needs further verification.

One group focused on an antiocyanin-enriched extract from strawberries, a compound known for its antioxidant, anti-inflammatory, and anti-apoptotic properties. They found that hSODG93A mice supplemented with the extract exhibited delayed disease onset and extended survival. Improved motor function in these mice was seen both through increased grip strength as well as histological

analysis, which revealed healthier neuromuscular junctions and reduced astrogliosis in the spinal cord [30]. Overall, these limited studies suggest that fruit and vegetable intake can be beneficial for ALS patients, with no known negative consequences. For a more in depth analysis of other various foods that affect ALS, from french fries to green tea, see [31]. In addition, dietary fiber intake has also been considered, with no significant association reported [32].

4.3.6 Gluten-free

A somewhat controversial diet thought to benefit some patients with ALS is a gluten-free diet. Initial studies reported a link between celiac disease or gluten insensitivity and ALS [33, 34]. However, many other studies have shown no link between the two diseases, and thus no benefit of a gluten-free diet [35, 36]. In addition, many neurologic manifestations that present with celiac disease may be misdiagnosed as ALS, suggesting that the link between ALS and celiac disease may not really exist [37]. A substantial amount of data will need to be presented for a gluten-free diet to be considered beneficial for those with ALS, unless the patient is diagnosed with gluten sensitivity or celiac disease in addition to ALS.

4.3.7 Vitamins

The study of how vitamins affect ALS patients is somewhat limited. Many ALS patients present with insufficient vitamin D levels, requiring vitamin D supplementation. Vitamin D supplementation has been associated with improved gross motor function both in human and mouse studies [38-40]. Vitamin D deficiency has had negative effects in patients and has been shown to significantly accelerate disease progression and shorten patient lifespan [41-44]. Thus, vitamin D supplementation may prove beneficial for ALS patients, especially when below a healthy level.

Vitamin E supplementation has been associated with a decreased risk for ALS, but studies have not shown it to slow disease progression or extend patient lifespan [45, 46]. As such, it has been

recommended to those with a history of familial ALS as a preventative measure [38]. For a more in depth review of these vitamins as well as additional vitamins and their effect on ALS development or progression see [38].

4.3.8 L-Serine

Dietary supplementation of the amino acid L-serine may also act as a neuro-protectant. Initial findings of Paul Cox correlated cyanobacterial toxin B-N-methylamino-L-alanine (BMAA), with the development of ALS in Guam populations [47]. This lead to further research that implicated BMAA in the formation of neurofibrillary tangles and beta-amyloid deposits in vivo, and suggested other at risk populations that near cyanobacterial reservoirs. This is one of the few studies on environmental factors, however the levels of BMAA required for these effects have remained controversial. Through this research, the supplementation of L-serine as a cellular protectant against BMAA poisoning has led to L-serine supplementation as a potential therapeutic treatment for ALS [48]. Phase 1 clinical trials were published in 2018 reporting a 34% reduction in progression slope [49, 50].

Table 4.1 A summary of reported dietary effects on ALS onset, progression or development

Diet	Model	Sex	Outcome	Survival	Time to onset	Other notable results	Source
High fat (PUFA)	Humans	M/F	+	n.r.	n.r.	↓ risk (50-60%.)	[7]
High fat	Humans	M/F	+	n.r.	n.r.	↓ risk (34%.)	[8]
High fat	TDP-43^{A315T} mice	M	+	↑	n.r.	Delayed AMPK activation.	[13]
High fat	SOD1^{G93A} mice	M	+	↑	↑	↑ fat storage, ↓ AMPK activity, ↑ motor function.	[12]
High fat	SOD1^{G86R} mice	M	+	↑	↑	↑ body mass, ↑ adipose tissue	[6]
Caloric restriction	TDP-43^{G93A} mice	M/F	-	n.c.	↓	↑ motor function	[14]
Caloric restriction	SOD1^{G93A} mice	M	-	↓	↓	↓ fat storage, ↑ AMPK activity, ↓ motor function.	[12]
Eicosapentaenoic acid	SOD1^{G93A} mice	F	-	↓	↑	EPA administered before disease onset was	[15]

						detrimental to the animal	
HC/HC	Humans	M/F	+	n.r.	n.r.	↑ weight gain	[17]
HF/HC	Humans	M/F	+/-	n.r.	n.r.	↓weight gain	[17]
Glucose	C. elegans ALS models	n/a	+	↑	n.c.	↓ autophagy, ER stress, and muscle damage.	[18]
Maple syrup	C. elegans (TDP-43)	n/a	+	↑	n.r.	Phenols GA and CA were responsible	[19]
Extra virgin olive oil	$SOD1^{G93A}$ mice	F	+	↑	n.c.	↓autophagy, ER stress and muscle damage.	[21]
Extra virgin olive oil extract	HEK cells/motoneurons/glia cultures from $SOD1^{G93A}$ mice	n.r.	+	n.r.	n.r.	Neuroprotective and prevented nitric oxide release.	[22]
Ketogenic	$SOD1^{G93A}$ mice	M	+	n.r.	n.r.	↑ complex I, ↑ ATP synthesis.	[25]
Ketogenic	$SOD1^{G93A}$ mice	M	+	n.c.	n.r.	↑ healthy energy metabolism and ↓ disease progression	[26]
The Deanna Protocol	$SOD1^{G93A}$ mice	M	+	↑	n.r.	↑ survival and motor function	[27]
Antioxidants, carotenes, fruits, vegetables	Humans	M/F	+	n.r.	n.r.	↑function	[28]
Fruits and beta-carotene	Humans	M/F	+	n.r.	n.r.	↓ risk	[29]

(M) male, (F) female, (+) positive, (-) negative, (↑) increased, (↓) decreased, (n.r.) not reported, (n.c.) no change, (HC/HC) high carbohydrate/high caloric, (HF/HC) high fat/high caloric

4.4 Metabolic factors associated with ALS (summary in Table 2)

4.4.1 BMI

The influential role of diet in ALS has brought with it a need for understanding the metabolic health of ALS patients with respect to their Body Mass Index (BMI). It has been shown that an increased BMI corresponds to an increased survival time in ALS [51-55], while a decreased BMI may increase disease severity [5]. However, how BMI acts as a protecting factor is largely unknown. As researchers have delved into this topic, sex-dependent differences have been revealed. A study conducted in Western Europe including over five-hundred thousand individuals showed that increased pre-diagnostic body fat reduced the risk of ALS mortality [56]. These risk factors varied between the sexes. Underweight women were three times more likely to die from ALS, while women with increased waist/hip ratio had a decreased risk. Men, on the other hand, showed a significant linear relationship with increased body mass index and decreased risk.

Furthermore, sex differences were seen when body fat distribution was studied to determine the protecting effects of visceral and subcutaneous fat [57]. Overall fat content was unchanged between ALS patients and controls, but the composition of the fat was different. Both males and females with ALS showed an increase in visceral fat and a decrease in subcutaneous fat when compared to healthy controls. However, this visceral fat did not impact ALS clinical severity or survival. Subcutaneous fat did predict survival in males, but not females, with an increase in fat corresponding to increased survival.

The differences seen in fat composition suggest there could be an alteration in fat metabolism in ALS patients. One study looked at the effect of TDP-43 overexpression in mice to determine changes in metabolism [58]. They observed that when TDP-43 is knocked out of

mice post-natal, they exhibit decreased weight loss, fat depletion, and rapid death. When TDP-43 is overexpressed, mice exhibit increased fat accumulation, adipocyte hypertrophy, and altered responses to insulin in skeletal muscle. This suggests TDP-43 as a regulator of body mass composition and glucose homeostasis, suggesting that mutations in TDP-43 may be a contributing factor to the metabolic abnormalities seen in ALS [58]. Future studies could include an investigation on fat composition in these mice compared to healthy controls as well as how diet could affect fat composition in ALS.

4.4.2 Hyperlipidemia

It is well documented that patients with ALS present with a lowered BMI and hypermetabolism, but they also present with hyperlipidemia. It is largely unknown what is causing hyperlipidemia in ALS patients, but research suggests that it a positive prognostic factor for ALS patients. A study was done in 655 humans measuring different metabolic factors including blood concentrations of triglycerides, cholesterol, low-density lipoprotein (LDL) and high-density lipoprotein (HDL), with hyperlipidemia being measured by the amount of total cholesterol or LDL in the serum [59]. The results revealed that hyperlipidemia was present in two-times as many ALS patients compared to controls, with a high LDL/HDL ratio significantly extending patient lifespan. Moreover, elevated levels of both fasting triglycerides and cholesterol have been shown to be positive prognostic factors in ALS. Serum triglycerides above median levels have been shown to extend patient lifespan by 14 months [60] and elevated cholesterol levels correlated with 3.25 times improved survival time [61].

Another study considered biological changes that accompany percutaneous endoscopic gastrostomy (gastrostomy), a process beneficial for ALS patients who have trouble swallowing or eating enough to meet their nutritional needs. They measured levels of total cholesterol and

low-density lipoprotein in patients before, at the time of, and after percutaneous endoscopic gastrostomy. Their results indicated that increased variation of total cholesterol between the three time points were indicative of decreased survival. They suggest that a diet focused on healthy cholesterol supplementation, especially in patients with gastrostomy, may prove beneficial in extending patient lifespan [62].

It is possible that hyperlipidemia is the result of a compensatory mechanism used to meet the altered energy demands in ALS. $SOD1^{G86R}$ mice were studied in the asymptomatic stage (65 days of age) and glycolytic muscles were shown to preferentially utilize lipids over glucose [63]. This may prove to be detrimental to the cell as an increase in lipid by-products can contribute to lipotoxicity and ROS production, eventually leading to denervation and having toxic effects on mitochondria. Interestingly, oxidative muscles such as the soleus showed no change.

In contrast, hyperlipidemia has been reported in $SOD1^{G93A}$ mice in the pre-symptomatic stage, with hyperlipidemia being significantly greater in males than in females [64]. Although in contrast to many studies reporting hyperlipidemia, it still suggests metabolic alterations are occurring before disease onset involving lipid metabolism. Lipid metabolism has also been shown to be altered in the gastrointestinal tract in mSOD1 mice. Lipids were both absorbed and triglyceride-rich lipoproteins cleared in greater frequency, resulting in decreased level of triglyceride-rich lipoproteins after eating, also known as postprandial lipemia. When supplemented with a high-fat diet, these alterations were ameliorated and neuroprotection occurred [65]. A high-fat diet also protected against a decrease in postprandial cholesterolemia. This study is in agreement with previous studies, suggesting an increased lipid intake for ALS patients to compensate for the increased energy needs.

Recently, a study was conducted to determine risk factors associated with ALS. LDL cholesterol and coronary heart disease were both identified as being causally linked to ALS, and further analysis showed that the link between ALS and coronary heart disease is due to elevated LDL cholesterol [66]. This agrees with the hyperlipidemia typically seen in ALS patients, but it brings into question if hyperlipidemia is a factor that is detectable before neurodegeneration occurs, and exactly why hyperlipidemia is promoted by ALS.

4.4.3 Type 2 diabetes mellitus

The contribution of type 2 diabetes to ALS development is under debate. Many studies have reported that type 2 diabetes protects against ALS development [67-70] and it may delay the onset of disease symptoms [71]. Others have reported that type 2 diabetes did not affect ALS phenotypes or prognosis [72]. These conflicting results may be because an increased BMI is often associated with type 2 diabetes and a high BMI is the underlying protecting factor. This had led scientists to delve deeper into specific phenotypes of the disease beyond an elevated BMI, specifically glucose homeostasis in ALS patients.

Glucose dysregulation is a common feature seen in both type 2 diabetes and ALS. A study done in 21 ALS patients and 21 control patients looked at the response of insulin to glucose using oral glucose tolerance tests. Those with ALS showed elevated blood glucose levels, impaired glucose tolerance, and elevated free-fatty acids [73]. Free-fatty acids are a known cause of insulin resistance, suggesting that ALS could be promoting type 2 diabetes-like phenotypes in humans. This result is contrary to mouse and human studies reported [6], but it suggested that because the patients in this study had non-SOD1 linked sporadic ALS they may exhibit different phenotypes than SOD1 linked ALS, highlighting a common found when studying ALS.

Table 4.2 A summary of reported metabolic factors associated with ALS onset, progression or development

Metabolic Factor	Model	Sex	Results	Reference(s)
BMI	Humans	Male/female	↑BMI associated with ↑survival time.	[51-55]
BMI	Humans	Male/female	↓BMI associated with ↑disease severity	[5]
BMI	Humans	Male/female	↓ BMI females have ↑ ALS (3x) , ↑ waist/hip ratio females have ↓ risk, ↑ BMI males correlated to ↓ risk.	[56]
Fat Distribution	Humans	Male/female	↑ subcutaneous fat ↑ survival in males only	[57]
Fat Metabolism	TDP-43 mice	Male	TDP-43 overexpression has ↑ fat accumulation, ↑ adipocyte hypertrophy, and altered insulin responses	[58]
Type 2 Diabetes Mellitus	Humans	Male/female	Protects against ALS development	[67-70]
Type 2 Diabetes Mellitus	Humans	Male/female	Delays onset of ALS symptoms	[71]
Type 2 Diabetes Mellitus	Humans	Male/female	Does not influence ALS phenotype or prognosis	[72]
Insulin sensitivity	Humans	Male/female	ALS patients had ↑ blood glucose levels, impaired glucose tolerance, and ↑ free fatty acids	[73]
LDL cholesterol	Humans	Male/female	Hyperlipidemia seen in 2x as many ALS patients, and ↑ LDL/HDL ratio extends patient lifespan.	[59]
Fasting triglycerides	Humans	Male/female	↑ triglycerides extend patient lifespan by 14 months.	[60]
Fasting cholesterol	Humans	Male/female	↑ cholesterol correlated with 3.25x improved survival	[61]
Cholesterol supplementation	Humans	Male/female	↑ lifespan, particularly in patients with gastrostomy	[62]
Lipid metabolism by glycolytic muscles	$SOD1^{G86R}$ mice	Male	Glycolytic muscles prefer lipids over glucose, while respiratory muscles show no change.	[63]
Hypolipidemia	$SOD1^{G93A}$ mice	Male/female	Hypolipidemia observed in the pre-symptomatic stage, significantly greater in male mice.	[64]
LDL cholesterol	Humans	Male/female	↑ LDL cholesterol and associated coronary heart disease correlated with ALS development	[66]

(M) male, (F) female, (+) positive, (-) negative, (↑) increased, (↓) (decreased), (BMI) body mass index, (LDL) low density lipoprotein, (HDL) high density lipoprotein

4.5 The effect of sex in ALS (summary in Table 3)

4.5.1 General sex differences

When reviewing diet and metabolic disease throughout this paper, it may be noticed that many of the in vivo experiments were performed in only one sex, usually male. In papers that included both sexes, sex specific differences were often seen [56, 57, 64]. Many studies state that because males are more susceptible to the disease and sometimes develop more severe disease symptoms they are a better model to study. However, differences between the sexes suggest that there is an underlying factor protecting females, and the application of various therapies may differ between sexes. This highlights both a need for understanding the mechanisms behind sex-dependent changes in ALS as well as the need for studies to be conducted in both sexes when possible.

The sex dependent differences in ALS point to sex hormones as being strong contributing factors between the sexes. Many epidemiological studies have shown that women are less susceptible to developing ALS and exhibit less severe disease progression [74-77]. However, these differences become less significant as patients age, with reports showing post-menopausal women being just as likely to develop ALS as men [78]. These findings point towards sex hormones as the strong contributing factor to sex-dependent differences. Many in vivo studies support the role of sex hormones in ALS pathology. ALS disease development and progression is varied amongst the sexes in many ALS mouse models [79-81]. Males typically exhibit an earlier onset of disease and females typically live longer, despite have similar symptomatic stage durations. In addition, it has been reported that male TDP-43 transgenic mice develop a stronger phenotype than females [82]. Males will exhibit abrupt onset of the disease around day 14-18, while females won't exhibit symptoms until around day 30, with only gradual development of

disease beginning with a small tremor. It is believed that this difference is due to an approximate 2-3 fold increase in TDP-43 accumulation in the male. These sex-dependent differences seen in disease onset and progression strongly suggest a role of sex hormones in ALS.

Sex-dependent differences have also been seen in response to exercise. Exercise is a somewhat controversial topic in ALS, with some reports claiming benefits to the patient, others claiming harm, and yet others reporting no change [83]. These conflicting reports are in part due to the short lifespan following diagnosis, making the effects of exercise difficult to measure in humans. A few groups have overcome this issue by studying the effect of exercise in mice. In $SOD1^{G93A}$ mice, high-intensity endurance training was beneficial for females only, with females having an increased survival time [84]. Male mice exhibited a hastened decrease in motor performance and death following clinical onset. It is unknown why the females are protected from the deleterious effects of exercise, but it is hypothesized that estrogen could be playing a role. It is also possible that female $SOD1^{G93A}$ mice live longer regardless of exercise, as has been reported [79, 80]. A second study measuring the effects of exercise in low-copy and high-copy human $SOD1^{G93A}$ mice found that exercise hastened clinical onset in males only [85]. In agreement with the previous study, exercise extended the lifespan of high-copy hSOD1 female mice only. They suggest that because non-exercising females had more irregular estrous cycles, they were exposed to less estrogen, and as such estrogen was acting as a protective factor in exercising female mice.

As mentioned previously, metabolism is altered in ALS. The effect of sex-hormones on metabolism in ALS is supported by an article showing leptin dependent changes in SOD1 mice [86]. Leptin is a hormone that regulates satiety and energy expenditure, changing the overall metabolic state of the organism. SOD1 mice typically exhibit hypermetabolism, but when placed

in a leptin-deficient background they exhibit sex-dependent improvements in energy homeostasis and decelerated disease progression [86]. Females exhibited a significant increase in survival and motor function and a decreased energy expenditure, while males showed similar changes but were much less drastic. Leptin is known to be affected by various hormones, including sex hormones, suggesting that the changes seen in this study are dependent upon the sex hormones present in the mice [86]. Further testing on how specific hormones are affecting these changes have not been conducted but would provide significant insight into how sex hormones are affecting metabolism in the SOD1 mouse model of ALS.

4.5.2 Endogenous estrogen

Estrogen and progesterone are the two most abundant female sex hormones. Estrogen is primarily an ovarian sex hormone, yet it has many functions outside of those related to reproduction. It has been reported to play a significant role in lipid and carbohydrate metabolism, electrolyte balance, and the central nervous system [87]. The higher prevalence of ALS in males points towards a protective effect of female sex hormones, primarily estrogen and progesterone. In epidemiological studies, a longer exposure to endogenous estrogen combined with a longer reproductive time-span significantly increases survival time in post-menopausal women with ALS [88].

Decreasing the amount of endogenous estrogen has proven to have deleterious effects on female mice. In $SOD1^{G93A}$ transgenic mice, ovariectomy led to acceleration of the disease, making disease progression and lifespan comparable to male mice [89, 90]. In addition, ovariectomy attenuated the anti-inflammatory and anti-apoptotic actions of estrogen [91]. When supplemented with a high dose of 17beta-estradiol (E2), a form of estrogen, ovariectomized females exhibited extended lifespan [89, 90]. In addition, male mice treated with E2 exhibited

significantly improved motor function in addition to inflammasome activity being ameliorated [92]. Combined, these data strongly suggest that estrogen is having a neuroprotective effect on disease onset and progression.

4.5.3 Endogenous progesterone

In both men and women, elevated endogenous progesterone levels show a positive correlation with survival time and time to diagnosis [93]. Few studies have been performed examining the effect of progesterone in an in vivo model. One study hypothesized that progesterone may be acting to delay neurodegeneration by activating autophagy in a $SOD1^{G93A}$ transgenic mouse model [94]. Although the onset of disease was not shown to be affected by progesterone, the progression of motor dysfunction was significantly delayed. After histological examination, it was clear that the progesterone treated group exhibited reduced spinal motor neuron death.

The effects of progesterone are reflected in the Wobbler mouse model of ALS, where progesterone is upregulated likely as a neuroprotective response to neurodegeneration [95]. There have been many studies conducted in Wobbler mice looking at the protective effects of progesterone (see [95-100]). However, it is important to note that the VPS54 mutation responsible for the Wobbler mouse has not been found in ALS patients, as such the specifics on these studies have not been included in this review [101]. It would be very interesting to replicate the experiments performed in the Wobbler mice in different ALS mouse models.

4.5.4 Endogenous testosterone

Testosterone is primarily a male sex hormone, but altered levels of testosterone have been reported in females with ALS. In one study, testosterone levels were elevated in females, and as the patient aged they remained elevated instead of declining with age as they do in healthy

controls [102]. A second study done in 92 patients reported no change in total testosterone in either males or females with ALS. However, they did report a significant decrease in free testosterone in those with ALS. They suggest that this difference is a result of testosterones inability to cross the blood brain barrier in its unbound form and that it is free testosterone impacts ALS development [103].

Interestingly, prenatal levels of testosterone may be an influencing factor in the development of sporadic ALS. There is some evidence suggesting that by measuring and comparing the lengths of the index finger and the ring finger (2D:4D ratio) you can crudely estimate the exposure of testosterone in utero for both males and female, with a reduced ratio associating with increased testosterone. In ALS patients, the 2D:4D ratio was lower than controls, suggesting increased prenatal testosterone levels were influencing ALS development [104]. These studies show that testosterone levels may be associated with ALS, but further understanding is needed to truly understand how testosterone is affecting ALS patients.

4.5.5 Exogenous sex hormones

In addition to endogenous hormones affecting ALS, exogenous hormones are also an important factor to consider, as approximately 80% of women in the United States use hormonal contraceptives to prevent pregnancy [105]. However, there is limited research into how exogenous hormones affect ALS onset and progression in females. In one epidemiological study consisting of 653 patients and 1,217 controls, exogenous estrogens and progestogens were shown decrease the chance of developing ALS in the female population [106]. In contrast, a study of 193 postmenopausal women reported oral contraceptive use was not associated with ALS risk [107]. It is important to note that this study did not consider the other various hormonal contraceptives, such as intrauterine devices or vaginal rings. Although inconclusive, the results

of these epidemiological studies have pushed for a deeper understanding of the function of exogenous sex hormones in ALS development and progression.

Table 4.3 A summary of reported sex-related differences associated with ALS onset, progression or development

Hormone	Treatment	Sex	Model	Out-come	Sur-vival	Time to Onset	Other notable results	Source
General sex hormones	Observa-tional	M/F	TDP-43 transgenic	+F -M	n.r.	n.r.	Abrupt disease onset in M ↑ TDP-43 accumulation	[82]
General sex hormones	High-endurance exercise	M/F	SOD1^{G93A} mice	+F -M	↑ F ↓ M	↑ F ↓ M	Exercise beneficial for F, deleterious for M	[84]
General sex hormones	Exercise	M/F	hSOD1 mice	+F -M	n.r.	↑ F ↓ M	Exercise benefit for F likely due to ↑ estrogen	[85]
Leptin	Leptin deficiency	M/F	SOD1 mice	+F +M	+F +M	↑ F ↑ M	↑ survival and motor function ↓ energy, stronger phenotypes in F	[86]
Estrogen	Lifelong exposure and reproductive timespan	F	Post-menopausal humans	+	↑	n.c.	↑ lifelong exposure ↑ reproductive timespan associated with ↓ risk	[88]
Estrogen	Ovariectomy	F	SOD1^{G93A} mice	-	↓	n.c.	↓ lifespan	[89, 90]
Estrogen	Ovariectomy + estrogen supplement ation	F	SOD1^{G93A} mice	+	↑	n.c	↓ ALS motor neuron progression, ↑ lifespan	[89, 90]
Estrogen	Estrogen supplement ation	M	SOD1^{G93A} mice	+	↑	n.c	↑ motor function ↓ neurodegeneratio n and ↓ inflammasome activity	[92]
N/A	Ovariectomy	F	hSOD1^{G93A} mice	-	↓	↑	↓ estrogen-dependent anti-inflammation and anti-apoptosis	[91]
Progesterone	Elevated pro-gesterone	M/F	Humans	+	↑	↓	↑ hypothalamic-pituitary-adrenal axis activation?	[93]
Progesterone	Pro-gesterone supplemen-tation	M	SOD1^{G93A} mice	+	↑	n.c.	↓ disease progression ↓ spinal motor neuron death	[94]
Testosterone	Obser-vational	M/F	Humans	n.r.	n.r.	n.r.	↑ testosterone levels in F ALS	[102]
Testosterone	Obser-vational	M/F	Humans	n.r.	n.r.	n.r.	↓ free testosterone in ALS	[103]

In utero testosterone	Obser-vational	M/F	Humans	-	n.r.	n.r.	↓ lower 2D:4D ratio in ALS, suggesting ↑ exposure to testosterone in utero contributed	[104]
Exogenous estrogen and progesterone	Obser-vational	F	Humans	+	n.r.	n.r.	Exogenous estrogens and progestogens contributed to a ↓ risk	[106]
Exogenous sex hormones	Oral contra-ceptive use	F	Post-menopausal women	n.c.	n.r.	n.r.	Oral contraceptive use did not impact ALS risk.	[107]

(M) male, (F) female, (+) positive, (-) negative, (↑) increased, (↓) decreased, (n.r.) not reported, (n.c.) no change, (N/A) not applicable

4.6 Concluding remark

ALS is a devastating neurodegenerative disease with few treatments and no cure. Although the cause of ALS is largely unknown, different factors have been studied in an effort to reduce disease risk, slow disease progression, and extend survival time (Figure 1). Three of these factors have been discussed in this review: diet, metabolic health, and sex. Diet and metabolic health go hand in hand. ALS patients often present with altered metabolic phenotypes, including altered fatty acid metabolism, which may be combated with the healthy dietary interventions discussed in this review. Furthermore, metabolic health both before and after disease onset has been shown to affect how the disease presents in the patient, with a higher BMI being associated with decreased risk and decreased disease progression. Consistent with this finding, diets that increase weight or contain certain poly unsaturated fatty acids (PUFAs) have been shown to decrease disease progression both in humans an mice. Combined, these studies review both current holistic therapies that can be applied to benefit ALS patients as well as molecular pathways that can be targeted for future drug development.

Sex is the third factor discussed in this review. Sex hormones play an important role in ALS independent of diet and metabolic health, with females protected from ALS development

and more severe disease progression. In addition, this review highlighted sex discrepancies seen in many studies involving diet and metabolic health. Unfortunately, most studies involving diet and metabolic health only include the male population. In cases where both sexes are included, differences between the sexes were seen which could be obstructing clear results from studies and contributing to contradictory reports. The impact of these findings is twofold: first, it highlights the importance of studying potential molecular pathways for drug development in both sexes, as they may be influenced by sex-dependent factors. It would be devastating to develop a drug intended for both sexes only to find it behaves very differently in males and females. Second, it suggests that the metabolic abnormalities seen in ALS may differ between sexes. This becomes important when applying holistic therapies altering diet or metabolism in both males and females. By considering each of these factors individually, and together, it will allow for more effective and safe therapies for ALS patients.

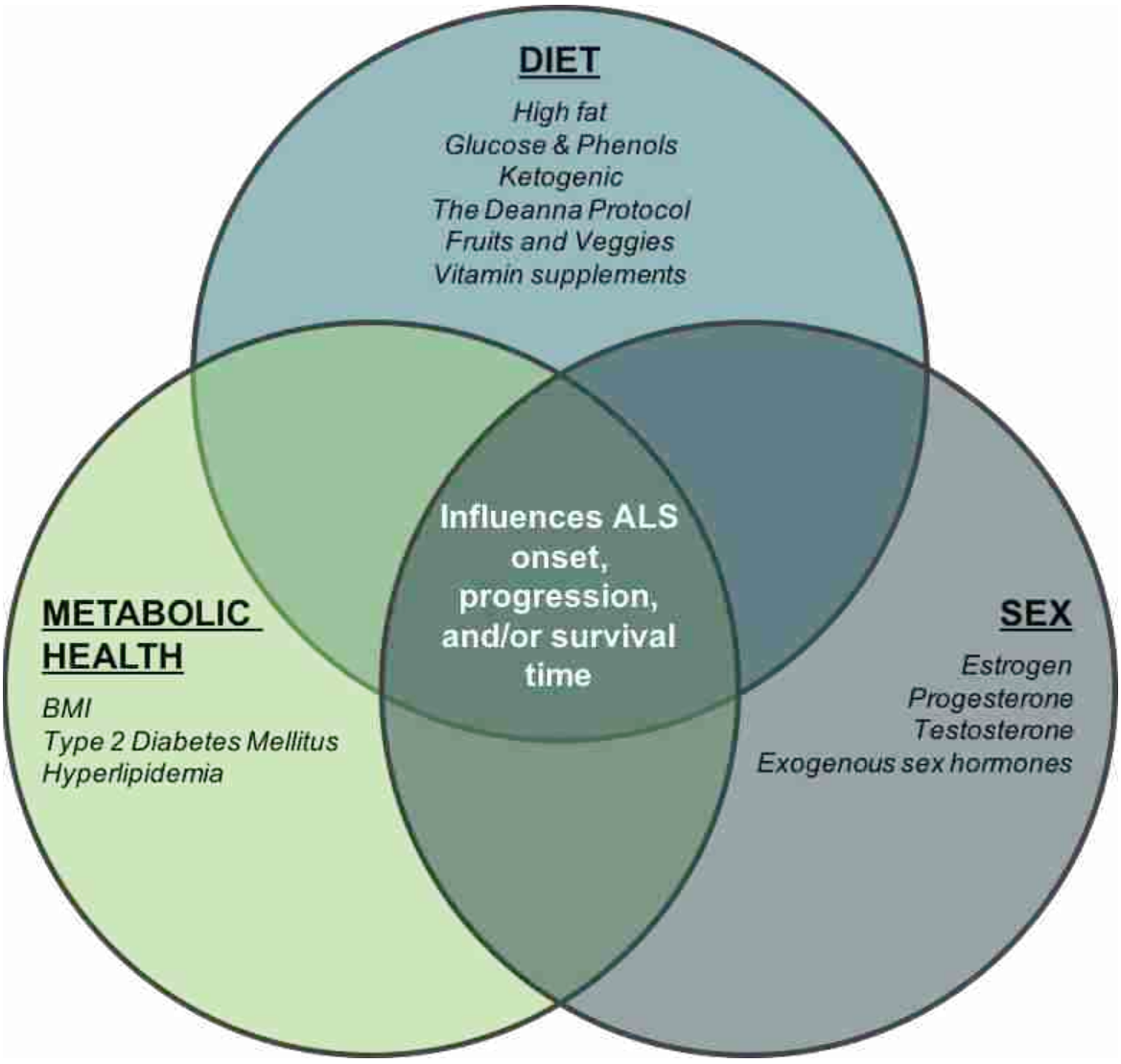

Figure 4.1 Diet, metabolic health, and sex are important contributing factors to ALS onset, progression and/or survival time . However, it is important to understand understand that each of these factors is linked to the other and that by altering one factor it may cause repercussions in another. This suggests mindfulness when developing models for the study of ALS.

REFERENCES

1. Association A. Quick Facts About ALS and the ALS Association 2019 [cited 2019 Jan. 10]. Available from: http://www.alsa.org/news/media/quick-facts.html.

2. Miller RG, Mitchell JD, Moore DH. Riluzole for amyotrophic lateral sclerosis (ALS)/motor neuron disease (MND). Cochrane Database Syst Rev. 2012(3):CD001447. doi: 10.1002/14651858.CD001447.pub3. PubMed PMID: 22419278.

3. Ajroud-Driss S, Siddique T. Sporadic and hereditary amyotrophic lateral sclerosis (ALS). Biochim Biophys Acta. 2015;1852(4):679-84. Epub 2014/09/07. doi: 10.1016/j.bbadis.2014.08.010. PubMed PMID: 25193032.

4. Bedlack RS, Joyce N, Carter GT, Paganoni S, Karam C. Complementary and Alternative Therapies in Amyotrophic Lateral Sclerosis. Neurol Clin. 2015;33(4):909-36. Epub 2015/10/31. doi: 10.1016/j.ncl.2015.07.008. PubMed PMID: 26515629; PMCID: PMC4712627.

5. Park Y, Park J, Kim Y, Baek H, Kim SH. Association between nutritional status and disease severity using the amyotrophic lateral sclerosis (ALS) functional rating scale in ALS patients. Nutrition. 2015;31(11-12):1362-7. doi: 10.1016/j.nut.2015.05.025. PubMed PMID: WOS:000362695100011.

6. Dupuis L, Oudart H, Rene F, Gonzalez de Aguilar JL, Loeffler JP. Evidence for defective energy homeostasis in amyotrophic lateral sclerosis: benefit of a high-energy diet in a transgenic mouse model. Proceedings of the National Academy of Sciences of the United States of America. 2004;101(30):11159-64. Epub 2004/07/21. doi: 10.1073/pnas.0402026101. PubMed PMID: 15263088; PMCID: PMC503756.

7. Veldink JH, Kalmijn S, Groeneveld GJ, Wunderink W, Koster A, de Vries JH, van der Luyt J, Wokke JH, Van den Berg LH. Intake of polyunsaturated fatty acids and vitamin E reduces the risk of developing amyotrophic lateral sclerosis. J Neurol Neurosurg Psychiatry. 2007;78(4):367-71. Epub 2006/05/02. doi: 10.1136/jnnp.2005.083378. PubMed PMID: 16648143; PMCID: PMC2077791.

8. Fitzgerald KC, O'Reilly EJ, Falcone GJ, McCullough ML, Park Y, Kolonel LN, Ascherio A. Dietary omega-3 polyunsaturated fatty acid intake and risk for amyotrophic lateral sclerosis. JAMA Neurol. 2014;71(9):1102-10. Epub 2014/07/16. doi: 10.1001/jamaneurol.2014.1214. PubMed PMID: 25023276; PMCID: PMC4160351.

9. Steyn FJ, Ioannides ZA, van Eijk RPA, Heggie S, Thorpe KA, Ceslis A, Heshmat S, Henders AK, Wray NR, van den Berg LH, Henderson RD, McCombe PA, Ngo ST. Hypermetabolism in ALS is associated with greater functional decline and shorter survival. J Neurol Neurosurg Psychiatry. 2018;89(10):1016-23. Epub 2018/05/01. doi: 10.1136/jnnp-2017-317887. PubMed PMID: 29706605; PMCID: PMC6166607.

10. Lee J, Baek H, Kim SH, Park Y. Association between estimated total daily energy expenditure and stage of amyotrophic lateral sclerosis. Nutrition. 2017;33:181-6. Epub 2016/08/22. doi: 10.1016/j.nut.2016.06.007. PubMed PMID: 27544003.

11. Desport JC, Torny F, Lacoste M, Preux PM, Couratier P. Hypermetabolism in ALS: correlations with clinical and paraclinical parameters. Neurodegener Dis. 2005;2(3-4):202-7. Epub 2006/08/16. doi: 10.1159/000089626. PubMed PMID: 16909026.

12. Coughlan KS, Halang L, Woods I, Prehn JH. A high-fat jelly diet restores bioenergetic balance and extends lifespan in the presence of motor dysfunction and lumbar spinal cord motor neuron loss in TDP-43A315T mutant C57BL6/J mice. Dis Model Mech. 2016;9(9):1029-37. Epub 2016/08/05. doi: 10.1242/dmm.024786. PubMed PMID: 27491077; PMCID: PMC5047697.

13. Zhao Z, Sui Y, Gao W, Cai B, Fan D. Effects of diet on adenosine monophosphate-activated protein kinase activity and disease progression in an amyotrophic lateral sclerosis model. J Int Med Res. 2015;43(1):67-79. Epub 2014/12/24. doi: 10.1177/0300060514554725. PubMed PMID: 25534414.

14. Hamadeh MJ, Rodriguez MC, Kaczor JJ, Tarnopolsky MA. Caloric restriction transiently improves motor performance but hastens clinical onset of disease in the Cu/Zn-superoxide dismutase mutant G93A mouse. Muscle Nerve. 2005;31(2):214-20. Epub 2004/12/31. doi: 10.1002/mus.20255. PubMed PMID: 15625688.

15. Yip PK, Pizzasegola C, Gladman S, Biggio ML, Marino M, Jayasinghe M, Ullah F, Dyall SC, Malaspina A, Bendotti C, Michael-Titus A. The omega-3 fatty acid eicosapentaenoic acid accelerates disease progression in a model of amyotrophic lateral sclerosis. PLoS One. 2013;8(4):e61626. Epub 2013/04/27. doi: 10.1371/journal.pone.0061626. PubMed PMID: 23620776; PMCID: PMC3631166.

16. Golko-Perez S, Mandel S, Amit T, Kupershmidt L, Youdim MB, Weinreb O. Additive Neuroprotective Effects of the Multifunctional Iron Chelator M30 with Enriched Diet in a Mouse Model of Amyotrophic Lateral Sclerosis. Neurotox Res. 2016;29(2):208-17. Epub 2015/11/20. doi: 10.1007/s12640-015-9574-4. PubMed PMID: 26581376.

17. Wills AM, Hubbard J, Macklin EA, Glass J, Tandan R, Simpson EP, Brooks B, Gelinas D, Mitsumoto H, Mozaffar T, Hanes GP, Ladha SS, Heiman-Patterson T, Katz J, Lou JS, Mahoney K, Grasso D, Lawson R, Yu H, Cudkowicz M, Network MDACR. Hypercaloric enteral nutrition in patients with amyotrophic lateral sclerosis: a randomised, double-blind, placebo-controlled phase 2 trial. Lancet. 2014;383(9934):2065-72. Epub 2014/03/04. doi: 10.1016/S0140-6736(14)60222-1. PubMed PMID: 24582471; PMCID: PMC4176708.

18. Tauffenberger A, Vaccaro A, Aulas A, Vande Velde C, Parker JA. Glucose delays age-dependent proteotoxicity. Aging Cell. 2012;11(5):856-66. Epub 2012/06/28. doi: 10.1111/j.1474-9726.2012.00855.x. PubMed PMID: 22734670; PMCID: PMC3470697.

19. Aaron C, Beaudry G, Parker JA, Therrien M. Maple Syrup Decreases TDP-43 Proteotoxicity in a Caenorhabditis elegans Model of Amyotrophic Lateral Sclerosis (ALS). J Agric Food Chem. 2016;64(17):3338-44. Epub 2016/04/14. doi: 10.1021/acs.jafc.5b05432. PubMed PMID: 27071850.

20. Angeloni C, Malaguti M, Barbalace MC, Hrelia S. Bioactivity of Olive Oil Phenols in Neuroprotection. Int J Mol Sci. 2017;18(11). Epub 2017/10/27. doi: 10.3390/ijms18112230. PubMed PMID: 29068387; PMCID: PMC5713200.

21. Olivan S, Martinez-Beamonte R, Calvo AC, Surra JC, Manzano R, Arnal C, Osta R, Osada J. Extra virgin olive oil intake delays the development of amyotrophic lateral sclerosis associated with reduced reticulum stress and autophagy in muscle of SOD1G93A mice. J Nutr Biochem. 2014;25(8):885-92. Epub 2014/06/12. doi: 10.1016/j.jnutbio.2014.04.005. PubMed PMID: 24917047.

22. De Paola M, Sestito SE, Mariani A, Memo C, Fanelli R, Freschi M, Bendotti C, Calabrese V, Peri F. Synthetic and natural small molecule TLR4 antagonists inhibit motoneuron death in cultures from ALS mouse model. Pharmacol Res. 2016;103:180-7. Epub 2015/12/08. doi: 10.1016/j.phrs.2015.11.020. PubMed PMID: 26640075.

23. Paoli A, Bianco A, Damiani E, Bosco G. Ketogenic diet in neuromuscular and neurodegenerative diseases. Biomed Res Int. 2014;2014:474296. Epub 2014/08/08. doi: 10.1155/2014/474296. PubMed PMID: 25101284; PMCID: PMC4101992.

24. Coussee E, De Smet P, Bogaert E, Elens I, Van Damme P, Willems P, Koopman W, Van Den Bosch L, Callewaert G. G37R SOD1 mutant alters mitochondrial complex I activity, Ca(2+) uptake and ATP production. Cell Calcium. 2011;49(4):217-25. Epub 2011/03/11. doi: 10.1016/j.ceca.2011.02.004. PubMed PMID: 21388680.

25. Zhao Z, Lange DJ, Voustianiouk A, MacGrogan D, Ho L, Suh J, Humala N, Thiyagarajan M, Wang J, Pasinetti GM. A ketogenic diet as a potential novel therapeutic intervention in amyotrophic lateral sclerosis. BMC Neurosci. 2006;7:29. Epub 2006/04/06. doi: 10.1186/1471-2202-7-29. PubMed PMID: 16584562; PMCID: PMC1488864.

26. Zhao W, Varghese M, Vempati P, Dzhun A, Cheng A, Wang J, Lange D, Bilski A, Faravelli I, Pasinetti GM. Caprylic triglyceride as a novel therapeutic approach to effectively improve the performance and attenuate the symptoms due to the motor neuron loss in ALS disease. PLoS One. 2012;7(11):e49191. Epub 2012/11/13. doi: 10.1371/journal.pone.0049191. PubMed PMID: 23145119; PMCID: PMC3492315.

27. Ari C, Poff AM, Held HE, Landon CS, Goldhagen CR, Mavromates N, D'Agostino DP. Metabolic therapy with Deanna Protocol supplementation delays disease progression and extends survival in amyotrophic lateral sclerosis (ALS) mouse model. PLoS One. 2014;9(7):e103526. Epub 2014/07/26. doi: 10.1371/journal.pone.0103526. PubMed PMID: 25061944; PMCID: PMC4111621.

28. Nieves JW, Gennings C, Factor-Litvak P, Hupf J, Singleton J, Sharf V, Oskarsson B, Fernandes Filho JA, Sorenson EJ, D'Amico E, Goetz R, Mitsumoto H, Amyotrophic Lateral Sclerosis Multicenter Cohort Study of Oxidative Stress Study G. Association Between Dietary Intake and Function in Amyotrophic Lateral Sclerosis. JAMA Neurol. 2016;73(12):1425-32. Epub 2016/10/25. doi: 10.1001/jamaneurol.2016.3401. PubMed PMID: 27775751; PMCID: PMC5370581.

29. Jin Y, Oh K, Oh SI, Baek H, Kim SH, Park Y. Dietary intake of fruits and beta-carotene is negatively associated with amyotrophic lateral sclerosis risk in Koreans: a case-control study. Nutr Neurosci. 2014;17(3):104-8. Epub 2013/05/29. doi: 10.1179/1476830513Y.0000000071. PubMed PMID: 23710627.

30. Winter AN, Ross EK, Wilkins HM, Stankiewicz TR, Wallace T, Miller K, Linseman DA. An anthocyanin-enriched extract from strawberries delays disease onset and extends survival in the hSOD1(G93A) mouse model of amyotrophic lateral sclerosis. Nutr Neurosci. 2018;21(6):414-26. Epub 2017/03/10. doi: 10.1080/1028415X.2017.1297023. PubMed PMID: 28276271.

31. Morozova N, Weisskopf MG, McCullough ML, Munger KL, Calle EE, Thun MJ, Ascherio A. Diet and amyotrophic lateral sclerosis. Epidemiology. 2008;19(2):324-37. Epub 2008/02/28. doi: 10.1097/EDE.0b013e3181632c5d. PubMed PMID: 18300717.

32. Fondell E, O'Reilly EJ, Fitzgerald KC, Falcone GJ, Kolonel LN, Park Y, McCullough ML, Ascherio A. Dietary fiber and amyotrophic lateral sclerosis: results from 5 large cohort studies. Am J Epidemiol. 2014;179(12):1442-9. Epub 2014/05/13. doi: 10.1093/aje/kwu089. PubMed PMID: 24816788; PMCID: PMC4051879.

33. Turner MR, Goldacre R, Ramagopalan S, Talbot K, Goldacre MJ. Autoimmune disease preceding amyotrophic lateral sclerosis: an epidemiologic study. Neurology. 2013;81(14):1222-5. Epub 2013/08/16. doi: 10.1212/WNL.0b013e3182a6cc13. PubMed PMID: 23946298; PMCID: PMC3795611.

34. Gadoth A, Nefussy B, Bleiberg M, Klein T, Artman I, Drory VE. Transglutaminase 6 Antibodies in the Serum of Patients With Amyotrophic Lateral Sclerosis. JAMA Neurol. 2015;72(6):676-81. Epub 2015/04/14. doi: 10.1001/jamaneurol.2015.48. PubMed PMID: 25867286.

35. Visser AE, Pazoki R, Pulit SL, van Rheenen W, Raaphorst J, van der Kooi AJ, Ricano-Ponce I, Wijmenga C, Otten HG, Veldink JH, van den Berg LH. No association between gluten sensitivity and amyotrophic lateral sclerosis. J Neurol. 2017;264(4):694-700. Epub 2017/02/09. doi: 10.1007/s00415-017-8400-8. PubMed PMID: 28168522; PMCID: PMC5374172.

36. Ludvigsson JF, Mariosa D, Lebwohl B, Fang F. No association between biopsy-verified celiac disease and subsequent amyotrophic lateral sclerosis--a population-based cohort study. Eur J Neurol. 2014;21(7):976-82. Epub 2014/04/09. doi: 10.1111/ene.12419. PubMed PMID: 24708265; PMCID: PMC4057356.

37. Ham H, Lee BI, Oh HJ, Park SH, Kim JS, Park JM, Cho YS, Choi MG. A case of celiac disease with neurologic manifestations misdiagnosed as amyotrophic lateral sclerosis. Intest Res. 2017;15(4):540-2. Epub 2017/11/17. doi: 10.5217/ir.2017.15.4.540. PubMed PMID: 29142524; PMCID: PMC5683987.

38. Karam CY, Paganoni S, Joyce N, Carter GT, Bedlack R. Palliative Care Issues in Amyotrophic Lateral Sclerosis: An Evidenced-Based Review. Am J Hosp Palliat Care. 2016;33(1):84-92. Epub 2014/09/10. doi: 10.1177/1049909114548719. PubMed PMID: 25202033; PMCID: PMC4439378.

39. Paganoni S, Macklin EA, Karam C, Yu H, Gonterman F, Fetterman KA, Cudkowicz M, Berry J, Wills AM. Vitamin D levels are associated with gross motor function in amyotrophic lateral sclerosis. Muscle Nerve. 2017;56(4):726-31. Epub 2017/01/04. doi: 10.1002/mus.25555. PubMed PMID: 28044349.

40. Gianforcaro A, Hamadeh MJ. Vitamin D as a Potential Therapy in Amyotrophic Lateral Sclerosis. Cns Neurosci Ther. 2014;20(2):101-11. doi: 10.1111/cns.12204. PubMed PMID: WOS:000329795000001.

41. Camu W, Tremblier B, Plassot C, Alphandery S, Salsac C, Pageot N, Juntas-Morales R, Scamps F, Daures JP, Raoul C. Vitamin D confers protection to motoneurons and is a prognostic factor of amyotrophic lateral sclerosis. Neurobiol Aging. 2014;35(5):1198-205. doi: 10.1016/j.neurobiolaging.2013.11.005. PubMed PMID: WOS:000332308300026.

42. Moghimi E, Solomon JA, Gianforcaro A, Hamadeh MJ. Dietary Vitamin D3 Restriction Exacerbates Disease Pathophysiology in the Spinal Cord of the G93A Mouse Model of Amyotrophic Lateral Sclerosis. PLoS One. 2015;10(5):e0126355. Epub 2015/05/29. doi: 10.1371/journal.pone.0126355. PubMed PMID: 26020962; PMCID: PMC4447353.

43. Libonati L, Onesti E, Gori MC, Ceccanti M, Cambieri C, Fabbri A, Frasca V, Inghilleri M. Vitamin D in amyotrophic lateral sclerosis. Funct Neurol. 2017;32(1):35-40. Epub 2017/04/06. PubMed PMID: 28380322; PMCID: PMC5505528.

44. Blasco H, Madji Hounoum B, Dufour-Rainfray D, Patin F, Maillot F, Beltran S, Gordon PH, Andres CR, Corcia P. Vitamin D is Not a Protective Factor in ALS. Cns Neurosci Ther. 2015;21(8):651-6. Epub 2015/06/23. doi: 10.1111/cns.12423. PubMed PMID: 26096806.

45. Ascherio A, Weisskopf MG, O'Reilly E J, Jacobs EJ, McCullough ML, Calle EE, Cudkowicz M, Thun MJ. Vitamin E intake and risk of amyotrophic lateral sclerosis. Ann Neurol. 2005;57(1):104-10. Epub 2004/11/06. doi: 10.1002/ana.20316. PubMed PMID: 15529299.

46. Wang H, O'Reilly EJ, Weisskopf MG, Logroscino G, McCullough ML, Schatzkin A, Kolonel LN, Ascherio A. Vitamin E intake and risk of amyotrophic lateral sclerosis: a pooled analysis of data from 5 prospective cohort studies. Am J Epidemiol.

2011;173(6):595-602. Epub 2011/02/22. doi: 10.1093/aje/kwq416. PubMed PMID: 21335424; PMCID: PMC3105261.

47. Cox PA, Davis DA, Mash DC, Metcalf JS, Banack SA. Dietary exposure to an environmental toxin triggers neurofibrillary tangles and amyloid deposits in the brain. Proc Biol Sci. 2016;283(1823). Epub 2016/01/23. doi: 10.1098/rspb.2015.2397. PubMed PMID: 26791617; PMCID: PMC4795023.

48. Metcalf JS, Dunlop RA, Powell JT, Banack SA, Cox PA. L-Serine: a Naturally-Occurring Amino Acid with Therapeutic Potential. Neurotox Res. 2018;33(1):213-21. Epub 2017/09/21. doi: 10.1007/s12640-017-9814-x. PubMed PMID: 28929385.

49. Bradley WG, Miller RX, Levine TD, Stommel EW, Cox PA. Studies of Environmental Risk Factors in Amyotrophic Lateral Sclerosis (ALS) and a Phase I Clinical Trial of L-Serine. Neurotox Res. 2018;33(1):192-8. Epub 2017/05/21. doi: 10.1007/s12640-017-9741-x. PubMed PMID: 28527102.

50. Levine TD, Miller RG, Bradley WG, Moore DH, Saperstein DS, Flynn LE, Katz JS, Forshew DA, Metcalf JS, Banack SA, Cox PA. Phase I clinical trial of safety of L-serine for ALS patients. Amyotroph Lateral Scler Frontotemporal Degener. 2017;18(1-2):107-11. Epub 2016/09/04. doi: 10.1080/21678421.2016.1221971. PubMed PMID: 27589995.

51. Mariosa D, Beard JD, Umbach DM, Bellocco R, Keller J, Peters TL, Allen KD, Ye W, Sandler DP, Schmidt S, Fang F, Kamel F. Body Mass Index and Amyotrophic Lateral Sclerosis: A Study of US Military Veterans. Am J Epidemiol. 2017;185(5):362-71. Epub 2017/02/06. doi: 10.1093/aje/kww140. PubMed PMID: 28158443; PMCID: PMC5860019.

52. Paganoni S, Deng J, Jaffa M, Cudkowicz ME, Wills AM. Body mass index, not dyslipidemia, is an independent predictor of survival in amyotrophic lateral sclerosis. Muscle Nerve. 2011;44(1):20-4. Epub 2011/05/25. doi: 10.1002/mus.22114. PubMed PMID: 21607987; PMCID: PMC4441750.

53. Paganoni S, Hyman T, Shui A, Allred P, Harms M, Liu J, Maragakis N, Schoenfeld D, Yu H, Atassi N, Cudkowicz M, Miller TM. Pre-morbid type 2 diabetes mellitus is not a prognostic factor in amyotrophic lateral sclerosis. Muscle Nerve. 2015;52(3):339-43. Epub 2015/04/23. doi: 10.1002/mus.24688. PubMed PMID: 25900666; PMCID: PMC4536144.

54. Reich-Slotky R, Andrews J, Cheng B, Buchsbaum R, Levy D, Kaufmann P, Thompson JL. Body mass index (BMI) as predictor of ALSFRS-R score decline in ALS patients. Amyotroph Lateral Scler Frontotemporal Degener. 2013;14(3):212-6. Epub 2013/03/05. doi: 10.3109/21678421.2013.770028. PubMed PMID: 23452274.

55. Traxinger K, Kelly C, Johnson BA, Lyles RH, Glass JD. Prognosis and epidemiology of amyotrophic lateral sclerosis: Analysis of a clinic population, 1997-2011. Neurol Clin Pract. 2013;3(4):313-20. Epub 2013/11/07. doi: 10.1212/CPJ.0b013e3182a1b8ab. PubMed PMID: 24195020; PMCID: PMC3787117.

56. Gallo V, Wark PA, Jenab M, Pearce N, Brayne C, Vermeulen R, Andersen PM, Hallmans G, Kyrozis A, Vanacore N, Vahdaninia M, Grote V, Kaaks R, Mattiello A, Bueno-de-Mesquita HB, Peeters PH, Travis RC, Petersson J, Hansson O, Arriola L, Jimenez-Martin JM, Tjonneland A, Halkjaer J, Agnoli C, Sacerdote C, Bonet C, Trichopoulou A, Gavrila D, Overvad K, Weiderpass E, Palli D, Quiros JR, Tumino R, Khaw KT, Wareham N, Barricante-Gurrea A, Fedirko V, Ferrari P, Clavel-Chapelon F, Boutron-Ruault MC, Boeing H, Vigl M, Middleton L, Riboli E, Vineis P. Prediagnostic body fat and risk of death from amyotrophic lateral sclerosis: the EPIC cohort. Neurology. 2013;80(9):829-38. Epub 2013/02/08. doi: 10.1212/WNL.0b013e3182840689. PubMed PMID: 23390184; PMCID: PMC3598455.

57. Lindauer E, Dupuis L, Muller HP, Neumann H, Ludolph AC, Kassubek J. Adipose Tissue Distribution Predicts Survival in Amyotrophic Lateral Sclerosis. PLoS One. 2013;8(6):e67783. Epub 2013/07/05. doi: 10.1371/journal.pone.0067783. PubMed PMID: 23826340; PMCID: PMC3694869.

58. Stallings NR, Puttaparthi K, Dowling KJ, Luther CM, Burns DK, Davis K, Elliott JL. TDP-43, an ALS linked protein, regulates fat deposition and glucose homeostasis. PLoS One. 2013;8(8):e71793. Epub 2013/08/24. doi: 10.1371/journal.pone.0071793. PubMed PMID: 23967244; PMCID: PMC3742534.

59. Dupuis L, Corcia P, Fergani A, De Aguilar JLG, Bonnefont-Rousselot D, Bittar R, Seilhean D, Hauw JJ, Lacomblez L, Loeffler JP, Meininger V. Dyslipidemia is a protective factor in amyotrophic lateral sclerosis. Neurology. 2008;70(13):1004-9. doi: DOI 10.1212/01.wnl.0000285080.70324.27. PubMed PMID: WOS:000254297500005.

60. Dorst J, Kuhnlein P, Hendrich C, Kassubek J, Sperfeld AD, Ludolph AC. Patients with elevated triglyceride and cholesterol serum levels have a prolonged survival in amyotrophic lateral sclerosis. J Neurol. 2011;258(4):613-7. Epub 2010/12/04. doi: 10.1007/s00415-010-5805-z. PubMed PMID: 21128082.

61. Ahmed RM, Highton-Williamson E, Caga J, Thornton N, Ramsey E, Zoing M, Kim WS, Halliday GM, Piguet O, Hodges JR, Farooqi IS, Kiernan MC. Lipid Metabolism and Survival Across the Frontotemporal Dementia-Amyotrophic Lateral Sclerosis Spectrum: Relationships to Eating Behavior and Cognition. J Alzheimers Dis. 2018;61(2):773-83. Epub 2017/12/20. doi: 10.3233/JAD-170660. PubMed PMID: 29254092.

62. Blasco H, Patin F, Molinier S, Vourc'h P, Le Tilly O, Bakkouche S, Andres CR, Meininger V, Couratier P, Corcia P. A decrease in blood cholesterol after gastrostomy could impact survival in ALS. Eur J Clin Nutr. 2017;71(9):1133-5. doi: 10.1038/ejcn.2017.54. PubMed PMID: WOS:000409341000017.

63. Palamiuc L, Schlagowski A, Ngo ST, Vernay A, Dirrig-Grosch S, Henriques A, Boutillier AL, Zoll J, Echaniz-Laguna A, Loeffler JP, Rene F. A metabolic switch toward lipid use in glycolytic muscle is an early pathologic event in a mouse model of amyotrophic lateral sclerosis. EMBO Mol Med. 2015;7(5):526-46. Epub 2015/03/31. doi: 10.15252/emmm.201404433. PubMed PMID: 25820275; PMCID: PMC4492815.

64. Kim SM, Kim H, Kim JE, Park KS, Sung JJ, Kim SH, Lee KW. Amyotrophic lateral sclerosis is associated with hypolipidemia at the presymptomatic stage in mice. PLoS One. 2011;6(3):e17985. Epub 2011/04/06. doi: 10.1371/journal.pone.0017985. PubMed PMID: 21464953; PMCID: PMC3064597.

65. Fergani A, Oudart H, Gonzalez De Aguilar JL, Fricker B, Rene F, Hocquette JF, Meininger V, Dupuis L, Loeffler JP. Increased peripheral lipid clearance in an animal model of amyotrophic lateral sclerosis. J Lipid Res. 2007;48(7):1571-80. Epub 2007/04/18. doi: 10.1194/jlr.M700017-JLR200. PubMed PMID: 17438338; PMCID: PMC1974855.

66. Bandres-Ciga S, Noyce AJ, Hemani G, Nicolas A, Calvo A, Mora G, Consortium I, International ALSGC, Tienari PJ, Stone DJ, Nalls MA, Singleton AB, Chio A, Traynor BJ. Shared polygenic risk and causal inferences in amyotrophic lateral sclerosis. Ann Neurol. 2019. Epub 2019/02/07. doi: 10.1002/ana.25431. PubMed PMID: 30723964.

67. Mariosa D, Kamel F, Bellocco R, Ye W, Fang F. Association between diabetes and amyotrophic lateral sclerosis in Sweden. European Journal of Neurology. 2015;22(11):1436-42. doi: 10.1111/ene.12632.

68. Kioumourtzoglou MA, Rotem RS, Seals RM, Gredal O, Hansen J, Weisskopf MG. Diabetes Mellitus, Obesity, and Diagnosis of Amyotrophic Lateral Sclerosis: A Population-Based Study. JAMA Neurol. 2015;72(8):905-11. doi: 10.1001/jamaneurol.2015.0910. PubMed PMID: 26030836; PMCID: PMC4975611.

69. D'Ovidio F, d'Errico A, Carna P, Calvo A, Costa G, Chio A. The role of pre-morbid diabetes on developing amyotrophic lateral sclerosis. Eur J Neurol. 2018;25(1):164-70. Epub 2017/09/19. doi: 10.1111/ene.13465. PubMed PMID: 28921834.

70. Sun Y, Lu CJ, Chen RC, Hou WH, Li CY. Risk of Amyotrophic Lateral Sclerosis in Patients With Diabetes: A Nationwide Population-Based Cohort Study. J Epidemiol. 2015;25(6):445-51. Epub 2015/05/08. doi: 10.2188/jea.JE20140176. PubMed PMID: 25947580; PMCID: PMC4444499.

71. Jawaid A, Salamone AR, Strutt AM, Murthy SB, Wheaton M, McDowell EJ, Simpson E, Appel SH, York MK, Schulz PE. ALS disease onset may occur later in patients with pre-morbid diabetes mellitus. Eur J Neurol. 2010;17(5):733-9. Epub 2010/01/16. doi: 10.1111/j.1468-1331.2009.02923.x. PubMed PMID: 20074230.

72. Moglia C, Calvo A, Canosa A, Bertuzzo D, Cugnasco P, Solero L, Grassano M, Bersano E, Cammarosano S, Manera U, Parals, Pisano F, Mazzini L, Dalla Vecchia LA, Mora G, Chio A. Influence of arterial hypertension, type 2 diabetes and cardiovascular risk factors on ALS outcome: a population-based study. Amyotroph Lateral Scler Frontotemporal Degener. 2017;18(7-8):590-7. Epub 2017/06/16. doi: 10.1080/21678421.2017.1336560. PubMed PMID: 28616937.

73. Pradat PF, Bruneteau G, Gordon PH, Dupuis L, Bonnefont-Rousselot D, Simon D, Salachas F, Corcia P, Frochot V, Lacorte JM, Jardel C, Coussieu C, Le Forestier N,

Lacomblez L, Loeffler JP, Meininger V. Impaired glucose tolerance in patients with amyotrophic lateral sclerosis. Amyotroph Lateral Scler. 2010;11(1-2):166-71. Epub 2010/02/27. doi: 10.3109/17482960902822960. PubMed PMID: 20184518.

74. McCombe PA, Henderson RD. Effects of gender in amyotrophic lateral sclerosis. Gend Med. 2010;7(6):557-70. Epub 2011/01/05. doi: 10.1016/j.genm.2010.11.010. PubMed PMID: 21195356.

75. Talbott EO, Malek AM, Lacomis D. The epidemiology of amyotrophic lateral sclerosis. Handb Clin Neurol. 2016;138:225-38. Epub 2016/09/18. doi: 10.1016/B978-0-12-802973-2.00013-6. PubMed PMID: 27637961.

76. Couratier P, Corcia P, Lautrette G, Nicol M, Preux PM, Marin B. Epidemiology of amyotrophic lateral sclerosis: A review of literature. Rev Neurol (Paris). 2016;172(1):37-45. Epub 2016/01/05. doi: 10.1016/j.neurol.2015.11.002. PubMed PMID: 26727307.

77. Zarei S, Carr K, Reiley L, Diaz K, Guerra O, Altamirano PF, Pagani W, Lodin D, Orozco G, Chinea A. A comprehensive review of amyotrophic lateral sclerosis. Surg Neurol Int. 2015;6:171. Epub 2015/12/03. doi: 10.4103/2152-7806.169561. PubMed PMID: 26629397; PMCID: PMC4653353.

78. Manjaly ZR, Scott KM, Abhinav K, Wijesekera L, Ganesalingam J, Goldstein LH, Janssen A, Dougherty A, Willey E, Stanton BR, Turner MR, Ampong MA, Sakel M, Orrell RW, Howard R, Shaw CE, Leigh PN, Al-Chalabi A. The sex ratio in amyotrophic lateral sclerosis: A population based study. Amyotroph Lateral Sc. 2010;11(5):439-42. doi: 10.3109/17482961003610853. PubMed PMID: WOS:000283069200005.

79. Cudkowicz ME, Pastusza KA, Sapp PC, Mathews RK, Leahy J, Pasinelli P, Francis JW, Jiang D, Andersen JK, Brown RH, Jr. Survival in transgenic ALS mice does not vary with CNS glutathione peroxidase activity. Neurology. 2002;59(5):729-34. Epub 2002/09/11. PubMed PMID: 12221165.

80. Snow RJ, Turnbull J, da Silva S, Jiang F, Tarnopolsky MA. Creatine supplementation and riluzole treatment provide similar beneficial effects in copper, zinc superoxide dismutase (G93A) transgenic mice. Neuroscience. 2003;119(3):661-7. Epub 2003/06/18. PubMed PMID: 12809687.

81. Hayworth CR, Gonzalez-Lima F. Pre-symptomatic detection of chronic motor deficits and genotype prediction in congenic B6.SOD1(G93A) ALS mouse model. Neuroscience. 2009;164(3):975-85. Epub 2009/08/25. doi: 10.1016/j.neuroscience.2009.08.031. PubMed PMID: 19699279; PMCID: PMC2783710.

82. Shan X, Chiang PM, Price DL, Wong PC. Altered distributions of Gemini of coiled bodies and mitochondria in motor neurons of TDP-43 transgenic mice. Proceedings of the National Academy of Sciences of the United States of America. 2010;107(37):16325-30. doi: 10.1073/pnas.1003459107. PubMed PMID: 20736350; PMCID: PMC2941282.

83. de Almeida JP, Silvestre R, Pinto AC, de Carvalho M. Exercise and amyotrophic lateral sclerosis. Neurol Sci. 2012;33(1):9-15. Epub 2012/01/10. doi: 10.1007/s10072-011-0921-9. PubMed PMID: 22228269.

84. Veldink JH, Bar PR, Joosten EA, Otten M, Wokke JH, van den Berg LH. Sexual differences in onset of disease and response to exercise in a transgenic model of ALS. Neuromuscul Disord. 2003;13(9):737-43. PubMed PMID: 14561497.

85. Mahoney DJ, Rodriguez C, Devries M, Yasuda N, Tarnopolsky MA. Effects of high-intensity endurance exercise training in the G93A mouse model of amyotrophic lateral sclerosis. Muscle Nerve. 2004;29(5):656-62. Epub 2004/04/30. doi: 10.1002/mus.20004. PubMed PMID: 15116368.

86. Lim MA, Bence KK, Sandesara I, Andreux P, Auwerx J, Ishibashi J, Seale P, Kalb RG. Genetically altering organismal metabolism by leptin-deficiency benefits a mouse model of amyotrophic lateral sclerosis. Hum Mol Genet. 2014;23(18):4995-5008. Epub 2014/05/17. doi: 10.1093/hmg/ddu214. PubMed PMID: 24833719; PMCID: PMC4140473.

87. Vrtacnik P, Ostanek B, Mencej-Bedrac S, Marc J. The many faces of estrogen signaling. Biochem Med (Zagreb). 2014;24(3):329-42. Epub 2014/10/30. doi: 10.11613/BM.2014.035. PubMed PMID: 25351351; PMCID: PMC4210253.

88. de Jong S, Huisman M, Sutedja N, van der Kooi A, de Visser M, Schelhaas J, van der Schouw Y, Veldink J, van den Berg L. Endogenous female reproductive hormones and the risk of amyotrophic lateral sclerosis. J Neurol. 2013;260(2):507-12. doi: 10.1007/s00415-012-6665-5. PubMed PMID: 22972621.

89. Choi CI, Lee YD, Gwag BJ, Cho SI, Kim SS, Suh-Kim H. Effects of estrogen on lifespan and motor functions in female hSOD1 G93A transgenic mice. J Neurol Sci. 2008;268(1-2):40-7. doi: 10.1016/j.jns.2007.10.024. PubMed PMID: 18054961.

90. Groeneveld GJ, Van Muiswinkel FL, Sturkenboom JM, Wokke JH, Bar PR, Van den Berg LH. Ovariectomy and 17beta-estradiol modulate disease progression of a mouse model of ALS. Brain Res. 2004;1021(1):128-31. doi: 10.1016/j.brainres.2004.06.024. PubMed PMID: 15328040.

91. Yan L, Liu Y, Sun C, Zheng Q, Hao P, Zhai J, Liu Y. Effects of Ovariectomy in an hSOD1-G93A Transgenic Mouse Model of Amyotrophic Lateral Sclerosis (ALS). Med Sci Monit. 2018;24:678-86. Epub 2018/02/03. PubMed PMID: 29394243; PMCID: PMC5806477.

92. Heitzer M, Kaiser S, Kanagaratnam M, Zendedel A, Hartmann P, Beyer C, Johann S. Administration of 17beta-Estradiol Improves Motoneuron Survival and Down-regulates Inflammasome Activation in Male SOD1(G93A) ALS Mice. Mol Neurobiol. 2017;54(10):8429-43. doi: 10.1007/s12035-016-0322-4. PubMed PMID: 27957680.

93. Monachelli GG, Meyer M, Rodriguez GE, Garay LI, Sica REP, De Nicola AF, Deniselle MCG. Endogenous progesterone is associated to amyotrophic lateral sclerosis prognostic factors. Acta Neurol Scand. 2011;123(1):60-7. doi: 10.1111/j.1600-0404.2010.01385.x. PubMed PMID: WOS:000284961100010.

94. Kim J, Kim TY, Cho KS, Kim HN, Koh JY. Autophagy activation and neuroprotection by progesterone in the G93A-SOD1 transgenic mouse model of amyotrophic lateral sclerosis. Neurobiol Dis. 2013;59:80-5. Epub 2013/07/31. doi: 10.1016/j.nbd.2013.07.011. PubMed PMID: 23891729.

95. Gonzalez Deniselle MC, Liere P, Pianos A, Meyer M, Aprahamian F, Cambourg A, Di Giorgio NP, Schumacher M, De Nicola AF, Guennoun R. Steroid Profiling in Male Wobbler Mouse, a Model of Amyotrophic Lateral Sclerosis. Endocrinology. 2016;157(11):4446-60. Epub 2016/11/02. doi: 10.1210/en.2016-1244. PubMed PMID: 27571131.

96. Gonzalez Deniselle MC, Carreras MC, Garay L, Gargiulo-Monachelli G, Meyer M, Poderoso JJ, De Nicola AF. Progesterone prevents mitochondrial dysfunction in the spinal cord of wobbler mice. J Neurochem. 2012;122(1):185-95. Epub 2012/04/11. doi: 10.1111/j.1471-4159.2012.07753.x. PubMed PMID: 22486171.

97. Gonzalez Deniselle MC, Lopez-Costa JJ, Saavedra JP, Pietranera L, Gonzalez SL, Garay L, Guennoun R, Schumacher M, De Nicola AF. Progesterone neuroprotection in the Wobbler mouse, a genetic model of spinal cord motor neuron disease. Neurobiol Dis. 2002;11(3):457-68. Epub 2003/02/15. PubMed PMID: 12586554.

98. Gonzalez Deniselle MC, Garay L, Gonzalez S, Guennoun R, Schumacher M, De Nicola AF. Progesterone restores retrograde labeling of cervical motoneurons in Wobbler mouse motoneuron disease. Exp Neurol. 2005;195(2):518-23. Epub 2005/08/13. doi: 10.1016/j.expneurol.2005.06.015. PubMed PMID: 16095593.

99. Gonzalez Deniselle MC, Garay L, Lopez-Costa JJ, Gonzalez S, Mougel A, Guennoun R, Schumacher M, De Nicola AF. Progesterone treatment reduces NADPH-diaphorase/nitric oxide synthase in Wobbler mouse motoneuron disease. Brain Res. 2004;1014(1-2):71-9. Epub 2004/06/24. doi: 10.1016/j.brainres.2004.04.004. PubMed PMID: 15212993.

100. Meyer M, Gonzalez Deniselle MC, Garay LI, Monachelli GG, Lima A, Roig P, Guennoun R, Schumacher M, De Nicola AF. Stage dependent effects of progesterone on motoneurons and glial cells of wobbler mouse spinal cord degeneration. Cell Mol Neurobiol. 2010;30(1):123-35. Epub 2009/08/21. doi: 10.1007/s10571-009-9437-8. PubMed PMID: 19693665.

101. Moser JM, Bigini P, Schmitt-John T. The wobbler mouse, an ALS animal model. Mol Genet Genomics. 2013;288(5-6):207-29. Epub 2013/03/30. doi: 10.1007/s00438-013-0741-0. PubMed PMID: 23539154; PMCID: PMC3664746.

102. Gargiulo-Monachelli GM, Sivori M, Meyer M, Sica RE, De Nicola AF, Gonzalez-Deniselle MC. Circulating gonadal and adrenal steroids in amyotrophic lateral sclerosis:

possible markers of susceptibility and outcome. Horm Metab Res. 2014;46(6):433-9. Epub 2014/05/09. doi: 10.1055/s-0034-1371891. PubMed PMID: 24806746.

103. Militello A, Vitello G, Lunetta C, Toscano A, Maiorana G, Piccoli T, La Bella V. The serum level of free testosterone is reduced in amyotrophic lateral sclerosis. Journal of the Neurological Sciences. 2002;195(1):67-70. doi: Pii S0022-510x(01)00688-8 Doi 10.1016/S0022-510x(01)00688-8. PubMed PMID: WOS:000174847900009.

104. Vivekananda U, Manjalay ZR, Ganesalingam J, Simms J, Shaw CE, Leigh PN, Turner MR, Al-Chalabi A. Low index-to-ring finger length ratio in sporadic ALS supports prenatally defined motor neuronal vulnerability. J Neurol Neurosurg Psychiatry. 2011;82(6):635-7. Epub 2011/05/10. doi: 10.1136/jnnp.2010.237412. PubMed PMID: 21551173.

105. Chandra A, Martinez GM, Mosher WD, Abma JC, Jones J. Fertility, family planning, and reproductive health of U.S. women: data from the 2002 National Survey of Family Growth. Vital Health Stat 23. 2005(25):1-160. Epub 2006/03/15. PubMed PMID: 16532609.

106. Rooney JPK, Visser AE, D'Ovidio F, Vermeulen R, Beghi E, Chio A, Veldink JH, Logroscino G, van den Berg LH, Hardiman O, Consortium E-M. A case-control study of hormonal exposures as etiologic factors for ALS in women Euro-MOTOR. Neurology. 2017;89(12):1283-90. doi: 10.1212/Wnl.0000000000004390. PubMed PMID: WOS:000410928600018.

107. Popat RA, Van Den Eeden SK, Tanner CM, Bernstein AL, Bloch DA, Leimpeter A, McGuire V, Nelson LM. Effect of reproductive factors and postmenopausal hormone use on the risk of amyotrophic lateral sclerosis. Neuroepidemiology. 2006;27(3):117-21. doi: 10.1159/000095550. PubMed PMID: WOS:000241773900001.

CHAPTER 5: Pbp1 Regulates Mitophagy through the Novel Binding Partner Ptc6

The following chapter is taken from a study currently in progress. All content and figures have been formatted for this dissertation.

5.1 Abstract

Mutations in ataxin-2 have recently been associated with an increased risk for Amyotrophic Lateral Sclerosis (ALS), yet little is known about the molecular pathways behind Ataxin-2 activity. Recently, PAS kinase was identified as a novel regulator of ataxin-2 function. In depth studies of the yeast homolog of ataxin-2, poly(A)- binding protein binding protein 1 (Pbp1), revealed that under glucose depravation, the nutrient sensing protein kinase PAS kinase phosphorylates and activates Pbp1. This activation inhibits TORC1 function through sequestration to stress granules, though the mechanism behind the Pbp1 and TORC1 interaction remains unclear. In this study, 32 novel interaction partners of Pbp1 were identified. Most the interacting partners were involved in RNA processing, but others were involved in DNA damage response, mitophagy, and the misfolded protein response respectively. Ptc6 was identified by yeast two-hybrid assay as a direct binding partner of Pbp1. Colocalization revealed sequestration of Ptc6 with Pbp1 to the stress granules under nutrient depravation. Mitophagy assays showed an expected decrease in Ptc6-deficient yeast, while Pbp1-deficient yeast exhibited a significant increase, suggesting Pbp1 activates Ptc6 to regulate mitophagy. In the absence of Pbp1, Ptc6 is hyperactive and the cell has increased levels of mitophagy. Quantification of total mitochondria revealed a significant increase in Ptc6-deficient yeast, suggesting that the decreased level of mitophagy is causing an accumulation of mitochondria. This is supported by plate respiration

assays that show increased colony size in Ptc6-deficient yeast. Further studies are needed to identify the health of the mitochondria in Ptc6-deficient yeast. Overall, this study provides further characterization of the ataxin-2/pbp1 pathways and yields valuable insight into the role of ataxin-2 in the development of ALS.

5.2 Introduction

Amyotrophic lateral sclerosis (ALS) is a devastating neurodegenerative disease. With no known cure and only a handful of known genetic components, treatment options for patients typically revolve around symptomatic management, such as physical therapy, pain relievers, and dietary supplementation [1, 2]. As such, there is a desperate need for an effective drug to be developed that will ameliorate disease symptoms and extend patient lifespan. Recently, intermediate-length ataxin-2 polyQ repeat expansions were identified to be significantly associated with susceptibility of ALS in humans [3]. While little is known about ataxin-2, initial studies have revealed that reducing ataxin-2 levels in an ALS mouse model (TDP-43 mutant mice) increases longevity [4]. These studies suggest that higher levels or altered activity of ataxin-2 are associated with ALS progression, while lower levels of ataxin-2 appear to be protective. Using ataxin-2 as a therapeutic target is promising, though not without side-effects, especially when considering complete inhibition of ataxin-2. Deletion of ataxin-2 in mice has been shown to have adverse side-effects, including obesity, insulin resistance, and hyperlipidemia [5, 6], suggesting that the deletion significantly impairs healthy cellular metabolism. It is unclear what other pathways are being altered in response to ataxin-2 deficiency, making regulation of ataxin-2 (restoring healthy function) an attractive therapeutic goal.

A newly identified regulator of ataxin-2 is PAS kinase. PAS kinase is a nutrient sensing protein kinase that is conserved between yeast, mice, and humans [7]. In yeast, PAS kinase has been shown directly phosphorylate and activate ataxin-2 as well as the yeast homolog of ataxin-2, Pbp1 (Choksi et al, *submitted*). Under cellular stress, PAS kinase phosphorylates and activates ataxin-2/Pbp1, sequestering it to the stress granule. This function is not surprising, as ATXIN-2/Pbp1 are both known to localize to stress granules. When ataxin-2/Pbp1 are phosphorylated and activated by PAS kinase in yeast, they also can sequester other proteins to stress granules. This model has been verified by monitoring the known interaction of Pbp1 and TORC1 (Figure 5.1). ataxin-2/Pbp1 overexpression in yeast causes caffeine sensitivity, resulting in inhibition of cellular growth through the sequestration of TORC1 to stress granules [10]. In PAS kinase-deficient yeast, ataxin-2/Pbp1 is no longer phosphorylated and activated by PAS kinase, thus preventing the sequestration of TORC1 to stress granules and promoting cellular growth on caffeine (11, Choksi et al, *submitted*).

Despite the clear importance of ataxin-2/Pbp1, only four binding partners have been identified (Pab1, Lsm12, Pbp4, and Dhh1, which are all thought to have roles in stress granule formation and mRNA regulation [12]. The aim of this study was to further characterize ataxin-2/Pbp1 through a Pbp1 interactome performed in yeast. Identifying additional binding partners will shed light onto the role of ataxin-2/Pbp1 in the cell, including pathways by which it may be affecting neurodegeneration and contributing to disease phenotypes.

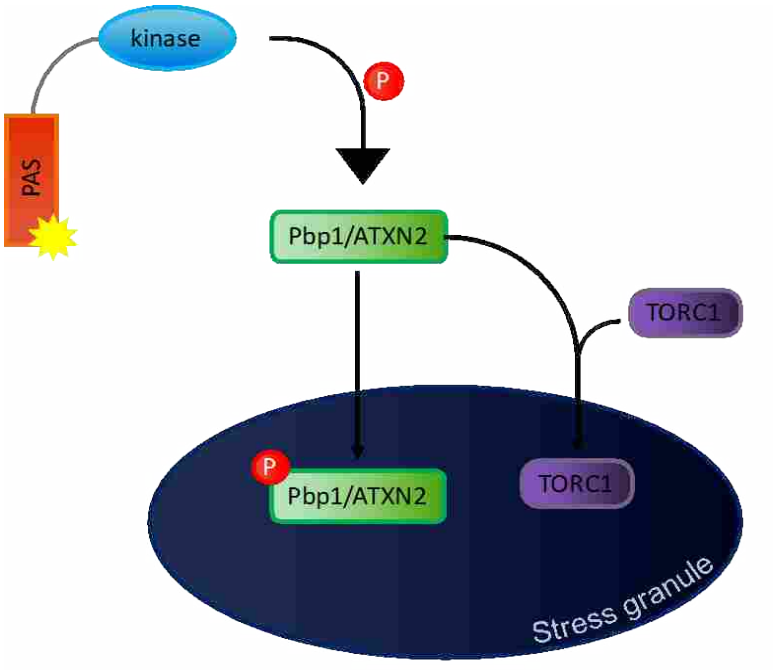

Figure 5.1 PAS kinase phosphorylates and activates Pbp1/ataxin-2, causing sequestration of Pbp1/ataxin-2. Pbp1/ataxin-2 also influences the sequestration of other proteins to the stress granules.

5.3 Materials and methods

5.3.1 Growth assays

Lists of strains, plasmids, and primers used in this study are provided in table 1. For plasmid construction, standard PCR-based cloning methods were used. Restriction enzymes were purchased from New England BioLabs (Ipswich, MA).

Yeast two-hybrid bait plasmid was made by PCR amplification of Pbp1 and subsequent cloning into the EcoRI/SalI sites of pGBD-C1 yeast two-hybrid Gal4 bait vector (pJG424) [13] (pJG1386 [JG2916/3163]). Yeast two-hybrid libraries are described in an earlier work [14]. Yeast two-hybrid Gold cells (Clontech, Mountain View, CA) were used to transform in bait and prey plasmids for interaction studies.

For serial dilution growth assays, spot-dilutions were performed by growing yeast in overnight liquid culture, serially diluted 1:10 in water and spotted on selective plates as well as control plates. Plates were incubated at 30°C for 7–10 d until colonies were apparent.

Table 5.1 Yeast strains used in this study

Strain	**Background**	**Genotype**	**Abbreviation**	**a/ α**	**Reference or source**
JGY1	W303	*ade2-1 can1-100 his3-11,15 leu2-3112 trp1-1 ura3-1*	WT	a	David Stillman (University of Utah, Salt Lake City, UT)
JGY2	W303	*Psk1*::his3 *ade2-1 can1-100 his3-11,15 leu2-3112 trp1-1 ura3-1*	*PSK2psk1*	a	Grose *et al.* (2007)
JGY3	W303	*psk2*::kan-MX4 *ade2-1 can1-100 his3-11,15 leu2-3112 trp1-1 ura3-1*	*PSK1psk2*	a	Grose *et al.* (2007)
JGY4	W303	*psk1*::*his3 psk2*::kan-MX4 *ade2-1 can1-100 his3-11,15 leu2-3112 trp1-1 ura3-1*	*psk1psk2*	a	Grose *et al.* (2007)
JGY299	S288C	*PSK2*-TAPtag::kanMX *ura3-0 trp1-0 SUC2 mal mel gal2 CUP1 flo1 flo8-1*	WT	α	Jared Rutter (University of Utah, Salt Lake City, UT)
Y2H Gold (JGY1031)		*LYS2*::*GAL1*UAS-*GAL1*TATA-His3, *GAL2*UAS-Gal2TATA-Ade2 *URA3::MEL1*UAS-*MEL1*TATA, *AUR1*-C*MEL1*, *ura3-52 his3-200 ade2-101 trp1-901 leu2-3, 112 gal4del gal80del met-*	Y2H Gold	a	Clontech
Y187 (JGY1073)		URA3::GAL1-GAL1-LacZ, MEL1, ura3-52, his3-200, ade2-101, trp1-901, leu2-3, 112, gal4del, gal80del, met-	Y187	α	Clontech
JGY1074		pGADT7 Mate and Plate stationary phase	YPAD library	α	DeMille *et al.* (2014)

		YPAD library in JGY1073			
JGY1098		pGADT7 Mate and Plate mid-log YPAGal library in JGY1073	YPAGal library	α	DeMille *et al.* (2014)
JGY1122	BY4743	*Pbp1::KanMx4* His3-1, leu2-0, lys2-0,ura3-0	*pbp1*	α	Janet Shaw (University of Utah, Salt Lake City, UT)
JGY1161	S288C	*psk1*::hygro *psk2*::NAT *ura3-0 trp1-0 SUC2 mal mel gal2 CUP1 flo1 flo8-1*	*psk1psk2*	α	DeMille *et al.* (2015)
JGY1383		*pJG1386 Pbp1 in Y2H bait* ura3-52, his3-200, ade2-101, trp1-901,leu2-3,112, gal4del	PBP1-Y2H Gold	a	This study
JGY43	BY4741	*His3d1, leu2DO, met15DO, ura3DO*	WT		Jared Rutter (University of Utah, Salt Lake City, UT)
JGY1244	BY4741	*Psk2::NAT, psk1::hygro, his3D1, leu2DO, met15DO, ura3DO.*	*psk1psk2*		Jared Rutter (University of Utah, Salt Lake City, UT)
JGY1598	BY4741	*Ptc6::kanMX, his3D1, leu2Do, met15DO, ura3DO*	*ptc6*		Tim Formosa (University of Utah, Salt Lake City, UT)
JGY1603	BY4741	*PTC6-GFP::HIS3MX6, his3-1, leu2-0, met15-0, ura3-0*	*ptc6-GFP*		O'shea collection (Thermo-Fisher)
JGY1591	BY4741	*OM45-GFP::His, leu2DO, met15DO, ura3DO*	WT		This study
JGY1593	BY4741	*OM45-GFP::His, leu2DO, met15DO, ura3DO*	*pbp1*		This study

JGY1624	BY4741	*OM45-GFP::His, leu2DO, met15DO, ura3DO*	*ptc6*		This study
JGY1594	BY4741	*OM45-GFP::His, psk1::hygro, psk2::nat, leu2DO, met15DO, ura3DO*	*psk1psk2*		This study
JGY1608	BY4741	*OM45-GFP::His, psk1::hygro, psk2::nat, pbp1::kanMX, leu2DO, met15DO, ura3DO*	*psk1psk2pbp1*		This study
JGY1623	BY4741	*OM45-GFP::His, psk1::hygro, psk2::nat, ptc6::kanMX, leu2DO, met15DO, ura3DO*	*psk1psk2ptc6*		This study
JGY1625	BY4741	*OM45-GFP::His, atg32::kanmx, leu2DO, met15DO, ura3DO*	*atg32*		This study

Table 5.2 Plasmids used in this study

Plasmid	**Gene**	**Description**	**Backbone**	**Yeast origin**	**Selection**	**Reference or source**
pJG9	*PSK1*	Psk1 in pRS424	pRS424	2u	Trp	Jared Rutter
pJG173	*PSK2*	Psk2 in pJR1765B	pJR1765B	2u	Ura	Jared Rutter
pJG174	*PSK2*	Psk2 K870R kinase dead mutant	pJR1765B	2u	Ura	Jared Rutter
pJG421	EV	pGAD-C1 empty Y2H prey vector	YEp-GAD	2u	Leu	James *et al.* (1996)
pJG424	EV	pGBD-C1 empty Y2H bait vector	YEp-GBD	2u	Trp	James *et al.* (1996)
pJG428	Library	pGAD-C2 genomic library	YEp-GAD	2u	LEU	James *et al*. (1996)
pJG429	Library	pGAD-C3 genomic library	YEp-GAD	2u	LEU	James *et al*. (1996)
pJG598	*PSK1*	ΔN692Psk1 in pJG425	YEp-GBD	2u	Trp	DeMille *et al.* (2014)
pJG725	*EV*	pADH-Myc	pRS416	CEN	Ura	David Stillman
pJG734	*PBP1*	ADH ∆N420Pbp1-Myc	pRS416	CEN	Ura	David Stillman
pJG858	*PSK1*	pGAL1-10, Psk1-HIS/HA	pRS426	2u	Ura	DeMille et al. (2014)

pJG859	EV	pGAL1-10, HIS/HA	pRS426	2u	Ura	DeMille et al. (2014)
pJG925	*PBP1*	Full-length Pbp1 in pJG859	pRS426	2u	Ura	DeMille et al. (2015)
pJG1250	*PBP1*	pGAL1-10, ΔN419Pbp1-Myc	pRS426	2u	Ura	DeMille et al. (2015)
pJG1251	*PBP1*	pGAL1-10, Full length Pbp1-Myc	pRS426	2u	Ura	DeMille et al. (2015)
pJG1271	*PSK1*	Psk1-D1230A kinase dead mutant	pRS426	2u	Ura	DeMille et al. (2014)
pJG1331	*ATXN2*	Full length ATXN2	pGEM-T	2u	Ura	Sino Biological Inc.
pJG1359	*ATXN2*	ΔN379 ATXN2 in pJG859	pRS426	2u	Ura	This Study
pJG1360	*ATXN2*	ΔN554 ATXN2 in pJG859	pRS426	2u	Ura	This Study
pJG1361	*ATXN2*	ΔN700 ATXN2 in pJG859	pRS426	2u	Ura	This Study
pJG1386	*PBP1*	ΔN419Pbp1 in pJG424	pRS416	CEN	Ura	This Study
pJG1409	*PBP1*	Full length Pbp1 in pJG725	pRS416	CEN	Ura	This Study
pJG1542	*PBP1*	Pbp1 with mutations: S106A, T193A, S436A, S479A,T708A,T718A made with pJG1251	pRS416	CEN	Ura	This Study
pJG1523	*PBP1*	Pbp1 with mutations: S106A, T193A, T355A, S436A, S479A,T708A made with pJG1251	pRS416	CEN	Ura	This Study
pJG1544	*PBP1*	Pbp1 with mutations: S106A, T215A, T355A, S436A, S479A,T708A,T718A made with pJG1251	pRS416	CEN	Ura	This Study
pJG1546	*PAT1*	PTA1 in Y2H bait			Leu	DeMille et al. (2014)
pJG1548	*Hypothetical gene*	Hypothetical gene in Y2H bait			Leu	DeMille et al. (2014)
pJG1549	*YEN1*	YEN1 in Y2H bait			Leu	DeMille et al. (2014)
pJG1560	*PBP1*	Full length Pbp1 in pJG859	pRS426	2u	Ura	This Study
pJG1561	*PBP1*	Pbp1 with mutations: S106A, T193A, S436A, S479A,T708A,T718A made with pJG12560	pRS426	2u	Ura	This Study
pJG1562	*PBP1*	Pbp1 with mutations: S106A, T193A, T355A, S436A,	pRS426	2u	Ura	This Study

		S479A,T708A made with pJG1560				
pJG1563	*PBP1*	Pbp1 with mutations: S106A, T215A, T355A, S436A, S479A,T708A,T718A made with pJG1560	pRS426	2u	Ura	This Study
pJG1572	*SEC61*	SEC61 in Y2H bait			Leu	DeMille et al. (2014)
pJG1573	*PTC6*	PTC6 in Y2H bait			Leu	DeMille et al. (2014)
pJG1574	*MUM2*	Mum2 in Y2H bait			Leu	DeMille et al. (2014)
pJG1575	*PKH1*	PKH1 in Y2H bait			Leu	DeMille et al. (2014)
pJG1669	*PBP1*	PBP1-RFP	pRS426	2u	Ura	This Study
pJG1690	*SEC63*	Sec63-RFP			Ura	Katrina Cooper

Table 5.3 Primers used in this study

Primer	**Sequence**
JG2335	TTCGATGATGAAGATACC
JG2761	CTATTCGATGATGAAGATACCCCACC
JG2762	AGATGGTGCACGATGCACAG
JG2916	GCCTCGAGGTTTATGGCCACTGGTACTACTATTATGG
JG2917	GGCGAATTCATGAAGGGAAACTTTAGGAAAAGAG
JG2953	GAAGGAAGGAAAGCTCAATTGGGAG
JG2954	GATTGAAATACTGATTACTTAAAATTTGC
JG2993	CGCCAGGGTTTTCCCAGTC
JG3037	CAACCATAGGATGATAATGCGATTAG
JG3136	GGCGAATTCTCGTTGCCTCCAAAACCGATCAGC
JG3384	GGCGAATTCATGTCGTTGCCTCCAAAACCGATCAGC
JG3704	GGCGTCGACTTACAACTGCTGTTGGTGGTGGGC
JG3758	GGCCAATTGATGCGCTCAGCGGCCGC
JG3759	GGCCAATTGATGACCCCCAGTGGGCCAGTTCTTG
JG3760	GGCCAATTGATGTCGCCTTGCCCATCTCCTTCC
JG3761	GGCCAATTGATGCTCACAGCCAATGAGGAACTTGAG
JG3854	GGCGTCGACGCAACTGCTGTTGGTGGTGGGC

5.3.2 Yeast 2-Hybrid screening

A yeast 2-hybrid system was used to look for a protein-protein interaction. The yeast 2-hybrid modifies the transcription factor for the Gal4 promoter. The transcription factor has a DNA binding domain and an activation domain that recruits RNA polymerase. The yeast 2-hybrid system cleaves the activation and binding domain and fuses them with a protein that will either serve as the bait (bound to binding domain) or prey (bound to activation domain). When

the two proteins interact in the cell it now allows for the Gal4 transcription factor binding domain and activation domain to become close enough to each other to recruit RNA polymerase to the promoter region and allow for expression of the reporter genes [15]. Pbp1 was cloned into binding domain (pJG1386) and the library was previously cloned into activation domain [14] (pJG428, pJG429, JGY1079 and JGY1098). Yeast containing both plasmids were selectively grown on SD-Leu-Trp. Colonies were then streaked onto selective media SD-Leu-Trp-His-Ade, where growth indicates a protein-protein interaction due to expression of reporter genes.

5.3.3 Yeast 2-Hybrid screening by mating

For cDNA library screens, α haploid yeast harboring a cDNA Y2H prey library (JGY1074 and JGY1098) [14] was mated to a haploid yeast harboring ΔN419Pbp1 Bait (JGY1383) in 2X YPAD for 24 hours at 30°C. Yeast cells where then pelleted and diluted using 10mL of SD-Leu-Trp media followed by plating 100uL on 100 SD-Leu-Trp-His-Ade plates.

5.3.4 Yeast 2-Hybrid screening by transformation

For genomic library screens, the Y2HGold (Clontech) strain bearing ΔN419Pbp1 Bait (JGY1383) was transformed with genomic libraries (pJG428, or pJG429) obtained from David Stillman, University of Utah [13]. Yeast cells where then pelleted and diluted using 10mL of SD-Leu-Trp media followed by plating 100uL on 100 SD-Leu-Trp-His-Ade plates.

5.3.5 Colony check and dependency assay

Colonies that arose on Y2H selection plates (SD-leu-trp-his-ade) were again patched on SD-leu-trp-his-ade plates for validation. The library plasmid inserts were then identified by colony PCR with subsequent sequencing (Brigham Young University DNA sequencing center) and national center for biotechnology information (NCBI) BLAST [16] analysis (an unambiguous hit with e-value of ≥10e−45). For verification and elimination of false positives,

library plasmids were purified from yeast [17], amplified in Escherichia coli (genelute plasmid mini-prep kit, sigma-aldrich, st. Louis, mo), and transformed into clontech matchmaker gold yeast with either the Pbp1 bait plasmid (pJG1386) or the empty bait plasmid (pJG424). Colonies arising on the SD-leu-trp transformation plates were then streaked onto SD-leu-trp-his-ade in duplicate and allowed to grow for 3–5 d to test for Pbp1 dependence. The strength of growth was determined by comparing growth of yeast on SD-leu-trp-his-ade plates, which is an indication of the interaction strength (s, strong; m, medium; w, weak) (Figure 5.2).

5.3.6 Mass spectrometry

Full length Pbp1 (pJG1560) into HIS expression under the GAL1-10 promoter was made by PCR amplifying Pbp1 with primers JG2916/2917 and cloning into the EcoRI/XhoI sites of pJG859. The protein was purified, run on 10% SDS PAGE, stained with coommassie blue and 78 kDa protein purified with it was cut from protein gel using a sterile razorblade. The gel slice was flash frozen at -80°C and sent to Majid Ghassemian, Department of Chemistry and Biochemistry, University of California, San Diego, for phosphosite mapping.

5.3.7 PTC6 colocalization

Ptc6-GFP fusion yeast (JGY1603) was obtained from the O'shea collection (ThermoFisher). Pbp1-RFP was transformed into JGY1603 to monitor colocalization of Pbp1 and Ptc6 to stress granules. Overnight samples were grown according to Demille *et al.* Briefly, samples were grown in in SD-Ura medium overnight, pelleted and re-suspended in SGal-Ura to induce expression of Pab1-RFP. Cultures were then grown 4 days, pelleted, washed, and re-suspended in synthetic complete medium. Cultures were grown for an additional hour at 30°C. Confocal fluorescent imaging stacks were acquired using an Olympus FV1000 confocal microscope. A 60x lens was used with 10x zoom, 0.4 μm step size and resolution of 640x640

pixels/frame for image acquisition. Deconvolution of images was performed using cellSens (Olympus).

5.3.8 Mitophagy assay

Mitophagy assays were performed via the method outlined by Kanki *et al.* Briefly, Om54-GFP DNA fragment was amplified from JGY1586 using JG4522 and JG4523. PCR product was transformed into JGY43, JGY1122, JGY 1598, and JGY1244 using standard yeast transformation methods. Correct integration was verified through fluorescence microscopy and PCR analysis of the genomic DNA (JG4524/JG4525).

Single colonies were picked and used to inncoluate 5mL YPD and grown to mid-log phase. Aliquots equal to OD~0.1 were collected for t=0, and the remaining cultures were centrifuged and re-suspended in a flask containing YPL (OD ~0.2). Cultures were grown shaking for 48 hours at 30°C, then aliquots equal to OD~0.1 were collected by centrifugation, re-suspended in 50 µL of 10% TCA, incubated on ice for 10 minutes, and frozen until ready to be broken open for SDS-Page. To break open, samples were thawed on ice and pelleted by centrifugation at 21,000xg for 10 minutes. Supernatant was removed, pellets were washed twice with 500 uL of cold acetone, and air dried. Samples were then re-suspended in 50 µL sample buffer (150 mM Tris-HCl, pH 8.8, 6% SDS, 25% glycerol, 6 mM EDTA, 0.5% 2-mercaptoethanol, and 0.05% bromophenol blue), disrupted by vortex with an equal amount of glass beads for 3 minutes, and incubated at 100°C for 3 minutes.

5 µL of sample was loaded on a 12% polyacrylamide gel and resolved. Transfer was completed using the TurboBlot program, 2 midi-gel mixed MW program, transferring onto a nitrocellulose membrane. Membranes were blocked with 5% milk, then probed with anti-GFP antibody (1:5000 TBST) at 4°C overnight, washed, then probed with HRP-conjugated anti-

mouse (1:10,000 TBS) for 1 hour at room temperature. Membranes were developed using the WesternBright ECL HRP substrate (Advansta Inc., San Jose, CA, USA, catalog number K-12045-D50) according to the manufacturer's protocol. Membranes were then striped and probed with anti-UGP1 to ensure equal loading between samples. Bands were quantified using the ImageJ software version 1.50i (National Institute of Health, Bethesda, MD, USA).

5.3.9 Plate respiration assays

Cultures were grown overnight in YPAD growth media. 1:10-fold serial dilutions were performed and 5 µL of each dilution tube was plated onto both SD-Ura and S-Gly-EtOH-Ura. Plates were grown for 2-3 days at 30°C and images acquired.

5.4 Results

5.4.1 A screen for Pbp1 binding partners reveals novel putative functions

Human ataxin-2 plays a pivotal role in the development of human ataxias (3, 4, 18), yet little is known about its function. A sensitive and reliable approach for identifying protein binding partners is copurification followed by quantitative mass spectrometry (MS). Full-length Pbp1 fused with a HIS epitope was affinity purified in triplicate, and samples were subjected to quantitative liquid chromatography (LC)–tandem MS. Twenty-five putative binding partners were identified for Pbp1 when compared with the empty HIS vector control also performed in triplicate (Table 5.4). Copurification screens retrieved both expected and novel binding partners. The copurification screen retrieved several proteins known to regulate Pbp1.

To further elucidate the function of this proteins, the yeast two-hybrid (Y2H) approach was employed utilizing the yeast ataxin-2 homolog, Pbp1 as bait. A truncation of Pbp1 (ΔN419Pbp1) was previously identified as active in Y2H screens and was screen against two yeast genomic libraries (pJG428, and pJG429) [13] and two cDNA libraries (JGY1098 and JGY1074) [14].

From ~10 million transformants and mated yeast screened, seven Pbp1 binding partners were identified (Table 5.5).

Table 5.4 Pbp1 binding partners identified by mass spectrometry

Gene	Human Homolog	Name description	Local-ization	# of times retrieved
RNA Processing				
IMP	IMP4	snoRNA-binding rRNA-processing protein	N	2
SSD1	N/A	mRNA-binding translational repressor	N/C	1
Protein Transporter				
TRS31	TRAPPC5	Core component of transport protein particle (TRAPP) complexes I-III	C/G	1
VPS29	VPS29	Vacuolar Protein Sorting	ES/ V	1
SSY1	N/A	Component of the SPS plasma membrane amino acid sensor system	PM	1
SEC24	SEC24	COPII vesicle coat component	ER/G/C	1
TIM9	TIMM9	Mitochondrial inner membrane translocase	M	1
Cell Cycle				
CDC50	TMEM30	Cell division control protein 50	ES	1
MCM5	MCM5	MiniChromosome maintenance protein 5	N	1
APC9	N/A	Anaphase Promoting Complex subunit 9	CD	1
BNR1	FMNL1	BNI1-related protein 1	CD	1
CYR1	PHLPP2	Adenylate Cyclase & magnesium ion binding	CD	1
CDC3	SEPT7	component of 10 nm filaments of mother-bud neck	CD	1
SPR28	SEPT1	Septin-related protein expressed during sporulation	W/ S	1
FUN19	TADA2A	SWIRM domain-containing protein	C	1
Other				
INA22	N/A	Inner membrane assembly complex subunit 22	M	2
RAD33	N/A	Nucleotide excision repair	N	1
APE3	ERMP1	Aminopeptidase Y	V	1
FRE7	CYBB	Ferric reductase PM	PM	1
NIT1	N/A	Nitrilase		1
ZRT2	N/A	low-affinity Zn(2+) transporter	PM	1
MOT3	N/A	Involved in cellular adjustment to osmotic stress	N/C	1
Protein of Unknown function				
YHR131 CP	N/A	Protein of Unknown function	C	1
FRT1	N/A	Tail-anchored ER membrane protein of unknown function	ER	1
SYG1	XPR1	Signal Transduction	PM/ER/ G	1

For localization: C, cytoplasm; M, mitochondrion; N, nucleus; ER, endoplasmic reticulum; PM, plasma membrane; W, cell wall; G, golgi; SG, stress granule; S, meiotic spindle; ES, Endosome; CD, cell division sites.

Table 5.5 Pbp1 binding partners identified by yeast two-hybrid

Gene	Human Homolog	Description	Loc.	# hits	Pray library	Construct (total aa)	Growth strength
RNA Processing							
MUM2	ERC2	mRNA methylation	N/C	3	cDNA	aa170 to aa298 (aa366)	W
PAT1	SLC36A1	Deadenylation-dependent mRNA-decapping factor	N/C	1	Gen	aa2 to aa192 (aa796)	S
PKH1	Pdpk1	Cytoplasmic mRNA processing body assembly	C/V	1	cDNA	aa649 to aa741 (aa766)	M
Hypothetical Protein (SGDID:S000003482)	-	Putative RNA binding protein	C/SG	2	Gen	aa509 to aa718 (aa718)	W
Other Functions							
YEN1	GEN1	Response to DNA damage stimulus	N/C	2	Gen	aa504 to aa759 (aa759)	W
PTC6	PPM1K	mitochondrion degradation, macroautophagy	M	1	Gen	aa1 to aa120 (aa442)	S
SEC61	SEC61A2	misfolded protein transport	ER/ MEM	1	Gen	aa407 to aa480 (aa480)	M

C corresponds to cytoplasm, MEM to membrane, M to mitochondrion, N to nucleus, ER to endoplasmic reticulum, V to vacuole and SG to stress granule. S, strong; M, medium; W, weak

Advantages of the Y2H approach include the identification of direct protein–protein interactions and sensitivity due to transcriptional amplification of an interaction [14]. However, the yeast two-hybrid can also yield false positives that allow growth independent of the bait. To minimize false positives, the Y2HGold strain was used, which harbors four different reporters control (Clontech Matchmaker Gold Yeast Two-hybrid System) [13], and each of these binding partners was verified by purifying the prey plasmid from yeast and retransforming into naive Y2HGold along with the ΔN419Pbp1 bait or an empty bait plasmid. The strength of growth is an indication of strength (Figure 5.2). The Y2H screen retrieved all novel binding partners including four involved in RNA processing. Although a role for Pbp1 in mRNA regulation was

known, these direct binding partners may reveal a more precise function through future study. The Y2H screen also revealed three additional proteins (YEN1, PTC6 and SEC61) all involved in stress response, specifically DNA damage response, mitophagy, and the misfolded protein response respectively.

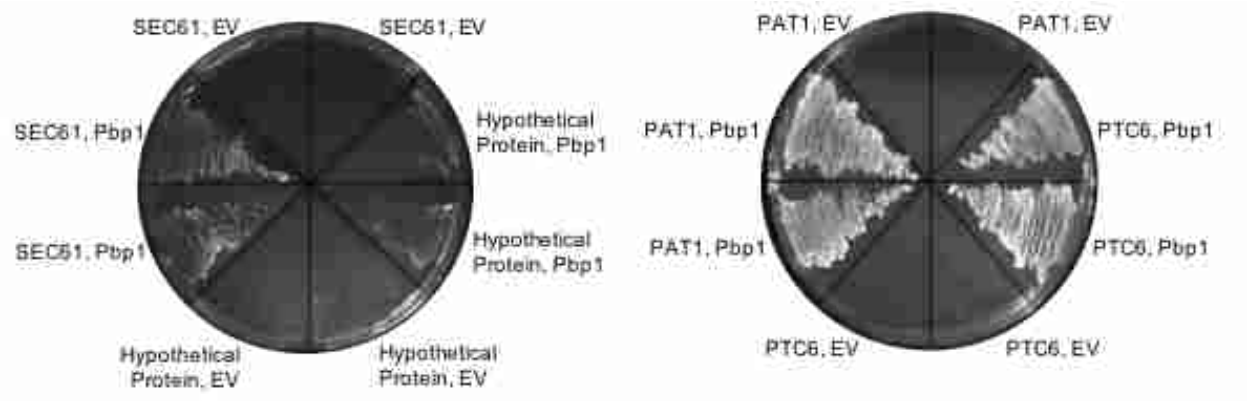

Figure 5.2 Dependency assay and growth comparison. For verification and elimination of false positives, library plasmids were purified and transformed into Clontech Matchmaker Gold yeast with either the bait plasmid (pJG1386) or the empty bait plasmid (pJG424). Colonies arising on the SD-Leu-Trp transformation plates were then streaked to SD-Leu-Trp-His-Ade in duplicate and allow growing for 3–5 d to test for Pbp1 dependence. The strength of growth was determined by comparing growth of yeast on SD-Leu-Trp-His-Ade plates, which is an indication of the interaction strength. (a) SEC61: Medium growth; Hypothetical Protein: Weak growth. (b) PAT1 and PTC6: Strong Growth.

5.4.2 Pbp1 sequesters Ptc6 at stress granules

Due to the metabolic alterations seen in ALS patients, as well as the role of mitophagy in ALS patients [19], Ptc6 was chosen for further study. Previous studies have revealed localization of Pbp1 to stress granules along with the Pbp1-dependent sequestration TORC1 at stress granules. To determine if Pbp1 is regulating Ptc6 activity via sequestration to stress granules, confocal microscopy was performed using Ptc6-GFP and Pbp1-RFP. Stress granule formation was induced by glucose deprivation. As shown in figure 5.3, Pbp1 and Ptc6 were shown to colocalize within the cell to cytoplasmic foci. This suggests that Pbp1 is sequestering Ptc6 to stress granules when the cell is under carbon starvation stress.

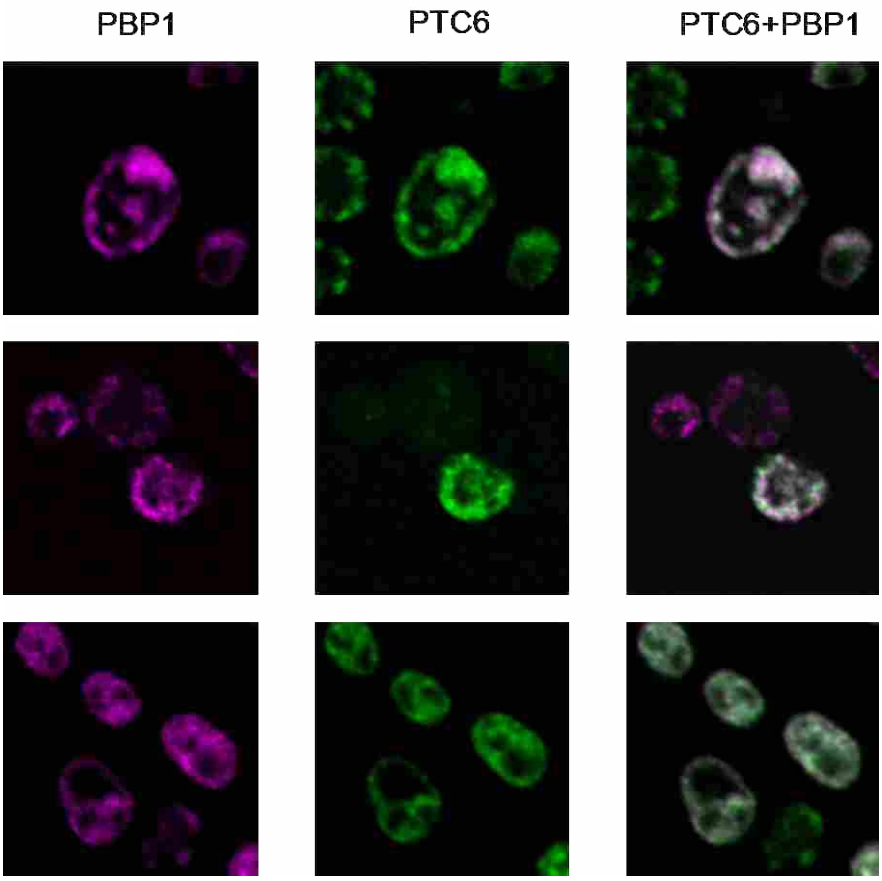

Figure 5.3 Colocalization of Pbp1 and Ptc6. Ptc6-GFP fusion yeast (ThermoFisher) was transformed with Pbp1-RFP (JG1669), grown under glucose deprivation, and imaged using an Olympus Fluoview confocal microscope.

5.4.3 Pbp1-deficient yeast exhibit increase mitophagy and mitophagy is restored in Pbp1/Ptc6-deficient yeast

Mitophagy is the process of clearing damaged mitochondria from the cell. It is thought that improper mitophagy can lead to the accumulation of dysfunctional or damaged mitochondria, contributing to neurodegeneration in ALS [19]. Ptc6 was chosen for further characterization as an interacting partner of Pbp1 because Ptc6 has been reported to be essential for mitophagy. Mitophagy assays were used to test our hypothesis that Pbp1 is inactivating Ptc6

by sequestration assays, just as it inactivates TORC1. If Pbp1 is absent from the cell, it is potentially not sequestering Ptc6 to stress granules allowing for increased mitophagy.

Mitophagy was induced through 48 hours growth in YPL and mitophagy was quantified by the amount of degraded OM45-GFP, measured through western blot. ATG1 was included as a control, as it should block mitophagy pathways. The level of mitophagy seen in *Ptc6* matched what has been reported in previous studies, with mitophagy being lowered in this strain (Figure 5.4). Pbp1-deficient yeast (*pbp1*) showed significantly elevated levels of mitophagy, suggesting a novel role of Pbp1 in regulating mitophagy within the cell. In addition, *pbp1ptc6* yeast showed mitophagy levels similar to wild-type consistent with elevated levels *pbp1* yeast due to increased activity of Ptc6. The return to wild type levels was, however, unexpected as Ptc6 has been reported as an essential gene necessary for mitophagy and suggests upregulation of unknown pathways in the Ppb1 knockout. The remaining strains tested revealed no significant changes. One-way ANOVA was performed using JMP Pro14 (version 14.0) software (SAS Institute, Cary, NC, USA) with Tukey's post-hoc test.

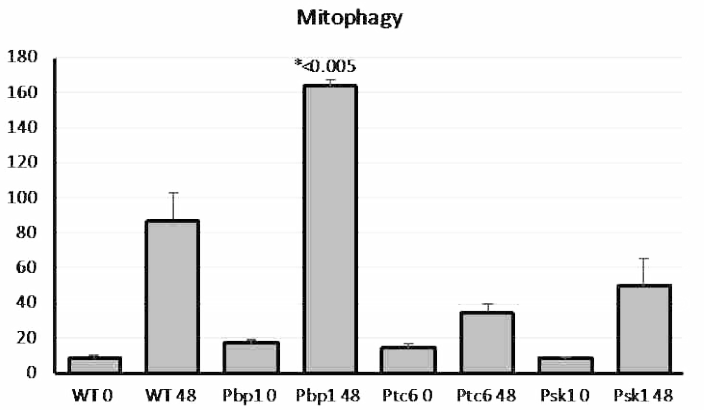

Figure 5.4 *Pbp1* yeast display increased levels of mitophagy . Mitophagy assays were conducted using the OM45-GFP processing assay developed by Kanki *et al.* Mitophagy was induced through growth in YPL and the amount of degraded GFP was measured as a marker for mitophagy. Bands were quantified using ImageJ. Significance was determined by one-way ANOVA and Tukey's post-hoc test. n=2.

5.4.4 PTC6-deficient yeast exhibit mitochondrial alterations

Due to the significant increase in mitophagy in Pbp1-deficient yeast and the significant decrease in mitophagy in Ptc6-defiicent yeast, mitochondria health was measured in each of the strains tested for the mitophagy assay. First, mitochondria content was quantified using flow cytometry. Mitochondria were tagged with OM45-GFP and endoplasmic reticulum was tagged with RFP. Endoplasmic reticulum was used as a cellular control. Consistent with a defect in mitophagy, our results show that PTC6-deficient yeast contain significantly more mitochondria (Figure 5.5A). However, PTC6/Pbp1-deficient yeast show levels similar to WT. One-way ANOVA was performed using JMP Pro14 (version 14.0) software (SAS Institute, Cary, NC, USA) with Tukey's post-hoc test.

This change in mitochondria content suggested that a change in respiration may also be seen due to the elevated mitochondrial content. The ability of each strain to grow on respiratory carbon source was utilized to determine if any noticeable respiratory differences could be detected. Each strain was grown up overnight and 1:10-fold serial dilution were performed and plated 1:100-fold serial dilutions were performed from the overnight and plated onto both glucose (a fermentative carbon source) and glycerol/ethanol (a respiratory carbon source). Following two days of growth, it was revealed that Ptc6-deficient yeast showed increased colony mass (Figure 5.5B), consistent with the increased mitochondria we observed (Figure 3A).

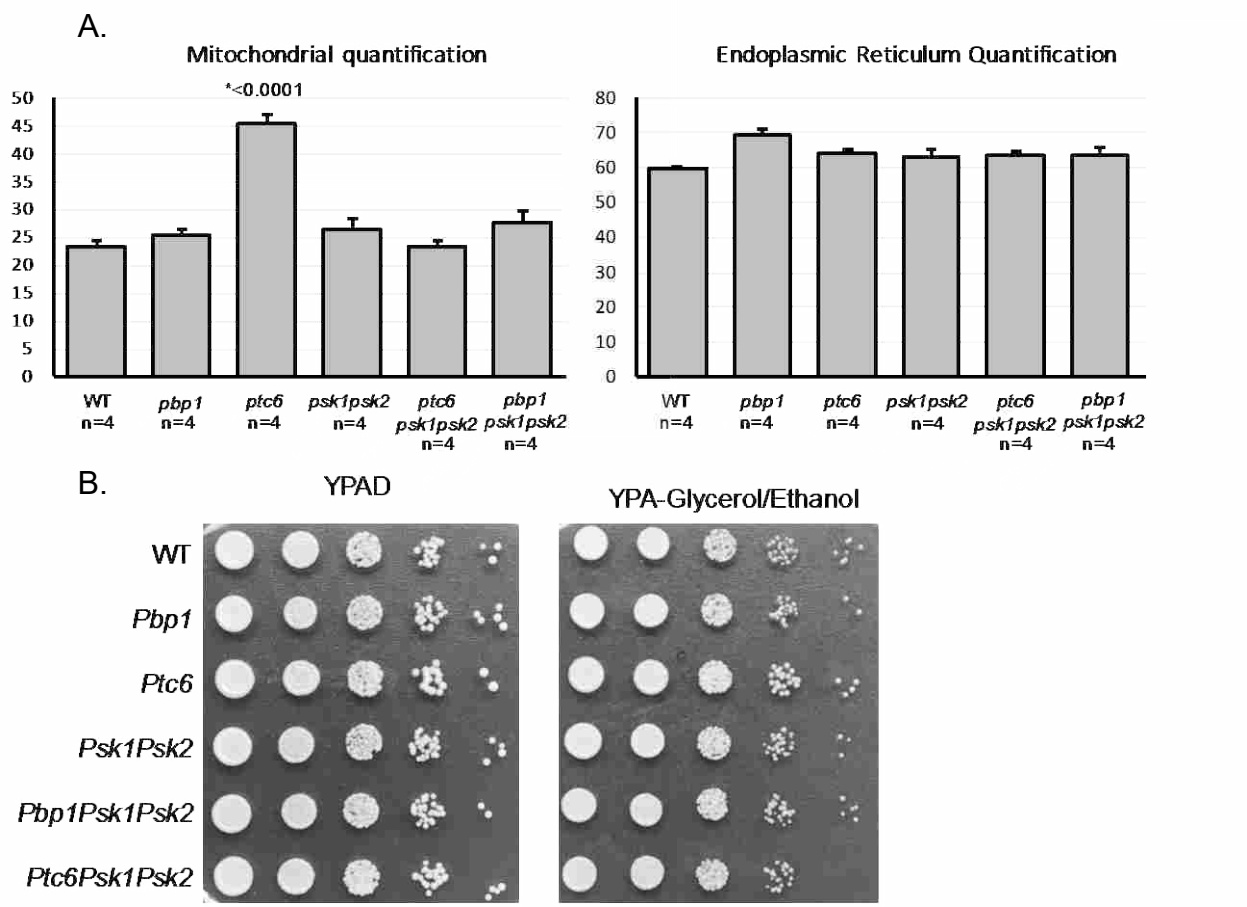

Figure 5.5 Evidence for *Ptc6* regulation of respiration. (A) Mitochondria was quantified using flow cytometry. OM45-GFP was used as a marker for mitochondrial content and the ER was quantified using Sec63-RFP, a protein in the ER. The ER was included as a control of overall cellular content. (B) Spot dilutions revealed increased respiration in Ptc6 yeast. Together, these results suggest the elevated mitochondrial content is contributing to elevated respiration.

5.5 Discussion

There are approximately 16,000 Americans living with ALS at any given moment. With a typical survival time of only 2-5 years, it can be a grim diagnosis with few treatment options. Fortunately, advances in technology have allowed for a more in-depth understanding of the pathways involved in the disease and subsequent potential drug targets [20]. Recently, ataxin 2 has been identified as a promising therapeutic target for ALS. It has been shown that intermediate-length polyglutamine expansions in the ataxin 2 gene increases the risk of ALS. Furthermore, it has been shown that by lowering the levels of ataxin 2 it is possible to mitigate

disease caused by TDP-43 proteinopathy in yeast, flies, and mice. As such, the regulation of ataxin 2 is a promising target for ALS treatment. PAS kinase has been identified as a protein kinase that regulates ataxin 2 activity. This is an extremely fortunate discovery as PAS kinase inhibitors have already been identified and are starting to be developed, making regulation of ataxin 2 through PAS kinase a very feasible task. PAS kinase is responsible for phosphorylating and activating ataxin-2, causing sequestration of various proteins to stress granules. As such, development of a PAS kinase inhibitor would result in a decreased ataxin-2 activity and resulting sequestration of proteins to stress granules. This study is focused on identifying proteins that interact with ataxin-2 through a study of its binding partners in yeast.

We performed a large-scale yeast interactome to identify Pbp1 binding partners through yeast-two hybrid and mass spectrometry. We identified 32 novel putative binding partners (7 from yeast two-hybrid and 25 from mass spectrometry). This has largely expanded the role of Pbp1 in yeast, which includes 6 proteins that are involved in RNA processing, 5 proteins involved in protein transportation, 8 cell cycle proteins, and 13 proteins with other unknown functions. In addition, 21 of the 32 identified binding partners have a homolog, suggested a possible conserved function between yeast and man.

Through the yeast two-hybrid assay we identified Ptc6 as a novel interacting partner of Pbp1. Ptc6 (also referred to as Aup1 or PPP2 in yeast) is a serine/threonine phosphatase that is localized to the mitochondria. Ptc6 was previously reported to be necessary for efficient mitophagy and cell survival in yeast [21]. This role in mitophagy was validated herein through the OM45-GFP processing assay, as *PTC6* yeast demonstrated decreased levels of mitophagy (Figure 5.4). Interestingly, *pbp1* yeast exhibited significantly increased levels of mitophagy. This result combined with our colocalization assays creates a model for how Pbp1 is interacting with

Ptc6. We hypothesize that when Pbp1 is activated, it sequesters Ptc6 to the stress granule, effectively deactivating Ptc6 function in the cell and decreasing mitophagy pathways (Figure 5.6). When Pbp1 is absent from the cell, Ptc6 is not sequestered to the stress granules, resulting in an increase in Ptc6 function and increased mitophagy. This result is especially interesting when looking at the context of ALS. In ALS, mitophagy pathways are often blocked, allowing for the accumulation of damaged mitochondria in the cell and contributing to neurodegeneration [19]. Elevated mitophagy in *Pbp1* yeast suggests yet another benefit of targeting Pbp1/ataxin-2 for ALS therapy, as lowering levels of Pbp1/ataxin-2 will result in increased mitophagy and decreased accumulation of damaged mitochondria. The regulation of mitophagy in ALS may be through the mammalian Ptc6 homolog PPM1K.

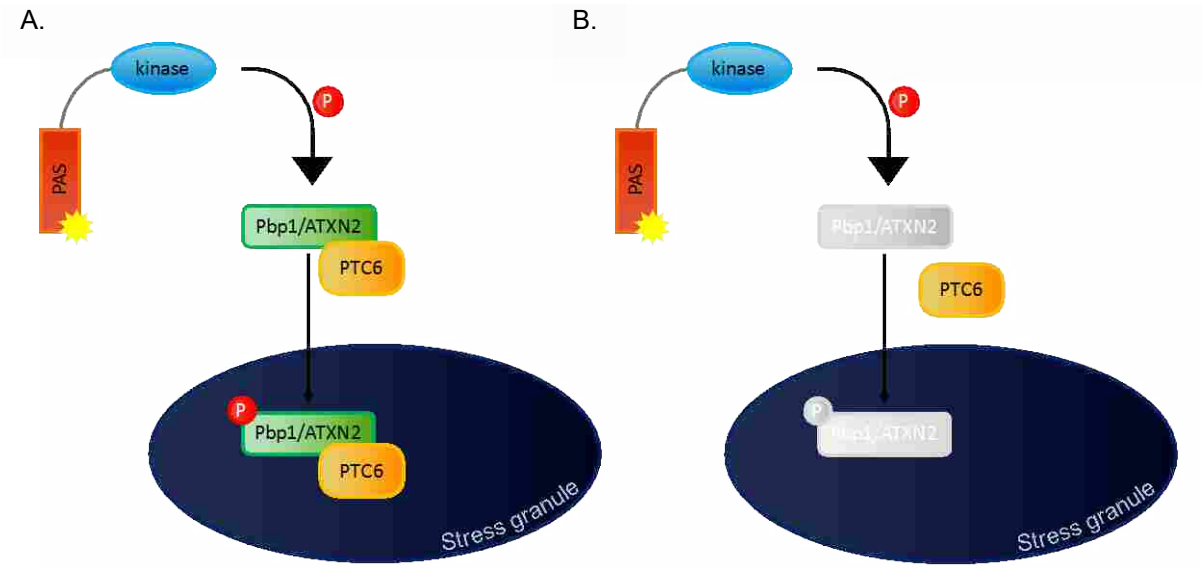

Figure 5.6 A model of Pbp1/ataxin-2 sequestration of Ptc6 to stress granules. (a) Pbp1 activation by PAS kinase results in sequestration of both Pbp1 and Ptc6, thus decreasing the function of Pbp1. (b) When Pbp1 is absent from the cell, Ptc6 is no longer sequestered to stress granules, remaining functional and possibly contributing to the increased mitophagy seen in Pbp1 yeast.

The defect of mitophagy in *ptc6* yeast prompted a deeper understanding of the mitochondria in these yeast strains. Flow cytometry assays revealed elevated mitochondria in

PTC6 yeast. This is supported by the mitophagy assays, as an inability to perform mitophagy would result in elevated levels of mitochondria in the cell. Furthermore, *PTC6* yeast appear to have increased respiration as shown by plate assay. As such, further characterization of the mitochondria is needed to determine if the yeast is accumulating damaged and dysfunctional mitochondria in the cell. This includes viewing mitochondrial morphology via confocal microscopy and measuring mitochondrial respiration via the Seahorse XF Cell Mito Stress Test. In addition to the mitochondrial phenotypes seen in *Ptc6* yeast, *Ptc6* yeast has been shown to be sensitive to rapamycin. This is very interesting because TORC1 is also sensitive to rapamycin. It

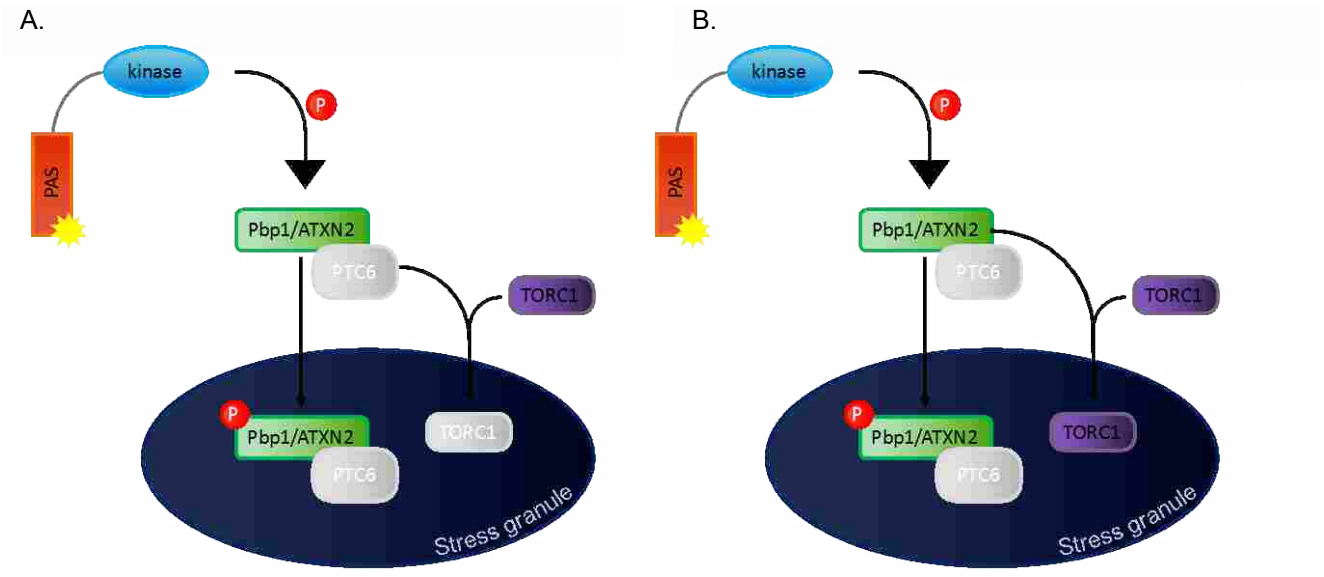

Figure 5.7 Possible models of Ptc6 dependent sequestration of TORC1 to stress granules . (a) Ptc6 is required for TORC1 sequestration to stress granules. In its absence, TORC1 is not sequestered to stress granules. (b) Ptc6 is not required for TORC1 sequestration to stress granules.

is known that Pbp1 sequesters TORC1 to stress granules, but it is unknown how that happens. It is possible that Pbp1 directly binds Ptc6 (as suggested by the yeast 2-hybrid assay, Table 3), and that Pbp1 is working through Ptc6 to sequester TORC1 to stress granules. This would also suggest that the *Ptc6* sensitivity to rapamycin could in part be due to it sequestering TORC1 to

stress granules. To test this theory, TORC1-GFP could be transformed into *Ptc6* yeast with Pabp1-RFP allowing for sequestration of TORC1 to stress granules to be monitored. If Ptc6 is responsible for sequestration, then TORC1 will not colocalize with Pab1-RFP in the stress granules (Figure 5.7A). If TORC1 does colocalize to the stress granules, it would suggest that Pbp1 is regulating the Ptc6 and TORC1 pathways separately (Figure 5.7B).

Through the identification of these 32 novel interacting partners of Pbp1 and the characterization of Ptc6, we have further solidified the importance of understand the role of Pbp1/ataxin-2 in ALS. By understanding both its upstream and downstream pathways, it will become more apparent how to best utilize it as a therapeutic target to help individuals with the disease.

REFERENCES

1. Hobson EV, McDermott CJ. Supportive and symptomatic management of amyotrophic lateral sclerosis. Nat Rev Neurol. 2016;12(9):526-38. Epub 2016/08/16. doi: 10.1038/nrneurol.2016.111. PubMed PMID: 27514291.

2. Soriani MH, Desnuelle C. Care management in amyotrophic lateral sclerosis. Rev Neurol (Paris). 2017;173(5):288-99. Epub 2017/05/04. doi: 10.1016/j.neurol.2017.03.031. PubMed PMID: 28461024.

3. Elden AC, Kim HJ, Hart MP, Chen-Plotkin AS, Johnson BS, Fang X, Armakola M, Geser F, Greene R, Lu MM, Padmanabhan A, Clay-Falcone D, McCluskey L, Elman L, Juhr D, Gruber PJ, Rub U, Auburger G, Trojanowski JQ, Lee VM, Van Deerlin VM, Bonini NM, Gitler AD. Ataxin-2 intermediate-length polyglutamine expansions are associated with increased risk for ALS. Nature. 2010;466(7310):1069-75. doi: 10.1038/nature09320. PubMed PMID: 20740007; PMCID: PMC2965417.

4. Becker LA, Huang B, Bieri G, Ma R, Knowles DA, Jafar-Nejad P, Messing J, Kim HJ, Soriano A, Auburger G, Pulst SM, Taylor JP, Rigo F, Gitler AD. Therapeutic reduction of ataxin-2 extends lifespan and reduces pathology in TDP-43 mice. Nature. 2017;544(7650):367-71. doi: 10.1038/nature22038. PubMed PMID: 28405022; PMCID: PMC5642042.

5. Meierhofer D, Halbach M, Sen NE, Gispert S, Auburger G. Ataxin-2 (Atxn2)-Knock-Out Mice Show Branched Chain Amino Acids and Fatty Acids Pathway Alterations. Mol Cell Proteomics. 2016;15(5):1728-39. Epub 2016/02/07. doi: 10.1074/mcp.M115.056770. PubMed PMID: 26850065; PMCID: PMC4858951.

6. Lastres-Becker I, Brodesser S, Lutjohann D, Azizov M, Buchmann J, Hintermann E, Sandhoff K, Schurmann A, Nowock J, Auburger G. Insulin receptor and lipid metabolism pathology in ataxin-2 knock-out mice. Hum Mol Genet. 2008;17(10):1465-81. Epub 2008/02/06. doi: 10.1093/hmg/ddn035. PubMed PMID: 18250099.

7. Rutter J, Michnoff CH, Harper SM, Gardner KH, McKnight SL. PAS kinase: an evolutionarily conserved PAS domain-regulated serine/threonine kinase. Proceedings of the National Academy of Sciences of the United States of America. 2001;98(16):8991-6. doi: 10.1073/pnas.161284798. PubMed PMID: 11459942; PMCID: PMC55361.

8. Pape JA, Newey CR, Burrell HR, Workman A, Perry K, Bikman BT, Bridgewater LC, Grose JH. Per-Arnt-Sim Kinase (PASK) Deficiency Increases Cellular Respiration on a Standard Diet and Decreases Liver Triglyceride Accumulation on a Western High-Fat High-Sugar Diet. Nutrients. 2018;10(12). Epub 2018/12/19. doi: 10.3390/nu10121990. PubMed PMID: 30558306; PMCID: PMC6316003.

9. Hao HX, Rutter J. The role of PAS kinase in regulating energy metabolism. IUBMB life. 2008;60(4):204-9. doi: 10.1002/iub.32. PubMed PMID: 18344204.

10. Takahara T, Maeda T. Transient sequestration of TORC1 into stress granules during heat stress. Mol Cell. 2012;47(2):242-52. doi: 10.1016/j.molcel.2012.05.019. PubMed PMID: 22727621.

11. DeMille D, Badal BD, Evans JB, Mathis AD, Anderson JF, Grose JH. PAS kinase is activated by direct SNF1-dependent phosphorylation and mediates inhibition of TORC1 through the phosphorylation and activation of Pbp1. Molecular biology of the cell. 2015;26(3):569-82. doi: 10.1091/mbc.E14-06-1088. PubMed PMID: 25428989; PMCID: PMC4310746.

12. Swisher KD, Parker R. Localization to, and effects of Pbp1, Pbp4, Lsm12, Dhh1, and Pab1 on stress granules in Saccharomyces cerevisiae. PLoS One. 2010;5(4):e10006. Epub 2010/04/07. doi: 10.1371/journal.pone.0010006. PubMed PMID: 20368989; PMCID: PMC2848848.

13. James P, Halladay J, Craig EA. Genomic libraries and a host strain designed for highly efficient two-hybrid selection in yeast. Genetics. 1996;144(4):1425-36. Epub 1996/12/01. PubMed PMID: 8978031; PMCID: PMC1207695.

14. DeMille D, Bikman BT, Mathis AD, Prince JT, Mackay JT, Sowa SW, Hall TD, Grose JH. A comprehensive protein-protein interactome for yeast PAS kinase 1 reveals direct inhibition of respiration through the phosphorylation of Cbf1. Molecular biology of the cell. 2014;25(14):2199-215. doi: 10.1091/mbc.E13-10-0631. PubMed PMID: 24850888; PMCID: PMC4091833.

15. Fields S, Song O. A novel genetic system to detect protein-protein interactions. Nature. 1989;340(6230):245-6. Epub 1989/07/20. doi: 10.1038/340245a0. PubMed PMID: 2547163.

16. Altschul SF, Gish W, Miller W, Myers EW, Lipman DJ. Basic local alignment search tool. J Mol Biol. 1990;215(3):403-10. Epub 1990/10/05. doi: 10.1016/S0022-2836(05)80360-2. PubMed PMID: 2231712.

17. Amberg DC, Burke D, Strathern JN, Burke D, Cold Spring Harbor Laboratory. Methods in yeast genetics : a Cold Spring Harbor Laboratory course manual. 2005 ed. Cold Spring Harbor, N.Y.: Cold Spring Harbor Laboratory Press; 2005. xvii, 230 p. p.

18. Pulst SM, Nechiporuk A, Nechiporuk T, Gispert S, Chen XN, Lopes-Cendes I, Pearlman S, Starkman S, Orozco-Diaz G, Lunkes A, DeJong P, Rouleau GA, Auburger G, Korenberg JR, Figueroa C, Sahba S. Moderate expansion of a normally biallelic trinucleotide repeat in spinocerebellar ataxia type 2. Nat Genet. 1996;14(3):269-76. Epub 1996/11/01. doi: 10.1038/ng1196-269. PubMed PMID: 8896555.

19. Evans CS, Holzbaur ELF. Autophagy and mitophagy in ALS. Neurobiol Dis. 2019;122:35-40. Epub 2018/07/10. doi: 10.1016/j.nbd.2018.07.005. PubMed PMID: 29981842; PMCID: PMC6366665.

20. Scott A. Drug therapy: On the treatment trail for ALS. Nature. 2017;550(7676):S120-S1. Epub 2017/10/19. doi: 10.1038/550S120a. PubMed PMID: 29045376.

21. Tal R, Winter G, Ecker N, Klionsky DJ, Abeliovich H. Aup1p, a yeast mitochondrial protein phosphatase homolog, is required for efficient stationary phase mitophagy and cell survival. J Biol Chem. 2007;282(8):5617-24. Epub 2006/12/15. doi: 10.1074/jbc.M605940200. PubMed PMID: 17166847.

CONCLUSIONS

Herein we characterized two novel substrates of PAS kinase, Cbf1 and Pbp1. First, we identified a novel role of Cbf1 in cellular respiration. In the absence of PAS kinase, Cbf1 is not inhibited by phosphorylation and shifts glucose towards respiration and away from lipogenesis. We further studied this shift in a mouse model of PAS kinase deficiency on either a normal chow diet or a high-fat high-sugar diet. We found that PAS kinase deficiency will shift glucose towards respiration and away from lipogenesis, just as it did in our yeast model. This was shown through respiration assays and through lipidomics analysis. These studies have deepened our understanding of how PAS kinase is functioning in both yeast and mice.

Next, we provided further characterization of the function of Pbp1. Pbp1 has a human homolog called ataxin-2. Mutations in ataxin-2 have been associated with amyotrophic lateral sclerosis (ALS), and removal of ataxin-2 in an ALS mouse model significantly increases the lifespan of the animal. ALS is a neurodegenerative disease, but it presents with many metabolic abnormalities that can be affected by diet, metabolic health, and sex. These changes were reviewed in-depth within this dissertation.

We furthered the understanding of Pbp1 function by identifying 32 interacting partners of Pbp1. We further characterized one of these partners identified by yeast-two hybrid assay, Ptc6. We provided evidence of Pbp1 regulation of Ptc6 by sequestration to stress granules. Initial studies show Pbp1 and Ptc6 regulation of mitophagy, and Ptc6 deficiency affecting mitochondrial content and function. These studies have provided insight into the interaction of Pbp1 and Ptc6 while also opening up exciting new questions about how Pbp1 and Ptc6 are involved in mitochondrial function, from respiration to mitophagy. The following experiments are suggested in order to answer these questions in the future:

Question 1: Is Pbp1 responsible for Ptc6 sequestration to stress granules

Experiment 1.1 Tag Ptc6 with GFP and Pabp1 (a known stress granule marker) with RFP. Transform these into Pbp1-deficeint yeast and view via confocal microscopy using the steps outlined in chapter 5. If Pbp1 is responsible for Ptc6 sequestration to stress granules, the in its absence we expect that Ptc6 will not be localized to stress granules.

Question 2. Is Ptc6 required for TORC1 sequestration to stress granules?

Experiment 2.1: Growth Assays to determine if TORC1 can be sequestered to stress granules in the absence of Ptc6. Spot wild-type, Ptc6-deficient, and Ptc6-deficient with Pbp1 overexpressing on a plasmid to caffeine plates. If the yeast can grow on caffeine in the absence of Ptc6, it suggests that Ptc6 is essential for TORC1 sequestration to stress granules.

Experiment 2.2 Colocalization analysis to determine of TORC1 can be sequestered to stress granules in the absence of Ptc6. Tag TORC1 with GFP in a Ptc6 knockout yeast strain. Follow the procedure outlined for colocalization analysis. Localization of TORC1 to the stress granules in the absence of Ptc6 suggests that Ptc6 is not responsible for the sequestration of TORC1 to stress granules.

Question 3: Do Ptc6-deficient yeast collect damaged mitochondria

Experiment 3.1 Our plate assays suggest that Ptc6-deficient yeast have increased respiration because of the increased colony size. We suggest performing respiration assays on the Seahorse XF Analyzer. We suggest performing this experiment in the strains shown in the spot dilutions, with the addition of the Pbp1/Ptc6 double knockout. This will help determine if the increased colony size is due to increased respiration.

Experiment 3.2 Our flow cytometry assays show Ptc6 deficient yeast have increased mitochondria. However, because Ptc6-deficient yeast show decreased mitophagy it is possible that damaged mitochondria is being collected. We suggest tagging the mitochondria with an RFP tag to determine morphological changes via confocal microscopy.

Ultimately, these experiments will shed light into how PAS kinase, Pbp1, and Ptc6 are interacting to regulate mitophagy and overall mitochondrial health within the cell. This pathway, along with the pathways mentioned throughout this dissertation, are promising targets for future drug development for metabolic and neurodegenerative disease. Further understanding of these pathways will provide for the most safe and effective therapies for patients.